Studies on non-equilibrium fluctuating motion as a rectifier

Tomohiko Sano

December 15, 2015

Acknowledgement

I would like to express my deep appreciation to my Ph.D supervisor, Professor Hisao Hayakawa. I am grateful that he taught me many things including physics, research, and scientific mind. I really appreciate all the advice he gave me in writing this thesis. I wish to acknowledge one of my collaborators Dr. Kiyoshi Kanazawa in Tokyo Institute of Technology for giving me critical comments on stochastic processes when he was in Kyoto University. I am grateful to Prof. Takahiro Sagawa in the University of Tokyo for extensive discussion on my work and kind invitation to his laboratory. I wish to acknowledge Prof. Eiki Iyoda in the University of Tokyo and Dr. Sosuke Ito in Tokyo Institute of Technology for constructive discussion. I would like to thank all of the present members, past members and visitors in Prof. Hayakawa's group for fruitful comments and discussions. I would like to thank Prof. Yu Watanabe for constructive comments on my presentation and providing easy-to-use computing environment in the laboratory. I am grateful to my colleague Mr. Satoshi Takada and members in the room K401, Mr. Kazuya Shinjo, Mr. Kazuhiko Tanimoto, and Mr. Kazuma Nagao for daily chatting even at midnight. I wish to acknowledge Mr. Takafumi Suzuki in the University of Tokyo for discussion of stochastic processes in quantum systems. I also thank students in condensed matter physics group, Mr. Takumi Ohta and Mr. Yukihisa Imamura for discussion and daily chatting.

I am grateful to Masato Itami in Kyoto University for valuable discussion for adiabatic piston problems at the beginning of the research. I appreciate helpful advice on finite-time thermodynamics to Prof. Yuki Izumida when I participated in the Japan Physics Society meeting. I would like to thank granular physicists, Prof. Takahiro Hatano in the University of Tokyo and Prof. Michio Otsuki in Shimane University for insightful comments on my research about granular physics. I would like to thank researchers from abroad for valuable comments. I wish to acknowledge Prof. Andrea Puglisi and Prof. Andrea Gnoli in Rome for their valuable comments on the experimental realization of my work on the granular rotor. I thank Prof. Antoine Naert in École Normale Supérieure de Lyon for extensive discussion on his experimental devices of granular rotors when I participated in Kyoto Winter School for Statistical Mechanics. I am grateful to Prof. Devaraj van der Meer in the University of Twente for constructive suggestions on the realization of non-Gaussian velocity distribution functions for granular gases when I joined the 2014 Gordon Conference on Granular and Granular-Fluid Flows. I thank my colleagues, Mr. Shinsuke Takasao and Mr.

Shinji Bono in Kyoto University and Mr. Seiya Sugo for discussion and daily chatting even at midnight.

I would like to thank researchers who gave me practical advice for my future works. I wish to acknowledge Prof. Adrian Baule and Mr. Andrea Cairoli in Queen Mary University of London for their useful comments and kind invitation to London. I am grateful to Prof. Hirofumi Wada in Ritsumeikan University and Prof. Tatsuo Shibata and Dr. Daiki Umetsu in RIKEN for stimulating discussion.

This thesis was partially supported by the Grant-in-aid of JSPS (Grant No. 26·2906) and JSPS research fellowship. This work was also supported by the JSPS core-to-core program for Non-equilibrium dynamics for soft matter and information. A part of the numerical calculations in this thesis was carried out on SR16000 at YITP in Kyoto University.

Lastly, I would like to thank my family Hiroyuki Sano, Masako Sano, and Fumihiko Sano for heartwarming support and express my deepest gratitude to my partner Karin Yamada for daily encouragement and considering about my life.

Contents

List of publications submitted for the requirement of the thesis

- **Chapter 5:**
  Tomohiko G. Sano and H. Hayakawa, "Roles of dry friction in the fluctuating motion of an adiabatic piston,"
  Physical Review E **89**, 032104 (2014).

- **Chapter 6:**
  Tomohiko G. Sano, K. Kanazawa and H. Hayakawa,"Granular rotor as a probe for a non-equilibrium bath," arXiv:1511.08594v1, submitted to Physical Review E

- **Chapter 7:**
  Tomohiko G. Sano and H. Hayakawa, "Efficiency at maximum power output for a passive engine," arXiv:1412.4468v2, resubmitted to Physical Review E

The other publications by the author

In addition, the author has published the following four papers in the peer-reviewed journals and one peer-reviewed proceedings for the international conference:

- Tomohiko G. Sano and Hisao Hayakawa, "Simulation of granular jets: Is granular flow really a perfect fluid?," Physical Review E **86**, 041308 (2012).

- Tomohiko G. Sano and Hisao Hayakawa, "Jet-induced jammed states of granular jet impacts," Progress of Theoretical and Experimental Physics, (**2013**) 103J02.

- Kiyoshi Kanazawa, Tomohiko G. Sano, Takahiro Sagawa, and Hisao Hayakawa, "Minimal Model of Stochastic Athermal Systems: Origin of Non-Gaussian Noise," Physical Review Letters **114**, 090601 (2015)

- Kiyoshi Kanazawa, Tomohiko G. Sano, Takahiro Sagawa, and Hisao Hayakawa, "Asymptotic Derivation of Langevin-like Equation with Non-Gaussian Noise and Its Analytical Solution," Journal of Statistical Physics **160**, 1294 (2015).

- Tomohiko G. Sano and Hisao Hayakawa, "Numerical analysis of impact processes of granular jets," AIP Conference Proceedings **1542**, 622 (2013), Powders and Grains 2013, Sydney, Australia

Abstract

The fluctuating motion of a tracer attached to non-equilibrium environments is theoretically studied as the rectifier. We clarify the following three properties of the fluctuating motion under non-equilibrium conditions in this thesis.

At first, we consider the motion of an adiabatic piston under sliding friction, which is located between two ideal gases in equilibrium characterized by two different temperatures and densities. In the absence of the sliding friction, the direction of the piston motion is known to be determined from the difference of temperature of two gases. However, if the sliding friction exists, we show that the direction of motion depends on the amplitude of the friction, and nonlinearity of the friction. Thus, the direction of momentum flux rectified from the fluctuation piston is not determined by temperature difference if the piston is attached to non-equilibrium environments. The fluctuation theorem under dry friction, which deviates from the conventional fluctuation theorem, is derived.

At second, the dynamics of a rotor under viscous or dry friction is investigated as a non-equilibrium probe of a granular gas numerically and analytically. To demonstrate a role of the rotor as a probe for a non-equilibrium bath, we perform the molecular dynamics (MD) simulation of the rotor under viscous or dry friction surrounded by a steady granular gas under gravity. We theoretically derive a one-to-one map between the velocity distribution function (VDF) for the granular gas and the angular one for the rotor. With the aid of the MD simulation, we demonstrate that the one-to-one map works well to infer the local VDF of the granular gas from the angular one of the rotor, and vice versa.

At third, we consider the cycle containing heating and cooling processes for an elastic hard core gas enclosed by a fluctuating piston. We study the efficiency at maximum power output (MP) for a passive engine without mechanical controls between two reservoirs. We enclose a hard core gas partitioned by a massive piston in a temperature-controlled container and theoretically analyze the efficiency at MP for heating and cooling protocols without controlling the pressure acting on the piston from outside.

Chapter 1

Introduction

1.1 Fluctuating motion under non-equilibrium situations

Studies on fluctuating motion have a history of nearly 200 years. An English botanist, Brown found the random motion of pollen grains on water, through his observation through a microscope in 1827 [1]. Although it is fascinating to observe the random motion of inactive grains as if they are organisms, the quantitative theory did not exist in the 19th century. In 1905, Einstein proposed the theory on the Brownian motion using a stochastic theory [2]. Einstein's work has greatly influenced the development of statistical mechanics, molecular kinetic theory and stochastic processes in the 20th century. Theory of Brownian motion has been developed by many researchers, including Langevin, Smoluchowski, Ornstein, and Uhlenbeck [3–9].

Equilibrium thermodynamics prohibits extracting work from a single environment without any energetic cost. However, one can expect to extract work from an isotropic thermal fluctuating environment such as the Feynman-Smoluchowski ratchet [10, 11]. Note that the ratchet has been originally proposed by Smoluchowski [10]. The symmetric vanes are connected to an asymmetric wheel with a pawl to rotate in one direction (Fig. 1.1). We call the whole system including vanes and the pawl "the ratchet." If the ratchet is placed in thermal equilibrium environment, we might expect to rectify the work from the single thermal equilibrium environment, which is in contradiction with the second law of equilibrium thermodynamics. To solve this contradiction, thermal fluctuation plays a key role. When the vanes are attached to the thermal equilibrium environment, they thermally fluctuate. As a result, the pawl thermally fluctuates and it does not work correctly. Thus, the ratchet cannot extract any work from the fluctuation in the single thermal equilibrium environment [10,11]. See Ref. [12] for the critical analysis of the ratchet as engines.

Nowadays, non-equilibrium Feynman-Smoluchowski ratchet is experimentally realized in a granular gas environment [13], where the asymmetric vanes

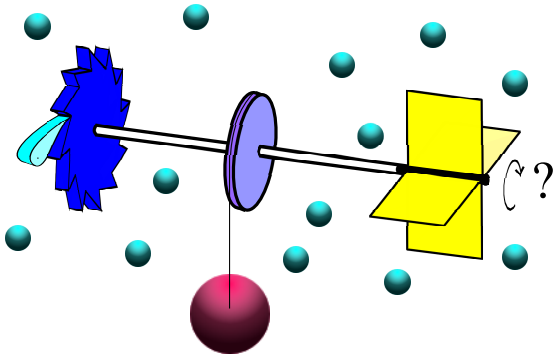

Figure 1.1: A schematic figure of the Feynman ratchet. The symmetric vanes are connected to the asymmetric wheel, where the pawl is placed to force the wheel to rotate in one direction. As is well known, no work can be rectified.

having coated the surfaces of different restitution coefficients are placed in the granular gas (Fig. 1.2). The difference of restitution coefficients corresponds to the pawl in the original Feynman-Smoluchowski ratchet, and thus, the vanes can rotate in one direction. It is essential that the ratchet is attached on a non-equilibrium environment. Because the kinetic energy of the granular gas is much higher than the room temperature and the asymmetric vanes can be regarded as the system attached to the zero-temperature environment, where thermalization of the pawl can be ignored. The realization of such a non-equilibrium Feynman-Smoluchowski ratchet has raised the natural question: *what can we rectify from the fluctuating motion under non-equilibrium?* This is the question addressed in this thesis.

The spirit of asking the previous question is as follows. Looking back the early history of equilibrium thermodynamics in the middle of 19th century, we should note that work of Carnot is remarkable [14]. Besides the discussion for the identity of heat, Carnot is the first person who considered the extraction of work from thermal equilibrium environments [1] and its maximum bound. In this thesis, we consider the extraction of work from environments including non-equilibrium ones.

1.2 Dry friction as a non-equilibrium environment

One of the typical couplings between the system and an environment is dry friction, when two solid bodies are in contact. Dry friction is ubiquitous throughout nature from a biological surface to an atomic-scale surface [15–17]. Recent developments in experimental technique enable us to control small systems and non-

[1] Needless to say, real engines are not in thermal equilibrium exactly.

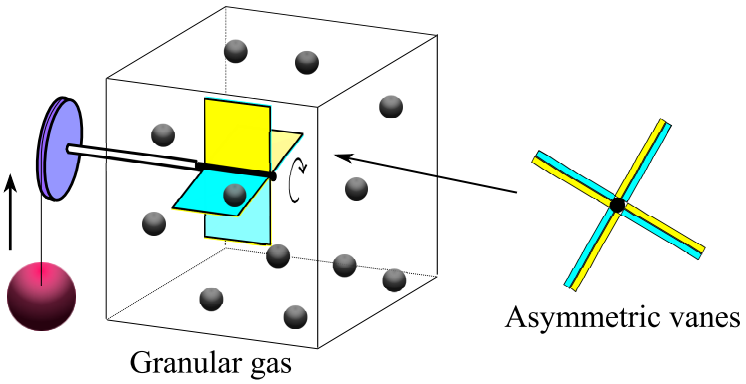

Figure 1.2: Schematic figure of the Feynman ratchet in a granular gas. The asymmetric vanes, whose surfaces are coated to have different restitution coefficients, are placed in granular gas.

equilibrium systems, such as nano-scale systems, single colloidal systems, and biological systems, to clarify their thermodynamic structures in detail [18–20]. One of the most important applications of manipulation techniques for small systems is the design of nano-machines or sub-micron machines [21–23]. The difficulty to realize efficient small machines is the existence of dry friction, because the dry friction wears down the small machines [24]. Thus, to control systems under dry friction is indispensable to invent small machines. There are many unavoidable obstacles which play central roles in small realistic systems, such as dry friction, wear, adhesion, electrification, and so on [25–28]. Experiments for macroscopic systems under dry friction reveal that the dry friction has an important role to extract work from an equilibrium environment [29, 30, 32]. The motor interacting with its supporting axis via dry friction rotates even in an equilibrium fluid. Recent studies on the Brownian motion under dry friction clarify that the motion of particles is characterized by non-Gaussian statistics [31, 33–43].

Although dry friction plays essential roles in non-equilibrium transport [24–28], the energetics for systems under dry friction has been elusive so far. For systems without dry friction, there exists the energetics in the Langevin description so-called stochastic energetics [44–46], in which the first law of thermodynamics holds at the level of single trajectory of a tracer particle. The original form of stochastic energetics has been restricted to systems of a single particle driven by a Gaussian white noise, while it is extended to those driven by a non-Gaussian white noise by introducing the new stochastic products [47].

1.3 Fluctuating motion of a symmetric rotor

In the previous section, we have shown that the asymmetry of vanes induces the directed motion. Then, we can ask a question: can we rectify useful quantities from the fluctuating motion of a symmetric rotor? From the fluctuation-dissipation relation (FDR), we expect that the fluctuation motion of symmetric vanes is directly related to the temperature of a non-equilibrium environment. Temperature is one of the most important quantities in equilibrium thermodynamics [48, 49]. One can generalize the concept of temperature to characterize various non-equilibrium systems. Although many authors have proposed non-equilibrium temperatures, their validity has not been sufficiently clarified so far [50–52]. Indeed, there are some reports that the effective temperatures in non-equilibrium systems do not satisfy the fundamental laws of thermodynamics, such as the zeroth law [53–57].

There are many attempts to introduce effective temperatures even for granular systems [58–61]. One of the most famous ones is the Edwards temperature, which is associated with the compactivity and is mainly used for static ensembles of granular particles [62–69]. Another well-known temperature is the kinetic temperature or the granular temperature, which is the second-order cumulant of the velocity distribution function (VDF) and is related to the kinetic energy of granular particles [70–86]. The latter effective temperature is appropriate in describing the granular flows even in the vicinity of jamming transition, whereas we do not have the consensus of what temperature is useful for general setups of granular systems [83–86]. Moreover, we have to take into account the effects of higher-order cumulants explicitly to characterize granular assemblies, because granular assemblies have non-Maxwellian nature of the VDF, i.e., the existence of higher-order cumulants [33, 57, 87–89].

For local thermal equilibrium gases, the local temperature can be measured through the observation of the motion of a Brownian tracer, because the second cumulant of the VDF of the tracer is directly related to the temperature according to the FDR. On the other hand, it is nontrivial whether we can infer the distributions of non-equilibrium environments only observing the motion of the tracer attached to environments such as granular gases [90, 91]. Kanazawa *et al.* suggested that such a characterization is possible through the analysis of a non-Gaussian Langevin equation [92, 93], where an inverse estimation formula is derived to infer the non-equilibrium granular VDF from the observation of the tracer. Although the usefulness of the inverse formula has already been numerically verified on the basis of the Boltzmann-Lorentz equation for spatially homogeneous and isotropic granular gases [3, 7, 8, 94–97], the model may not be sufficiently realistic because inhomogeneity and anisotropy exist in real granular gases such as vertically vibrated granular systems under gravity [88]. This implies that more realistic formulation is necessary for experimental measurement of high-order cumulants by observation of the tracer dynamics.

1.4 Efficiency with finite power

Equilibrium thermodynamics reveals the relation between work and heat, and the upper bound for extracted work from an arbitrary heat cycle [98, 99]. The milestone of equilibrium thermodynamics is that thermodynamic efficiency for any heat cycle between two reservoirs characterized by the temperatures $T_{\rm H}$ and $T_{\rm L}$ ($T_{\rm H} > T_{\rm L}$) is bounded by the Carnot efficiency:

$$\eta_{\rm C} \equiv 1 - \frac{T_{\rm L}}{T_{\rm H}}, \tag{1.1}$$

achieved by a quasi-static operation [100]. There are many studies on the efficiency of engines including both external and internal combustion engines. The steam engines and steam turbines belong to the former category whose ideal cycles are the Carnot cycle, the Stirling cycle, and so on [100, 101]. The diesel and free-piston engines are examples of the latter, and their ideal cycles are the Otto cycle, the Brayton cycle, and so on [102, 103]. It is also known that the maximum efficiency for the ideal external combustion engines is $\eta_{\rm C}$, while that for the ideal internal ones is usually smaller than $\eta_{\rm C}$. For a practical point of view, an engine with $\eta_{\rm C}$ is useless, because its power is zero.

The extension of thermodynamics toward finite-time operations, so-called finite time thermodynamics, has been investigated by many authors [104–129]. Chambadal and Novikov independently proposed, and later Curzon and Ahlborn rediscovered that the efficiency at maximum power (MP) output is given by the Chambadal-Novikov-Curzon-Ahlborn (CNCA) efficiency [104–109]:

$$\eta_{\rm CA} \equiv 1 - \sqrt{\frac{T_{\rm L}}{T_{\rm H}}}. \tag{1.2}$$

Recently it is found that Reitlinger originally proposed $\eta_{\rm CA}$ in 1929 [104, 105]. The validity of the CNCA efficiency near equilibrium has been justified through the linear irreversible thermodynamics [111], molecular kinetics [112, 113] or low-dissipation assumption [114]. It is believed that the CNCA efficiency is, in general, only the efficiency at MP near equilibrium situations. Indeed, there are many situations to exceed the CNCA efficiency in idealized setups [112,114,116]. Although there are several studies for finite time thermodynamics including external and internal combustion engines or fluctuating heat engines [125–129], they are mostly interested in force-controlled engines [112,113,115–118,121–126, 128,129], where a piston or a partitioning potential is controlled by an external agent. On the other hand, the efficiency at MP for an engine without any external force control, which we call a passive engine, has not been well-studied so far.

1.5 The aim of this thesis

The aim of this thesis is to clarify the role of the fluctuating motion of the tracer under non-equilibrium conditions as a rectifier. In this thesis, we study

the motion of the tracer (piston or rotor) attached to no-equilibrium baths in the following three setups: (i) an adiabatic piston under sliding friction, (ii) a rotor in granular gases and (iii) a piston attached to a hard core gas under cyclic heating and cooling operations. The aim of this thesis is to verify the properties of a rectified quantity, such as work, from the observation of the tracer motion.

1.6 The organization of this thesis

This thesis is organized as follows: In Chapter 2, we review studies of finite time thermodynamics including the early history of equilibrium thermodynamics. In Chapter 3, basic relations, techniques, and definitions of stochastic calculus including recent results used in this thesis are summarized, which would be useful to readers. We review basic relations of the energetics on the basis of the Langevin equation, i.e. stochastic energetics and the fluctuating engine in Chapter 4. In Chapter 5, we study the fluctuating motion of an adiabatic piston under the sliding friction, which is located between two equilibrium environments characterized by two different temperatures and densities. The direction of the piston motion is known to be determined from the difference of temperature of two gases. However, if sliding friction exists, we show that the direction of motion depends on the amplitude of the friction, and nonlinearity of the friction if the piston is attached to non-equilibrium environments. We also derive the fluctuation theorem under dry friction. In Chapter 6, the dynamics of a rotor under viscous or dry friction is investigated as a non-equilibrium probe of a granular gas numerically and analytically. To demonstrate a role of the rotor as a probe for a non-equilibrium bath, we perform the molecular dynamics (MD) simulation of the rotor under viscous or dry friction surrounded by a steady granular gas under gravity. In Chapter 7, the efficiency at MP for a passive engine without mechanical controls between two reservoirs is studied. We enclose a hard core gas partitioned by a massive piston in a temperature-controlled container and analyze the efficiency at MP for heating and cooling protocols without controlling the pressure acting on the piston from outside. In Chapter 8, we conclude a thesis with some remarks. In Appendix A, we explain the detailed derivation of the fluctuation relation under dry friction. In Appendix B, we show the benchmark test of the simulation of the granular rotor. In Appendices C and D, we show both the detailed theoretical calculations and the numerical procedure for the rotor under viscous and dry frictions, respectively. In Appendix. E, we review the kinetic theory and the Boltzmann equation. Transport coefficients for granular flow are also summarized in this appendix. In Appendix. F, we discuss the velocity autocorrelation function for the piston. We discuss the definition of work for a passive engine in Appendix. G and the effect of side-wall friction on the efficiency in Appendix H. Throughout this thesis, variables with "$\hat{}$" denote stochastic variables.

Chapter 2

Finite time thermodynamics

Abstract

In this chapter, we review equilibrium thermodynamics and finite time thermodynamics focusing on thermodynamic efficiency. In Sec. 2.1, we briefly summarize historical achievements of equilibrium thermodynamics. In Sec. 2.2, we classify heat engines and explain their ideal theoretical cycles. In Sec. 2.3, we review the progress on the efficiency at MP for heat and chemical engines.

2.1 Equilibrium Thermodynamics

Equilibrium thermodynamics is one of the most established achievements in classical physics. It is well known that many scientists struggled to establish equilibrium thermodynamics. In Sec. 2.1.1, we briefly explain the early history of equilibrium thermodynamics to see the important contribution by Carnot, who brings the viewpoint of *work* into thermodynamics. We call thermodynamics before Carnot's work "thermology" to distinguish them. In Sec. 2.1.2, we explain the Carnot theorem in a sophisticated manner on the basis of the entropy function. In Sec. 2.1.3, the chemical version of the Carnot cycle is explained.

2.1.1 Early History of Equilibrium Thermodynamics

In the late 18th century and the beginning of the 19th century, heat and temperature are thought to be extensive and intensive quantities for *caloric*, respectively. Today, they are well-established concepts: heat is a kind of energy transfer, and temperature can be defined the efficiency of an ideal thermodynamic cycle [14]. Let us briefly summarize the early history of equilibrium thermodynamics, following the historical books written by Yamamoto [14].

The modern view of nature starts from the mathematical positivism and the mechanistic view of nature, where targets are abstracted to be geometrical objects. Although such views of nature are not directly related to the beginning of thermodynamics, Galileo is the first person to quantify the heat phenomena as the volume change of the gas. One of the early significant discoveries in the science of gases would be the existence of atmospheric pressure and vacuum, through experiments for columns of mercury by Torricelli and Pascal, and the demonstration by von Guericke, who invented a vacuum pump [130–132].

The discovery of atmospheric pressure and vacuum had been succeeded to Boyle and Hooke, who examined the first qualitative law for gaseous physics, known as Boyle's law, though Boyle was interested in the "elasticity" of the air. Boyle's law states that the pressure of the gas is inversely proportional to the volume. Hooke, who performed the experiments as an assistant of Boyle, revisited Boyle's law from the viewpoint of the elastic theory for spring. Boyle and Hooke regard gas as a static object, e.g. elastic wool. Then, they regarded its vibration as the heat. Their idea is not succeeded to the kinetic theory by Maxwell and other people in the late 19th century. However, it should be stressed that they came up with the idea that the motion (vibration) can be transformed into heat [133].

The reason why the idea by Boyle and Hooke is not succeeded to the kinetic theory is the strong influence of Newtonian mechanics. Newton showed that the pressure of the gas is inversely proportional to the volume, if repulsive force between gas particles is inversely proportional to their distance [134]. In those days, people believed that the origin of the pressure is not the collision of particles, but the repulsive force between static gas particles.

The origin of thermology is the proposal of *materia ignis*, which is the inert substance playing a role of all of the thermal phenomena, by Boerhaave [135]. He assumed the existence of *materia ignis*. Franklin considered the conservation and its equilibrium of *materia ignis*, as a principle, through the analogy between electric and thermal phenomena. In 1774, de Lavoisier, who is known to be a giant of chemistry, proposed *caloric*, which is the similar concept of *materia ignis*. Then, the *caloric theory* had been popular in the late 18th century.

Besides the prosperity of thermology, Black indicated the difference between temperature and heat introducing the concept of heat capacity [136]. Black revisited the idea of equilibrium, not as the principle, but as the experimental and empirical fact: the fact that two systems are in thermal equilibrium is recognized by the observation of a thermometer. Emphasizing the important role of a thermometer, he distinguished temperature from heat. Although Black distinguished them, he avoided answering the question: *what is heat?* Because the concept of heat capacity is consistent with the idea that the heat is a matter (a calorific matter or a matter of heat), the heat had been thought as a static matter yet.

de Lavoisier tried to formulate thermology more concretely. He and Laplace formulated thermology at the level of mathematical physics. For example, they introduced the conservation law for the caloric, which is in contrast to the first law of thermodynamics [137]. Although Rumford, who is known as Sir Ben-

jamin Thompson, experimentally showed that frictional heat is inexhaustible in 1798, where the heat produced by boring a cannon could boil water, his experimental facts without any new theoretical support seemed to be too weak to deny thermology [138].

Carnot is the first person to bring the viewpoint of work into thermology, which gives the birth to the Carnot theorem and its corollaries [100]. It is surprising that the work by Carnot was almost ignored by the community in those days. Although Carnot presented his theory in 1824 and Clapeyron reformulated the work by Carnot in 1834, almost nobody mentioned his papers until 1844. In 1848, at last, Thomson, who is known as Lord Kelvin, found and spread papers by Carnot. Carnot proved that the maximum work obtained between two heat sources corresponds to the material-independent function called the Carnot function, which is now called the Carnot efficiency. Clapeyron and Thomson tried to identify the Carnot function experimentally, though their accuracy were not sufficient. Right after the discovery of papers by Carnot, the first law of thermodynamics was established by Mayer, Joule, Clausius, Clapeyron, Thomson.

2.1.2 Heat Engine

Here, let us introduce the modern proof of Carnot's theorem [139]. We consider a heat cycle which is connected with a hot and a cold system. Let $S_\nu = S_\nu(U_\nu)$ be the entropy for the engine $S_{\rm E}$, the hot system (H) $S_{\rm H}$, the cold system (L) $S_{\rm L}$, external system $S_{\rm ex}$, and $U_\nu(\nu = {\rm E}, {\rm H}, {\rm L}, \text{ and ex})$ is the internal energy of each system. $S_\nu = S_\nu(U_\nu)$ is assumed to be a concave function of U_ν. We assume that the external system is thermally insulated from H or L. Note that H and L are not necessary reservoirs, and, therefore their internal energy can change. During the cycle, the engine converts the energy gain $Q_{\rm H}$ from H to the work W toward the external system and $Q_{\rm L}$ flows into L. After the cycle, the internal energy for hot and cold reservoirs, respectively, changes as $U_{\rm H} \to U_{\rm H} - Q_{\rm H}$ and $U_{\rm L} \to U_{\rm L} + (Q_{\rm H} - W)$. Because the total entropy increases after the cycle, we obtain the following inequality:

$$\begin{aligned} &S_{\rm E} + S_{\rm H}(U_{\rm H} - Q_{\rm H}) + S_{\rm L}(U_{\rm L} + Q_{\rm H} - W) + S_{\rm ex} + \Delta S_{\rm ex} \\ &\geq S_{\rm E} + S_{\rm H}(U_{\rm H}) + S_{\rm L}(U_{\rm L}) + S_{\rm ex}, \end{aligned} \tag{2.1}$$

where $S_{\rm ex}$ represents the entropy change of the external system. It should be noted that $S_{\rm E}$ does not change after the cycle because the engine is assumed to come back to the initial state. Equation (2.1) can be rewritten as

$$\{S_{\rm H}(U_{\rm H} - Q_{\rm H}) - S_{\rm H}(U_{\rm H})\} + \{S_{\rm L}(U_{\rm L} + Q_{\rm H} - W) - S_{\rm L}(U_{\rm L})\} + \Delta S_{\rm ex} \geq 0. \tag{2.2}$$

Recalling the following inequality for an arbitrary concave function $f(x)$:

$$(x - x_0) f'(x_0 \pm 0) \geq f(x) - f(x_0), \tag{2.3}$$

Eq. (2.2) is reduced to

$$\frac{-Q_{\rm H}}{T_{\rm H}(U_{\rm H})} + \frac{Q_{\rm H} - W}{T_{\rm L}(U_{\rm L})} + \Delta S_{\rm ex} \geq 0. \tag{2.4}$$

$T_\nu(U_\nu) \equiv (\partial S_\nu/\partial U_\nu)^{-1}$ has the meaning of temperatures follows. Because temperature is a monotonic function of the internal energy, $T_{\rm H}(U_{\rm H}) \geq T_{\rm H}(U_{\rm H} - Q_{\rm H})$ and $T_{\rm L}(U_{\rm L}) \leq T_{\rm L}(U_{\rm L} + Q_{\rm H} - W)$ hold. $T_{\rm H}(U_{\rm H})$ and $T_{\rm L}(U_{\rm L})$, respectively, means the hottest and coldest temperatures for H and L during their contact to the system. If H and L are reservoirs, i.e. their changes of the internal energy are negligible, $U_{\rm H} - Q_{\rm H} \simeq U_{\rm H}$ and $U_{\rm L} \simeq U_{\rm L} + Q_{\rm H} - W$. We write $T_{\rm H} = T_{\rm H}(U_{\rm H})$ and $T_{\rm L} = T_{\rm L}(U_{\rm L})$ as abbreviation. Using Eq. (2.4), we obtain the inequality for the efficiency $\eta_{Q\to W} \equiv W/Q_{\rm H}$:

$$\eta_{Q\to W} \leq 1 - \frac{T_{\rm L}}{T_{\rm H}} + \frac{T_{\rm L}\Delta S_{\rm ex}}{Q_{\rm H}}. \tag{2.5}$$

Note that $\Delta S_{\rm ex} \geq 0$ and $\Delta S_{\rm ex} = 0$ for a reversible work source. If $\eta_{Q\to W}$ is realized for one system, the external work source can be replaced by the reversible one with the identical efficiency $\eta_{Q\to W}$. Therefore we can choose $\Delta S_{\rm ex} = 0$ in Eq. (2.5), and the inequality becomes more strict. Thus, Carnot's theorem is proved:

$$\eta_{Q\to W} \leq 1 - \frac{T_{\rm L}}{T_{\rm H}}. \tag{2.6}$$

Here, the equality is realized for a quasi-static operation, if H and L are reservoirs and the temperature of the engine and that of the reservoir are the same when they are attached.

2.1.3 Multi-component Chemical Engine

One can consider a chemical engine, where the work is extracted from particle reservoirs. For example, living systems use adenosine triphosphate hydrolysis as one of energy sources. Let us introduce the following general chemical reaction [140] at temperature T as

$$\sum_{i=1}^{n} \nu_i M_i \rightleftharpoons 0, \tag{2.7}$$

where ν_i and M_i represent the stoichiometric coefficient and the symbol for i th component, respectively. Note that $\nu_i > 0$ is a product and $\nu_i < 0$ is a reactant of the reaction. There are $n = n_r + n_p$ kinds of chemical substances, where n_p products are produced from n_r reactants. We consider an isothermal engine consisting of n uptake or release processes and n expansion or compression processes as discussed in Ref. [140]. The schematic figure is shown in Fig. 2.1. The volume of the solution in the container $V_{\rm cont}$ is perfectly controlled by the external agent through the pressure control from the outside. The container can uptake or release the ith substance to the ith particle reservoir of the chemical potential μ_i^0 through a semipermeable membrane. This configuration is similar to the Van't Hoff reaction box [141]. The change of the number of ith component dN_i is caused by the change due to the chemical reaction $dN_i^{\rm in}$ and the exchange from the reservoir $dN_i^{\rm ex}$:

$$dN_i \quad = \quad dN_i^{\rm in} + dN_i^{\rm ex}. \tag{2.8}$$

In chemical thermodynamics, $dN_i^{\rm in}$ is expressed in terms of the extent of reaction ξ:

$$dN_i^{\rm in} = \nu_i d\xi. \tag{2.9}$$

Let $\mu_i < 0$ and $\mu_i^0 < 0$ be the chemical potential for i th component in the container and that for the particle reservoir, respectively. It is convenient to introduce the chemical affinity:

$$A^0 \equiv -\sum_i \nu_i \mu_i^0, \tag{2.10}$$

which represents how far from the chemical equilibrium the reaction is, or equivalently, the sum of the Gibbs free energy per a unit mol. We assume that the affinity is positive $A^0 > 0$, which means that the reaction proceeds in the direction that the amount of products increases.

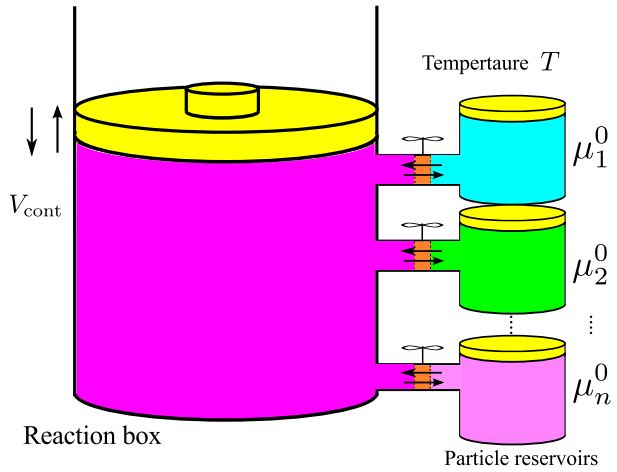

Figure 2.1: The schematic figure of the chemical engine [140]. The container can uptake or release the ith substance to the ith particle reservoir of the chemical potential μ_i^0 through a semipermeable membrane. This configuration is similar to the Van't Hoff reaction box [141].

The protocol for the engine is the following $2n$ steps: Initially, we assume $\mu_1 = \mu_1^0$. (1): By changing $V_{\rm cont}$, the container absorbs (releases) 1st component. (2): The volume of the solution $V_{\rm cont}$ is changed to satisfy the relation $\mu_2 = \mu_2^0$. (3): $\cdots$. $(2i-1)$: By changing $V_{\rm cont}$, the container absorbs (releases) i th component. $(2i)$: The volume of the solution $V_{\rm cont}$ is changed to satisfy the relation $\mu_{i+1} = \mu_{i+1}^0$. $(2i+1)$: $\cdots$. $(2n)$: The volume of the solution $V_{\rm cont}$ is changed to satisfy the relation $\mu_1 = \mu_1^0$. For isothermal chemical engine, the

efficiency $\eta_{\rm chem}$ is defined as

$$\eta_{\rm chem} \equiv \frac{W_{\rm chem}}{G_+}, \tag{2.11}$$

$$W_{\rm chem} \equiv \sum_{i=1}^{n} \mu_i^0 \int_{2i-1}^{2i} dN_i^{\rm ex}, \tag{2.12}$$

$$G_+ \equiv \sum_{\nu_i>0} \mu_i^0 \int_{2i-1}^{2i} dN_i^{\rm ex}. \tag{2.13}$$

Using the relation $\oint dN_i = 0$ and Eqs. (2.8)-(2.10), we obtain the following expressions:

$$W_{\rm chem} = -\sum_i \nu \mu_i^0 \oint d\xi, \tag{2.14}$$

$$G_+ = -\sum_{\nu_i>0} \nu \mu_i^0 \oint d\xi. \tag{2.15}$$

Introducing the chemical affinities for products and reactants,

$$A_+^0 \equiv -\sum_{\nu_i>0} \nu \mu_i^0, \tag{2.16}$$

$$A_-^0 \equiv \sum_{\nu_i<0} \nu \mu_i^0, \tag{2.17}$$

the efficiency for the equilibrium chemical engine is expressed as the ratio of chemical affinities for products and reactants:

$$\eta_{\rm chem} = \frac{A_+^0 - A_-^0}{A_+^0} = 1 - \frac{A_-^0}{A_+^0} \equiv \eta_{\rm CC}, \tag{2.18}$$

which we can called the chemical Carnot efficiency. We comment on the special case with $n_r = 0, n_p = 1, \nu_1 > 0$, where any reactions do not exist [142]. In this case, because all molecules absorbed in the container are removed in the quasi-static limit, the efficiency is apparently $\eta_{\rm chem} = 1$.

2.2 Classification of engines and ideal theoretical cycles

In this section, we classify heat engines and explain their ideal theoretical cycles. Heat engines are categorized into two types, external (Sec. 2.2.1) and internal combustion engines (Sec. 2.2.2), in which the heat sources are prepared outside and inside the engine, respectively. Although real engines are influenced by friction or wear, idealized engines consisting of ideal gases and frictionless piston are analyzed for the estimation of the maximum efficiency.

2.2.1 External combustion engine

External combustion engines are the engines, where the working fluids inside the container are heated or cooled by external heat sources. The merit of external combustion engines is the broad utility. We can use any materials as heat sources for an external combustion engine, while this is not true for internal combustion engines. The demerit of the external combustion engine is the limitation of the size. We cannot gain sufficient work from small external combustion engines. Right after the industrial revolution, external combustion engines became popular because of its broad utility. At present, external combustion engines can be found as thermal or nuclear power plants. For example, steam engines are external combustion engines, because working fluid heated by an external heat source rotates the turbine. The Carnot cycle and the Stirling cycle are examples of ideal theoretical cycles. Note that the maximum efficiencies for both the Carnot and Stirling cycle are identical to η_C.

2.2.2 Internal combustion engine

Internal combustion engines are the engines, whose works are extracted by the explosion or reaction of working fluids [103]. The name of internal combustion engine comes from the fact that the source of work is inside the engine. We usually pour the mixture of air and reactant into the container and collect their products. To keep the inside of the container clean, we cannot choose arbitrary substances in contrast to external combustion engines. However, internal combustion engines can work well, even if the size is small. Therefore, internal combustion engines can be found in many places, e.g. the engine of motorcycles. To discuss the efficiency of internal combustion engine, hydrodynamics or thermal conduction of reactants and explosion processes of reactants are important. However, we usually replace explosion processes by heating or cooling processes to consider the efficiency for ideal theoretical cycles. The Otto cycle and the Brayton cycle are typical examples. Note that the maximum efficiency for an internal combustion engine is usually smaller than η_C.

2.3 Efficiency at Maximum Power Output

We have discussed the maximum efficiency of the engine up to the previous section. Although the maximum efficiency derived in equilibrium thermodynamics is general, the thermodynamic bound itself is practically useless when we discuss an actual engine. Indeed, the power of the quasi-static cycle, i.e. the work per a unit time is zero, while the actual engine has the finite power. From the practical point of view, we are interested in the efficiency at MP. The energetics considering a finite-time cycle is now called finite time thermodynamics. In this section, we review the recent progress on the finite time thermodynamics. In the following, we discuss the efficiency for the engine, when the power is maximized. In Sec. 2.3.1, we introduce the derivation of the CANA efficiency by Curzon and Ahlborn in Ref. [109]. In Sec. 2.3.2, we derive the CNCA efficiency on the basis

of the linearly irreversible thermodynamics [111]. In Sec. 2.3.3 and 2.3.4, we discuss the efficiency at MP under nonlinear non-equilibrium situations on the basis of the low-dissipation assumptions and the extended Onsager relations, respectively. In Sec. 2.3.5, we derive the efficiency at MP for chemical engines on the basis of the low-dissipation assumption.

2.3.1 Derivation by Curzon and Ahlborn

The most famous formula known as the efficiency at MP is the CNCA efficiency:

$$\eta_{\rm CA} = 1 - \sqrt{\frac{T_{\rm L}}{T_{\rm H}}}. \tag{2.19}$$

For the simplicity of the derivation by Curzon and Ahlborn [109] in 1975, $\eta_{\rm CA}$ is sometimes called the CA efficiency, while Eq. (2.19) has already been derived by Reitlinger in 1929 [104, 105].

Let us derive Eq. (2.19) following the argument by Curzon and Ahlborn [109]. Let $T_{\rm H}^{(w)}$ and $T_{\rm L}^{(w)}$ be, respectively, the temperatures of the working fluids when hot $T_{\rm H}$ and cold $T_{\rm L}$ reservoirs are attached. We assume that the heat fluxes through the vessel containing the working fluid are proportional to the temperature difference, i.e. the heat fluxes from $T_{\rm H}$ and T_L are, respectively, assumed to be $\alpha_{\rm H}(T_{\rm H} - T_{\rm H}^{(w)})$ and $\alpha_{\rm L}(T_{\rm L}^{(w)} - T_{\rm L})$. Here, $\alpha_{\rm H}$ and $\alpha_{\rm L}$ are constants which depend on thermal conductivity of working fluid. In the isothermal expansion and compression processes, the input energy $W_{\rm H}$ and the discarded energy $W_{\rm L}$ can be written as

$$W_{\rm H} = \alpha_{\rm H} t_{\rm H}(T_{\rm H} - T_{\rm H}^{(w)}), \tag{2.20}$$

$$W_{\rm L} = \alpha_{\rm L} t_{\rm L}(T_{\rm L}^{(w)} - T_{\rm L}), \tag{2.21}$$

where $t_{\rm H}$ and $t_{\rm L}$ are the operation times for heating and cooling processes, respectively. During the adiabatic processes, we assume that there is no heat exchange with the surroundings. Requiring that adiabatic processes are reversible, we obtain the condition

$$\frac{W_{\rm H}}{T_{\rm H}^{(w)}} = \frac{W_{\rm L}}{T_{\rm L}^{(w)}},$$

i.e.

$$\frac{t_{\rm H}}{t_{\rm L}} = \frac{\alpha_{\rm L} T_{\rm H}^{(w)}(T_{\rm L}^{(w)} - T_{\rm L})}{\alpha_{\rm H} T_{\rm L}^{(w)}(T_{\rm H} - T_{\rm H}^{(w)})}, \tag{2.22}$$

where $t_{\rm H}$ and $t_{\rm L}$ are not independent. Assuming that the adiabatic processes spend the same time to the isothermal ones [1], the power P of the engine is given

[1] In the original paper [109], the adiabatic processes are assumed to take $(\gamma_{\rm ad} - 1)(t_{\rm H} + t_{\rm L})$, where $\gamma_{\rm ad}$ is a constant. However, the assumption does not change the maximum power condition.

by

$$P = \frac{W_{\rm H} - W_{\rm L}}{2(t_{\rm H} + t_{\rm L})}. \tag{2.23}$$

Using the relation (2.22), we eliminate $t_{\rm H}/t_{\rm L}$ from Eq. (2.23):

$$P = \frac{\alpha_{\rm L}\alpha_{\rm H}}{2} \frac{x_{\rm H}x_{\rm L}(T_{\rm H} - T_{\rm L} - x_{\rm H} - y_{\rm L})}{\alpha_{\rm L}T_{\rm H}x_{\rm L} + \alpha_{\rm H}T_{\rm L}x_{\rm H} + x_{\rm H}x_{\rm L}(\alpha_{\rm H} - \alpha_{\rm L})} \tag{2.24}$$

$$x_{\rm H} \equiv T_{\rm H} - T_{\rm H}^{(w)} \tag{2.25}$$

$$x_{\rm L} \equiv T_{\rm L}^{(w)} - T_{\rm L}. \tag{2.26}$$

The maximum power conditions $\partial P/\partial x = 0$ and $\partial P/\partial y = 0$ are written as

$$\frac{x_{\rm H}}{T_{\rm H}} = \frac{1 - \sqrt{T_{\rm L}/T_{\rm H}}}{1 + \sqrt{\alpha_{\rm H}/\alpha_{\rm L}}}, \tag{2.27}$$

$$\frac{x_{\rm L}}{T_{\rm L}} = \frac{\sqrt{T_{\rm H}/T_{\rm L}} - 1}{1 + \sqrt{\alpha_{\rm L}/\alpha_{\rm H}}}. \tag{2.28}$$

Thus, we obtain the expression for the efficiency at maximum power output:

$$\begin{aligned} \eta &= \frac{W_{\rm H} - W_{\rm L}}{W_{\rm H}} = 1 - \frac{T_{\rm L}^{(w)}}{T_{\rm H}^{(w)}} = 1 - \frac{T_{\rm L} + y}{T_{\rm H} - x} \\ &= 1 - \sqrt{\frac{T_{\rm L}}{T_{\rm H}}} = \eta_{\rm CA}, \end{aligned} \tag{2.29}$$

which is independent of $\alpha_{\rm H}$ and $\alpha_{\rm L}$.

2.3.2 Derivation from linearly irreversible thermodynamics

Although derivation by Curzon and Ahlborn is simple, their derivation contains some strong assumption. Moreover, the applicability of their derivation for a cycle consisting of isothermal and adiabatic processes is not clear. Van den Broeck has proved that the CNCA efficiency is the universal one at MP, at least, for systems near equilibrium by using the linearly irreversible thermodynamics [111].

We consider an engine working between two temperature reservoirs, where the temperature difference is sufficiently small so that linearly irreversible thermodynamics can be used. The engine performs work $W_l = -F_{\rm ex}x_l$ toward the external force $F_{\rm ex}$ with a conjugate thermodynamic variable x_l (e.g. the position of the piston or the volume of the working fluid). The corresponding thermodynamic force is $\mathcal{X}_1 = F_{\rm ex}/T$, where T denotes the temperature of the system. The thermodynamic flux is $\mathcal{J}_1 = \dot{x}_l = dx_l/dt$. The power of the engine is described as

$$P = \dot{W}_l = -F_{\rm ex}\dot{x}_l = -\mathcal{J}_1\mathcal{X}_1 T. \tag{2.30}$$

The engine gains the energy from the hot reservoir, which is the corresponding thermodynamic flux $\mathcal{J}_2 = \dot{Q}_{\rm H}$. The corresponding thermodynamic force is the temperature difference $\mathcal{X}_2 = 1/T_{\rm L} - 1/T_{\rm H} \simeq \Delta T/T^2$, where $\Delta T = T_{\rm H} - T_{\rm L}$ and $T \equiv T_{\rm H}$. Then the Carnot efficiency is $\eta_C = \Delta T/T$.

Linearly irreversible thermodynamics stems from the fact that the fluxes $\mathcal{J}_i$ are linear combination of thermodynamic variables $\mathcal{X}_i$ [149]:

$$\mathcal{J}_1 = L_{11}\mathcal{X}_1 + L_{12}\mathcal{X}_2, \tag{2.31}$$

$$\mathcal{J}_2 = L_{21}\mathcal{X}_1 + L_{22}\mathcal{X}_2, \tag{2.32}$$

where the Onsager coefficients $L_{ij}(i,j=1,2)$ satisfy the relation

$$L_{11} \geq 0,\ L_{22} \geq 0,\ L_{11}L_{22} - L_{12}L_{21} \geq 0, \tag{2.33}$$

and the microscopic irreversibility leads to the reciprocal relation

$$L_{12} = L_{21}. \tag{2.34}$$

Let us introduce the coupling strength q as

$$q \equiv \frac{L_{12}}{\sqrt{L_{11}L_{22}}}, \tag{2.35}$$

with $-1 \leq q \leq 1$.

Assuming that the control parameter for the power of the engine is only $\mathcal{X}_1$, we can write the maximum power condition:

$$\frac{\partial}{\partial \mathcal{X}_1} P = -\frac{1}{T}\frac{\partial}{\partial \mathcal{X}_1}(L_{11}\mathcal{X}_1^2 + L_{12}\mathcal{X}_1\mathcal{X}_2) = 0. \tag{2.36}$$

Thus, $\mathcal{X}_1$ for MP is given by

$$\mathcal{X}_1^{\rm MP} = -\frac{1}{2}\frac{L_{12}\mathcal{X}_2}{L_{11}}. \tag{2.37}$$

The obtained efficiency at MP is described as

$$\begin{aligned} \eta &= \frac{\dot{W}}{\dot{Q}_{\rm H}} = -\frac{\Delta T}{T}\frac{\mathcal{J}_1\mathcal{X}_1}{\mathcal{J}_2\mathcal{X}_2} \\ &= \frac{1}{2}\frac{\Delta T}{T}\frac{q^2}{2-q^2} \end{aligned} \tag{2.38}$$

Taking the tight coupling limit $|q| \to 1$, where the fluxes and forces are tightly coupled, the efficiency corresponds to $\eta_{\rm CA} \simeq \Delta T/2T$, which is the half of the maximum efficiency η_C in $\Delta T/T \ll 1$ limit and is identical to the CNCA efficiency in this limit.

So far, we have considered a finite power engine in the linear non-equilibrium regime. In the following two subsections, to go beyond the linear regime, we introduce two methods for finite power engines in the nonlinear non-equilibrium regime. It should be noted that although two methods result in the same results, the obtained efficiency does not always correctly predicts the efficiency for real engines.

2.3.3 Asymptotic derivation of the Chambadal-Novikov-Curzon-Ahlborn efficiency

Instead of assuming linear non-equilibrium relations (2.31) and (2.32), we start from the following low-dissipation assumptions:

$$Q_{\rm H} = T_{\rm H}\left(\Delta S - \frac{\Sigma_{\rm H}}{t_{\rm H}} + O\left(t_{\rm H}^{-2}\right)\right), \tag{2.39}$$

$$Q_{\rm L} = T_{\rm L}\left(-\Delta S - \frac{\Sigma_{\rm L}}{t_{\rm L}} + O\left(t_{\rm L}^{-2}\right)\right), \tag{2.40}$$

where ΔS represents the entropy change in the long time limit $t_{\rm H}, t_{\rm L} \to \infty$. $\Sigma_{\rm H}$ and $\Sigma_{\rm L}$ represent the amounts of dissipation induced by the heat currents from hot and cold reservoirs, respectively [114]. It is easy to recover the Carnot efficiency in $t_{\rm H}, t_{\rm L} \to \infty$ limit as $\eta = (Q_{\rm H} + Q_{\rm L})/Q_{\rm H} = 1 - T_{\rm L}/T_{\rm H} = \eta_C$ from the relations (2.39) and (2.40). When the power

$$P \equiv \frac{Q_{\rm H}(t_{\rm H}) + Q_{\rm L}(t_{\rm L})}{t_{\rm H} + t_{\rm L}} \tag{2.41}$$

is maximized, we obtain the conditions for $t_{\rm H}$ and $t_{\rm L}$ by solving equations $\partial P/\partial t_{\rm H} = 0$ and $\partial P/\partial t_{\rm L} = 0$. Their physical reasonable solutions are

$$t_{\rm H} = \frac{2}{(T_{\rm H} - T_{\rm L})\Delta S}\sqrt{\Sigma_{\rm H} T_{\rm H}}\left(\sqrt{\Sigma_{\rm H} T_{\rm H}} + \sqrt{\Sigma_{\rm L} T_{\rm L}}\right), \tag{2.42}$$

$$t_{\rm L} = \frac{2}{(T_{\rm H} - T_{\rm L})\Delta S}\sqrt{\Sigma_{\rm L} T_{\rm L}}\left(\sqrt{\Sigma_{\rm H} T_{\rm H}} + \sqrt{\Sigma_{\rm L} T_{\rm L}}\right). \tag{2.43}$$

Thus, we obtain the efficiency at MP under the low-dissipation assumption: $\eta_{\rm LD} = \eta_{\rm LD}\left(T_{\rm L}/T_{\rm H}, \Sigma_{\rm L}/\Sigma_{\rm H}\right)$

$$\eta_{\rm LD}\left(\frac{T_{\rm L}}{T_{\rm H}}, \frac{\Sigma_{\rm L}}{\Sigma_{\rm H}}\right) = \frac{\eta_C\left(1 + \sqrt{\frac{\Sigma_{\rm L} T_{\rm L}}{\Sigma_{\rm H} T_{\rm H}}}\right)}{\left(1 + \sqrt{\frac{\Sigma_{\rm L} T_{\rm L}}{\Sigma_{\rm H} T_{\rm H}}}\right)^2 + \frac{T_{\rm L}}{T_{\rm H}}\left(1 - \frac{\Sigma_{\rm L}}{\Sigma_{\rm H}}\right)}. \tag{2.44}$$

It should be noted that Eq. (2.44) recovers the CNCA efficiency in the symmetric dissipation limit $\Sigma_{\rm H} = \Sigma_{\rm L}$:

$$\lim_{\Sigma_{\rm L}/\Sigma_{\rm H} \to 1} \eta_{\rm LD}\left(\frac{T_{\rm L}}{T_{\rm H}}, \frac{\Sigma_{\rm L}}{\Sigma_{\rm H}}\right) = 1 - \sqrt{\frac{T_{\rm L}}{T_{\rm H}}} = \eta_{\rm CA}. \tag{2.45}$$

On the other hand, by taking the asymmetric limit $\Sigma_{\rm L}/\Sigma_{\rm H} \to 0, +\infty$, we obtain

$$\lim_{\Sigma_{\rm L}/\Sigma_{\rm H} \to 0} \eta_{\rm LD}\left(\frac{T_{\rm L}}{T_{\rm H}}, \frac{\Sigma_{\rm L}}{\Sigma_{\rm H}}\right) = \frac{\eta_C}{2 - \eta_C} \equiv \eta_+, \tag{2.46}$$

$$\lim_{\Sigma_{\rm L}/\Sigma_{\rm H} \to \infty} \eta_{\rm LD}\left(\frac{T_{\rm L}}{T_{\rm H}}, \frac{\Sigma_{\rm L}}{\Sigma_{\rm H}}\right) = \frac{\eta_C}{2} \equiv \eta_-. \tag{2.47}$$

We can show the relation

$$\eta_- \leq \eta_{\rm LD} \leq \eta_+. \tag{2.48}$$

Expanding Eq. (2.44), in terms of η_C, we obtain

$$\eta_{\rm LD} = \frac{\eta_C}{2} + \frac{\eta_C^2}{4 + 4\sqrt{\Sigma_{\rm L}/\Sigma_{\rm H}}} + O(\eta_C^3). \tag{2.49}$$

Thus, the analysis on the basis of the assumptions (2.39) and (2.40) recovers the CNCA efficiency in the limit $\eta_C \to 0$. It is interesting that the inequality (2.48) is consistent with the efficiency of actual power plants as is shown in Fig. 2.2 [114].

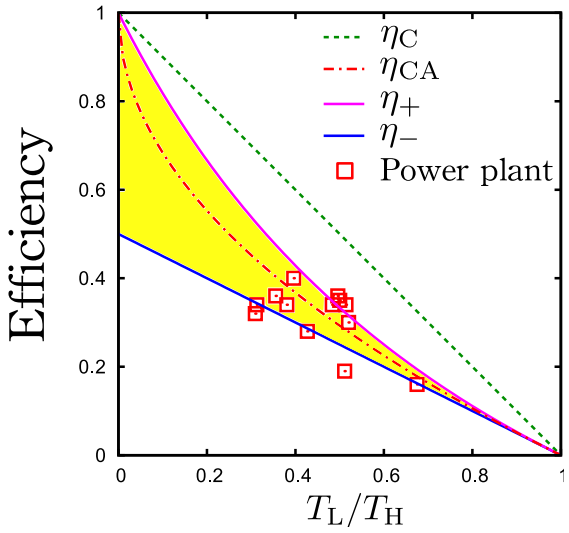

Figure 2.2: The comparison between results in Sec. 2.3.3 and efficiencies for the actual power plants. Although the assumptions (2.39) and (2.40) are strong, Eq. (2.48) works well even for actual engines. The data points are obtained from Ref. [114].

2.3.4 Minimally nonlinear irreversible heat engines

In the previous subsection, we start from phenomenological assumptions and obtain the reasonable expression for the efficiency at MP. In this subsection, we introduce the engine called "the minimally nonlinear irreversible heat engine" [115] by extending the Onsager relation as

$$\mathcal{J}_1 = L_{11}\mathcal{X}_1 + L_{12}\mathcal{X}_2, \tag{2.50}$$

$$\mathcal{J}_2 = L_{21}\mathcal{X}_1 + L_{22}\mathcal{X}_2 - \bar{\gamma}_{\rm H}\mathcal{J}_1^2. \tag{2.51}$$

The last nonlinear term with the constant $\bar{\gamma}_{\rm H} > 0$ in Eq. (2.51) is introduced in addition to the conventional linear relations (2.31) and (2.32). Here, we consider the heat flux from the cold reservoir $\mathcal{J}_3$ as

$$\mathcal{J}_3 \equiv \dot{Q}_{\rm L} = \dot{W} - \dot{Q}_{\rm H} = -\mathcal{J}_1 \mathcal{X}_1 T_{\rm L} - \mathcal{J}_2. \tag{2.52}$$

We rewrite the relations (2.50) and (2.51) in terms of $\mathcal{J}_2$ and $\mathcal{J}_3$ as

$$\mathcal{J}_2 = \frac{L_{21}}{L_{11}}\mathcal{J}_1 + L_{22}(1-q^2)\mathcal{X}_2 - \bar{\gamma}_{\rm H}\mathcal{J}_1^2, \tag{2.53}$$

$$\mathcal{J}_3 = -\frac{L_{21}T_{\rm L}}{L_{11}T_{\rm H}}\mathcal{J}_1 - L_{22}(1-q^2)\mathcal{X}_2 - \bar{\gamma}_{\rm L}\mathcal{J}_1^2, \tag{2.54}$$

where a new positive constant is introduced $\bar{\gamma}_{\rm L} \equiv (T_{\rm L}/L_{11}) - \bar{\gamma}_{\rm H} > 0$. When we use equations (2.53) and (2.54), instead of Eqs. (2.50) and (2.51), J_1 is the control parameter.

The power and efficiency for the minimally nonlinear irreversible heat engine is $P = -\mathcal{J}_1\mathcal{X}_1 T_{\rm L} = \mathcal{J}_2 + \mathcal{J}_3$ and $\eta = W/Q_{\rm H} = P/\mathcal{J}_2$, respectively. Considering the maximum power condition $\partial P/\partial \mathcal{J}_1 = 0$, the efficiency at maximum power output can be obtained as

$$\eta = \frac{\eta_C}{2}\frac{q^2}{2 - q^2(1 + \eta_C/\{2(1+\bar{\gamma}_{\rm L}/\bar{\gamma}_{\rm H})\})}. \tag{2.55}$$

It should be noted that the obtained efficiency is bounded as

$$\eta_-^q \le \eta \le \eta_+^q, \tag{2.56}$$

where we have introduced

$$\eta_-^q \equiv \frac{\eta_C}{2}\frac{q^2}{2-q^2}, \tag{2.57}$$

$$\eta_+^q \equiv \frac{\eta_C}{2}\frac{q^2}{2 - q^2(1+\eta_C/2)}. \tag{2.58}$$

By taking the asymmetric dissipation limit $\bar{\gamma}_{\rm L}/\bar{\gamma}_{\rm H} \to +\infty$ and $\bar{\gamma}_{\rm L}/\bar{\gamma}_{\rm H} \to 0$, Eqs. (2.57) and (2.58) are derived, respectively. It is interesting that the tight coupling limit $|q| \to 1$ reduces the previous results as $\eta_-^q \to \eta_-$ and $\eta_+^q \to \eta_+$.

2.3.5 Efficiency at maximum power output for multi-component chemical engine

Although the low-dissipation assumptions for heat engines (2.39) and (2.40) in Sec. 2.3.3 are simple, their results are consistent with the efficiency for actual power plants. Let us adopt the low-dissipation assumptions to the chemical engine in Sec. 2.1.3. In this subsection, we extend the result of a single-component chemical engine in Ref. [142] toward a multi-component chemical engine. Here

we assume that the chemical solution is well stirred to avoid the phase separation, where the system can be described by the kinetic equations without spatial inhomogeneity. To treat the phase separation effect, we need to take into account the Doi-Peliti formalism [143–148] for finite-time thermodynamics.

Once the operation is performed in the finite-time $\{t_i\}_{i=1}^n$, $\eta_{\rm chem}$ cannot reach $\eta_{\rm CC}$, because $\mu_i \neq \mu_i^0$ for the $(2i-1)$th step and the container cannot absorb or release ideal molar number for the $i+1$th molecule in the $(2i)$th step [142]. On the basis of the low-dissipation assumption, the chemical energy collected or produced through the cycle are expressed as

$$W_{\rm chem}(\{t_i\}_{i=1}^n) = (A_+^0 - A_-^0)\oint d\xi - \sum_i a_i^c \frac{\tau_i}{t_i}\oint d\xi + O\left(\frac{\tau_i^2}{t_i^2}\right), \quad (2.59)$$

$$G_+(\{t_i\}_{i=1}^n) = A_+^0 \oint d\xi - \sum_{\nu_i>0} a_i^c \frac{\tau_i}{t_i}\oint d\xi + O\left(\frac{\tau_i^2}{t_i^2}\right), \quad (2.60)$$

where $a_i^c > 0$ and τ_i are the loss of the chemical energy due to the finite-time-operation and the relaxation time for the change of the ith molecule number, respectively. The power P_w of the chemical engine can be defined as

$$P_w \equiv \frac{W_{\rm chem}(\{t_i\}_{i=1}^n)}{\sum_i t_i}. \quad (2.61)$$

$\{t_i\}_{i=1}^n$ at MP is derived from $\partial P_w/\partial t_i = 0$ $(i = 1, 2, \cdots, n)$:

$$t_i^{\rm MP} = \frac{2\sqrt{a_i^c\tau_i}}{A_+^0 - A_-^0}\left(\sum_{j=1}^n \sqrt{a_j^c\tau_j}\right). \quad (2.62)$$

Thus, the efficiency at maximum power output can be derived as

$$\eta_{\rm chem}(\{t_i^{\rm MP}\}_{i=1}^n) = \frac{\eta_{\rm CC}}{2}\left(1 - \frac{\eta_{\rm CC}}{2}\frac{\sum_{\nu_i>0}\sqrt{a_i^c\tau_i}}{\sum_i \sqrt{a_i^c\tau_i}}\right)^{-1}. \quad (2.63)$$

If the dissipation is symmetric: $a_1^c\tau_1 = a_2^c\tau_2 = \cdots = a_n^c\tau_n$, Eq. (2.63) becomes simpler:

$$\eta_{\rm chem}(\{t_i^{\rm MP}\}_{i=1}^n) = \frac{\eta_{\rm CC}}{2}\left(1 - \frac{\eta_{\rm CC}}{2}\frac{n_p}{n}\right)^{-1} \quad (2.64)$$

We note that the efficiency at MP is given by the half of the maximum efficiency $\eta_{\rm chem}(\{t_i^{\rm MP}\}_{i=1}^n) \simeq \eta_{\rm CC}/2$ in the linear non-equilibrium limit $\eta_{\rm CC} \to 0$.

Chapter 3

A Short Course of stochastic analysis

Abstract

In this chapter, we briefly summarize the formulas of stochastic analysis used in this thesis. We only consider white processes, where the noise is delta-correlated. In Sec. 3.1 we introduce stochastic integrals and derive formulas for the master equation of the given stochastic differential equation (SDE), in Sec. 3.2. In Sec. 3.3, we apply the derived formulas to physical systems. We discuss the system size expansion method proposed by van Kampen [7] and its extension to non-Gaussian processes [92, 93] in Sec. 3.4.

3.1 Stochastic integrals

For stochastic quantities, it is well-known that the integral depends on the method of the discretization. The familiar methods of the division are called the Itô type and the Stratonovich type, which are, respectively, represented as $\cdot$ and $\circ$. In this section, we introduce the corresponding stochastic integrals.

For a white Gaussian noise $\hat{\xi}_{\rm G}(t)$, the Wiener process $\hat{B}(t)$ is defined as

$$\hat{B}(t) \equiv \int_0^t \hat{\xi}_{\rm G}(s) ds \tag{3.1}$$

and its time differential $d\hat{B}(t)$ are introduced for convenience. Formally, we write the time differential as $\hat{\xi}_{\rm G}(t)dt = d\hat{B}(t)$. For the Wiener process, we know the convenient properties

$$d\hat{B}^2 = O(dt),\ d\hat{B}^n = o(dt)\ (n \geq 3). \tag{3.2}$$

In parallel to the Gaussian noise, we introduce the Lévy process $\hat{L}(t)$ as

$$\hat{L}(t) \equiv \int_0^t \hat{\xi}_{\rm NG}(s)ds, \tag{3.3}$$

where $\hat{\xi}_{\rm NG}$ represents the non-Gaussian noise. We can formally write the time differential as $d\hat{L}(t) = \xi_{\rm NG}(t)dt$. We should note that

$$d\hat{L}^n = O(dt), \tag{3.4}$$

is satisfied, which is the significant difference from Eq. (3.2).

3.1.1 Itô type stochastic integral

In this subsection, we define the Itô type stochastic integral:

$$\int_0^t dsb(s,\hat{x}(s)) \cdot \hat{\xi}_{\rm NG}(s) \quad \equiv \quad \lim_{\Delta t\to 0}\sum_{k=0}^{N}\left\{\Delta\hat{L}(t_k)b(t_k,\hat{x}(t_k))\right\}, \tag{3.5}$$

where we have introduced $t_i \equiv i\Delta t$, $\Delta t \equiv t/N$, $t_{N+1} \equiv t$ and $\Delta\hat{L}(t_k) \equiv \hat{L}(t_{k+1}) - \hat{L}(t_k)$. $b(t,x)$ is a continuous function of t and x. The important property for the Itô type stochastic integral is *martingale*, i.e.,

$$\langle b(s,\hat{x}(s)) \cdot d\hat{L}(s)\rangle = \langle b(s,\hat{x}(s))\rangle\langle d\hat{L}(s)\rangle, \tag{3.6}$$

where $\langle\cdots\rangle$ represents the ensemble average. Because Eq. (3.6) is useful to calculate the average, the Itô type integral is often used. For $\hat{\xi}_{\rm G}$, we can define the integral replacing $\hat{\xi}_{\rm NG}$ by $\hat{\xi}_{\rm G}$.

3.1.2 Stratonovich type stochastic integral

The Stratonovich product is often used for thermal processes, such as the stochastic energetics, which will be discussed in Chapter 4. We note that the corresponding product is ill-defined for the Lévy process. We introduce the Stratonivich product for the Wiener process

$$\int_0^t dsb(s,\hat{x}(s)) \circ \hat{\xi}_{\rm G}(s) \equiv \lim_{\Delta t\to 0}\sum_{k=0}^{N}\left\{\Delta\hat{B}(t_k)b\left(t_k,\frac{\hat{x}(t_{k+1})+\hat{x}(t_k)}{2}\right)\right\}. \tag{3.7}$$

It should be noted that martingale property Eq. (3.6) is no longer valid for the Stratonivich product, while the ordinary calculus, e.g. $dh(\hat{x}(t)) = h'(\hat{x}(t))\circ d\hat{x}(t)$ for an arbitrary analytic function $h(x)$, can be used for the Wiener process as is shown later. Instead of the Stratonovich product, a different product "$*$" is used for the ordinary calculus of the Lévy process as is discussed in Ref. [47].

3.2 Stochastic differential equation and master equation

Let us consider the following stochastic differential equation (SDE) driven by a non-Gaussian noise $\hat{\xi}_{\rm NG}(t)$:

$$\frac{d\hat{x}}{dt} = a(t,\hat{x}(t)) + b(t,\hat{x}(t))\hat{\xi}_{\rm NG}(t). \tag{3.8}$$

This equation is ambiguous because the product for $b(t,\hat{x}(t))\hat{\xi}_{\rm NG}(t)$ is not explicitly declared. The SDE with the Itô type stochastic integral is called the Itô type SDE:

$$\frac{d\hat{x}}{dt} = a(t,\hat{x}(t)) + b(t,\hat{x}(t)) \cdot \hat{\xi}_{\rm NG}(t). \tag{3.9}$$

If $b(t,\hat{x})$ does not depend on $\hat{x}$, the SDE is called to be additive, otherwise, it is called multiplicative. In this section, we define the Itô type SDEs and derive the corresponding Master equation.

Itô type SDE driven by a non-Gaussian noise

We write the evolution of a stochastic quantity $\hat{x}(t)$ by the discretized method:

$$\hat{x}(t) - \hat{x}(0) \equiv \sum_{k=0}^{N} \left\{ \Delta t a(t_k,\hat{x}(t_k)) + \Delta\hat{L}(t_k) b(t_k,\hat{x}(t_k)) \right\}. \tag{3.10}$$

Taking the continuous limit $\Delta t \to 0$ for Eq. (3.10), we obtain the stochastic *integral* equation for $\hat{x}_{\rm NG}(t)$:

$$\hat{x}(t) - \hat{x}(0) = \int_0^t ds a(s,\hat{x}(s)) + \int_0^t ds b(s,\hat{x}(s)) \cdot \hat{\xi}_{\rm NG}(s). \tag{3.11}$$

The stochastic *differential* equation for $\hat{x}(t)$ is defined as the differential of Eq. (3.11):

$$\frac{d\hat{x}}{dt} = a(t,\hat{x}(t)) + b(t,\hat{x}(t)) \cdot \hat{\xi}_{\rm NG}(t). \tag{3.12}$$

Similarly, we can define the Itô type SDE driven by a Gaussian noise.

Here, let us derive the time evolution for the distribution $f(x,t) \equiv {\rm Prob}(x = \hat{x}(t))$, following Ref. [8]. For an arbitrary analytic function $g(x)$, its derivative is calculated through the Taylor expansion:

$$\begin{aligned} dg(\hat{x}) &\equiv g(\hat{x}+d\hat{x}) - g(\hat{x}) && (3.13)\\ &= \sum_{n=1}^{\infty} \frac{\partial^n g}{\partial \hat{x}^n} \frac{(d\hat{x})^n}{n!} && (3.14)\\ &= \sum_{n=1}^{\infty} \frac{\partial^n g}{\partial \hat{x}^n} \frac{(adt + b\cdot d\hat{L})^n}{n!} && (3.15)\\ &= \frac{\partial g}{\partial \hat{x}} a dt + \sum_{n=1}^{\infty} \frac{1}{n!} \left\{ \frac{\partial^n g}{\partial \hat{x}^n} (b\cdot d\hat{L})^n \right\} && (3.16) \end{aligned}$$

It should be noted that $d\hat{L}^n = O(dt)$ holds. By taking the ensemble average of Eq. (3.16), we obtain

$$\begin{aligned}\int \frac{\partial f}{\partial t} g(x) dx &= \int dx \frac{\partial g}{\partial x} a(t,x) f(x,t) \\ &\quad + \sum_{n=1}^{\infty} \int dx \frac{\partial^n g}{\partial x^n} \left(\frac{b^n(t,x)}{n!} \frac{\langle d\hat{L}^n \rangle}{dt} f(x,t) \right) \qquad (3.17) \\ &= \int dx g(x) \frac{\partial}{\partial x} \left(-a(t,x) f(x,t) \right) \\ &\quad + \sum_{n=1}^{\infty} \int dx g(x) \frac{\partial^n}{\partial x^n} \left\{ \frac{(-b(t,x)^n)}{n!} K_n f(x,t) \right\}, \qquad (3.18)\end{aligned}$$

where we have introduced $\langle d\hat{L}^n \rangle \equiv K_n dt$. Here, we have used the martingale property Eq. (3.6). Because $g(x)$ is an arbitrary function, we obtain Master equation for Eq. (3.12):

$$\frac{\partial f}{\partial t} = \frac{\partial}{\partial x} \left(-a(t,x) f(x,t) \right) + \sum_{n=1}^{\infty} \frac{\partial^n}{\partial x^n} \left\{ \frac{(-b(t,x))^n}{n!} K_n f(x,t) \right\}. \qquad (3.19)$$

Ito type SDE driven by many independent non-Gaussian noises

Because the extension toward the SDE driven by many independent non-Gaussian noises $\hat{\xi}_\nu(t) (\nu = 1, 2, \cdots, n)$ is straightforward, we skip the derivation. The SDE driven by many independent non-Gaussian noises is defined as

$$\begin{aligned}\frac{d\hat{x}}{dt} &= a(t,\hat{x}) + \sum_{\nu=1}^{n} b_\nu(t,\hat{x}) \cdot \hat{\xi}_\nu(t), \qquad (3.20) \\ \hat{L}_\nu(t) &\equiv \int_0^t ds \hat{\xi}_\nu(s), \qquad (3.21) \\ \langle d\hat{L}_\nu^n(t) \rangle &\equiv K_n^{(\nu)} dt. \qquad (3.22)\end{aligned}$$

The corresponding master equation is represented as

$$\frac{\partial f}{\partial t} = \frac{\partial}{\partial x} \left(-a(t,x) f(x,t) \right) + \sum_{n=1}^{\infty} \frac{\partial^n}{\partial x^n} \left\{ \sum_{\nu=1}^{n} \frac{(-b_\nu(t,x))^n}{n!} K_n^{(\nu)} f(x,t) \right\}. \qquad (3.23)$$

Stratonovich type SDE driven by a Gaussian noise

Let us consider the Stratonovich type SDE driven by a Gaussian noise. Similar to Eq. (3.10), we discretize $\hat{x}(t)$ as

$$\hat{x}(t) - \hat{x}(0) \equiv \sum_{k=0}^{N} \left\{ \Delta t a(t_k, \hat{x}(t_k)) + \Delta \hat{B}(t_k) b \left(t_k, \frac{\hat{x}(t_{k+1}) + \hat{x}(t_k)}{2} \right) \right\}. \qquad (3.24)$$

By taking the continuous limit $\Delta t \to 0$, we obtain the stochastic integral equation for $\hat{x}(t)$

$$\hat{x}(t) - \hat{x}(0) = \int_0^t dsa(s, \hat{x}(s)) + \int_0^t dsb(s, \hat{x}(s)) \circ \hat{\xi}_{\rm G}(s). \tag{3.25}$$

Taking the differential of Eq. (3.25), we can define the SDE for $\hat{x}(t)$ driven by a Gaussian noise:

$$\frac{d\hat{x}}{dt} = a(t, \hat{x}(t)) + b(t, \hat{x}(t)) \circ \hat{\xi}_{\rm G}(t). \tag{3.26}$$

We can derive the Master equation for Eq. (3.26) as follows.

$$\begin{aligned} dg(\hat{x}) &= \sum_{n=1}^{\infty} \frac{\partial^n g}{\partial \hat{x}^n} \frac{(adt + b \circ d\hat{B})^n}{n!} & (3.27) \\ &= \sum_{n=1}^{\infty} \frac{1}{n!} \left\{ \frac{\partial g}{\partial \hat{x}} adt + \frac{\partial^n g}{\partial \hat{x}^n} (b \circ d\hat{B})^n \right\} & (3.28) \end{aligned}$$

We note that the martingale property cannot be used when we take the ensemble average of Eq. (3.28). From Eq. (3.2), the master equation for Eq. (3.26) can be obtained as:

$$\frac{\partial f}{\partial t} = \frac{\partial}{\partial x} \left(-a(t,x) f(x,t) \right) + \frac{1}{2} \left\{ \left(-\frac{\partial}{\partial x} b(t,x) \right)^2 f(x,t) \right\}. \tag{3.29}$$

Here, we have assumed $\langle d\hat{B}(t) \rangle = 0$ and $\langle d\hat{B}^2(t) \rangle = dt$.

For later convenience, we derive the formula, which connects the Itô type stochastic integral with the Stratonovich one. For an arbitrary analytic function $h(x)$, the differential is given by

$$\begin{aligned} dh(\hat{x}(t)) &= h'(\hat{x}(t)) d\hat{x}(t) + \frac{h''(\hat{x}(t))}{2} d\hat{x}(t)^2 + \cdots \\ &= \left\{ h'(\hat{x}(t)) + h''(\hat{x}(t)) \frac{d\hat{x}(t)}{2} \right\} d\hat{x}(t) + \cdots & (3.30) \\ &= h' \left(\hat{x}(t) + \frac{d\hat{x}(t)}{2} \right) d\hat{x}(t) + \cdots \\ &= \frac{h'(\hat{x}(t+dt)) + h'(\hat{x}(t))}{2} d\hat{x}(t) + \cdots \\ &= h'(\hat{x}(t)) \circ d\hat{x}(t). & (3.31) \end{aligned}$$

Introducing the $H(x) \equiv h'(x)$ and comparing Eqs. (3.30) and (3.31), we obtain the formula:

$$H(\hat{x}(t)) \circ d\hat{x}(t) = H(\hat{x}(t)) \cdot d\hat{x}(t) + \frac{H'(\hat{x}(t))}{2} (d\hat{x}(t))^2, \tag{3.32}$$

where we have abbreviated "$\cdot$" in the second term on the right-hand side for simplification. For example, substituting Eq. (3.26) and $H = b(\hat{x}(t), t)$ into Eq. (3.32), we obtain the Itô formula:

$$b(\hat{x}(t), t) \circ d\hat{B}(t) = b(\hat{x}(t), t) \cdot d\hat{B}(t) + \frac{b(\hat{x}(t), t)}{2} \frac{\partial b(\hat{x}(t), t)}{\partial \hat{x}(t)} dt, \tag{3.33}$$

which enable us to transform Eq. (3.26) into the Itô type SDE.

3.3 Application to physical systems

In this section, we apply the obtained formulas in the previous section to physical systems.

3.3.1 Langevin equation driven by a Gaussian noise

Langevin equation without potential under a Gaussian noise

A Langevin equation without potential under a Gaussian noise is written as

$$M\frac{d\hat{V}}{dt} = -\gamma\hat{V} + \sqrt{2\gamma k_B T}\xi_{\mathrm{G}}(t), \tag{3.34}$$

$$\langle \xi_{\mathrm{G}}(t) \rangle = 0, \tag{3.35}$$

$$\langle \xi_{\mathrm{G}}(t)\xi_{\mathrm{G}}(s) \rangle = \delta(t-s) \tag{3.36}$$

We use the relation between Eqs. (3.12) and (3.19), changing $x \to V$, $a \to -\gamma V/M$, and $b \to \sqrt{2\gamma k_B T}/M$, to obtain the master equation. The corresponding master equation for Eq. (3.34) is obtained as

$$\frac{\partial f}{\partial t} = \frac{\partial}{\partial V}\frac{\gamma}{M}Vf + \frac{\gamma k_B T}{M^2}\frac{\partial^2 f}{\partial V^2} \tag{3.37}$$

We note that $K_n = 0$ $(n \geq 3)$.

Langevin equation with potential under a Gaussian noise

A Langevin equation with potential under a Gaussian noise is written as

$$M\frac{d\hat{V}}{dt} = -\gamma\hat{V} - \frac{\partial U}{\partial \hat{x}} + \sqrt{2\gamma k_B T}\xi_{\mathrm{G}}(t), \tag{3.38}$$

$$\frac{d\hat{X}}{dt} = \hat{V} \tag{3.39}$$

The corresponding master equation is written as

$$\frac{\partial f}{\partial t} = -\frac{\partial}{\partial X}Vf + \frac{\partial}{\partial V}\left(\frac{\gamma}{M}V + \frac{\partial U}{\partial X}\right)f + \frac{\gamma k_B T}{M^2}\frac{\partial^2 f}{\partial V^2}. \tag{3.40}$$

3.3.2 Langevin equation driven by non-Gaussian noises

Langevin equation driven by a state-dependent Poissonian noise

We consider the Langevin equation driven by a state-dependent Poissonian noise whose amplitude is I and the birth rate is λ.

$$\begin{aligned}
\frac{d\hat{V}}{dt} &= -\gamma\hat{V} + I\hat{\xi}_{\mathrm{P}}(t,\hat{V}) && (3.41)\\
\xi_{\mathrm{P}}(t,\hat{V}) &\equiv \sum_i \delta(t-\hat{t}_i) && (3.42)\\
\hat{L}_P(t,\hat{V}) &\equiv \int_0^t \hat{\xi}_{\mathrm{P}}(s,\hat{V})ds && (3.43)\\
\langle d\hat{L}_P^n(t,\hat{V})\rangle &= \lambda(V)dt && (3.44)
\end{aligned}$$

The Poissonian noise is state-dependent in the sense that $\lambda(V)$ depends on V. Replacing $x \to V$, $a \to -\gamma V$, $b \to I$ and $K_n \to \lambda(V)$ in Eq. (3.19), we obtain the corresponding Master equation:

$$\frac{\partial f}{\partial t} = \frac{\partial}{\partial V}\left(\gamma V f(V,t)\right) + \sum_{n=1}^{\infty}\frac{\partial^n}{\partial V^n}\left\{\frac{(-I)^n}{n!}\lambda(V)f(V,t)\right\}. \tag{3.45}$$

Stochastic equation of motion driven by many state-dependent Poissonian noises

We consider the following SDE:

$$\begin{aligned}
M\frac{d\hat{V}}{dt} &= \hat{F} && (3.46)\\
\hat{F} &\equiv \sum_v P_v(\hat{V})\cdot\hat{\xi}_v(t|\hat{V}) && (3.47)\\
\hat{L}_v(t) &\equiv \int_0^t \xi_v(s|\hat{V})ds && (3.48)\\
\langle d\hat{L}_v^n(t)\rangle &\equiv \lambda_v(V)dt && (3.49)
\end{aligned}$$

By setting $a \to 0$, $b_\nu \to P_\nu/M$ and $K_n^\nu \to \lambda_\nu$, the corresponding Master equation is obtained from Eq. (3.23):

$$\frac{\partial f}{\partial t} = \sum_{n=1}^{\infty}\frac{\partial^n}{\partial V^n}\sum_v\left\{\left(-\frac{P_v}{M}\right)^n\frac{\lambda_v(V)}{n!}f(V,t)\right\}. \tag{3.50}$$

We note that the obtained equation corresponds to the one-dimensional Boltzmann-Lorentz equation, if we interpret $\lambda_v(V)$ and P_v as

$$\begin{aligned}
\lambda_v(V) &= |v-V|\rho S\phi(v)dv, && (3.51)\\
P_v(V) &= \frac{2mM}{m+M}(v-V), && (3.52)
\end{aligned}$$

respectively and replace $\sum_v$ by the integral $\int$. This is known as the Rayleigh piston (Fig. 3.1) [150]. Here, ρS is the one dimensional density and $\phi(v)$ is the VDF for colliding elastic molecules of mass m. $\lambda_v(V)$ represents the collision probability of a molecule with the velocity between v and $v + dv$ against the massive tracer M. P_v is the momentum change due to the collisions.

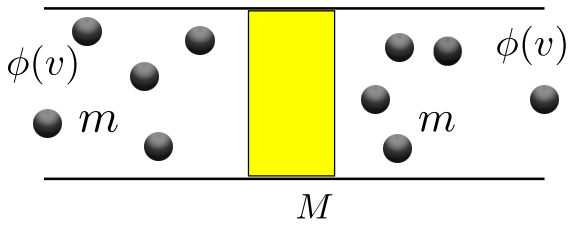

Figure 3.1: A schematic figure of the Rayleigh piston. The piston moves one dimensionally in the bath whose VDF is given by $\phi(v)$.

3.4 System size expansion method

We introduce the system size expansion methods to derive state-independent SDEs from master equations.

3.4.1 van Kampen's system size expansion

We consider a stochastic variable $\hat{V}$, which represents, for example, the velocity of the piston moving in one-dimensional direction without any side-wall friction (the Rayleigh piston). The time evolution of the probability distribution function (PDF) $P = P(V,t) \equiv \mathrm{Prob}(\hat{V}(t) = V)$ driven by the state-dependent white noise can be described by the Boltzmann-Lorentz equation [7, 8]:

$$\frac{\partial P}{\partial t} = \int dy \left\{ \mathbb{W}_{\epsilon_\Omega}(V-y;y)P(V-y,t) - \mathbb{W}_{\epsilon_\Omega}(V;y)P(V,t) \right\}, \quad (3.53)$$

where $\mathbb{W}_{\epsilon_\Omega}(V;y)$ represents the transition probability of the jump amplitude y when the piston velocity is V, i.e. the noise is state-dependent. We have also introduced the small parameter ϵ_Ω, which corresponds to the inverse of the system size. We note that $\mathbb{W}_{\epsilon_\Omega}(V;y)$ satisfies the relation with $\mathcal{Y} \equiv y/\epsilon_\Omega$

$$\bar{W}(V;\mathcal{Y})d\mathcal{Y} = \mathbb{W}_{\epsilon_\Omega}(V;y)dy, \quad (3.54)$$

where $\bar{W}$ is ϵ_Ω independent [7].

Introducing and substituting the scaled variables

$$V_{\mathrm{G}} \equiv \frac{V}{\sqrt{\epsilon_\Omega}}, \quad (3.55)$$

$$\tau \equiv \epsilon_\Omega t \quad (3.56)$$

and $P^{(G)} = P^{(G)}(V_{\rm G}, \tau) \equiv \sqrt{\epsilon_\Omega} P(\sqrt{\epsilon_\Omega} V_{\rm G}, \tau/\epsilon_\Omega)$ into Eq. (6.6), we obtain the Fokker-Planck equation in the limit $\epsilon_\Omega \to 0$:

$$\frac{\partial P^{(G)}}{\partial \tau} = -\frac{\partial}{\partial V_{\rm G}} K_1'(0) V_{\rm G} P^{(G)} + \frac{\partial^2}{\partial V_{\rm G}^2} K_2(0) P^{(G)} + O(\sqrt{\epsilon_\Omega}), \quad (3.57)$$

$$K_n(V) \equiv \int d\mathcal{Y} \mathcal{Y}^n \bar{W}(V; \mathcal{Y}), \quad (3.58)$$

which is equivalent to the Langevin equation

$$M \frac{d\hat{V}_{\rm G}}{d\tau} = -\gamma_{\rm G} \hat{V}_{\rm G} + \sqrt{2\gamma_{\rm G} T_{\rm eff}} \hat{\xi}_{\rm G}(\tau), \quad (3.59)$$

Here, $\gamma_{\rm G} \equiv M K_1'(0)$, $\langle \hat{\xi}_{\rm G}(\tau) \rangle = 0$ and $\langle \hat{\xi}_{\rm G}(\tau_1) \hat{\xi}_{\rm G}(\tau_2) \rangle = \delta(\tau_1 - \tau_2)$. We have introduced the effective temperature $T_{\rm eff}$ as

$$T_{\rm eff} \equiv \frac{M K_2(0)}{K_1'(0)}. \quad (3.60)$$

Therefore, as expected, the steady state distribution function $P_{\rm ss}^{(G)} \equiv \lim_{\tau \to \infty} P^{(G)}$ is Gaussian:

$$P_{\rm ss}^{(G)} = \sqrt{\frac{M}{2\pi T_{\rm eff}}} \exp\left[-\frac{M V_{\rm G}^2}{2 T_{\rm eff}} \right]. \quad (3.61)$$

3.4.2 Generalized system size expansion

We consider the case that a stochastic variable coupled with two environments. One is the same as Eq. (6.6), and another one is the viscous environment $F_{\rm fri} = -\gamma_{\rm vis} V$ [92,93]. Note that the detailed discussion when $F_{\rm fri}$ is a nonlinear function or $F_{\rm fri}$ is driven by a noise is found in Ref. [93]. The starting point is

$$\frac{\partial P}{\partial t} = \frac{\gamma_{\rm vis}}{M} \left\{ \frac{\partial}{\partial V} V P \right\} + \int dy \left\{ \mathbb{W}_{\epsilon_\Omega}(V - y; y) P(V - y, t) - \mathbb{W}_{\epsilon_\Omega}(V; y) P(V, t) \right\}, \quad (3.62)$$

We assume that the friction satisfies the relation $\gamma_{\rm vis}/\gamma_G = O(1)$. Introducing the scaled variable:

$$\mathcal{V} \equiv \frac{V}{\epsilon_\Omega}, \quad (3.63)$$

and taking the limit $\epsilon_\Omega \to 0$ in Eq. (3.62), we obtain the time evolution for $\mathcal{P} = \mathcal{P}(\mathcal{V}, t) = \epsilon_\Omega P(\epsilon_\Omega V, t)$:

$$\frac{\partial \mathcal{P}}{\partial t} = \frac{\gamma_{\rm vis}}{M} \left\{ \frac{\partial}{\partial \mathcal{V}} \mathcal{V} \mathcal{P} \right\} + \int_{-\infty}^{\infty} d\mathcal{Y} \mathcal{W}(\mathcal{Y}) \left\{ \mathcal{P}(\mathcal{V} - \mathcal{Y}, t) - \mathcal{P}(\mathcal{V}, t) \right\}, \quad (3.64)$$

which is equivalent to the Langevin equation driven by additive non-Gaussian noises:

$$M \frac{d\hat{\mathcal{V}}}{dt} = -\gamma_{\rm vis} \hat{\mathcal{V}} + \hat{\xi}_{\rm NG}(t). \quad (3.65)$$

Here, the transition rate for $\hat{\xi}_{\rm NG}(t)$ is given by $\mathcal{W}(\mathcal{Y}) \equiv \bar{W}(V=0;\mathcal{Y})$. The steady state distribution function for Eq. (3.64) is solved by introducing the Fourier transform $\tilde{P}_{\rm ss}(s) \equiv \int dV e^{isV} P_{\rm ss}(V)$ with $P_{\rm ss} \equiv \lim_{t\to\infty} \mathcal{P}(\mathcal{V},t)$ [151]:

$$\tilde{P}_{\rm ss}(s) \quad = \quad \exp\left[\frac{M}{\gamma_{\rm vis}}\int_0^s \frac{\Phi(s')}{s'}ds'\right], \tag{3.66}$$

where $\Phi(s)$ represents the cumulant generating function:

$$\Phi(s) \equiv \int_{-\infty}^{\infty} d\mathcal{Y}\mathcal{W}\left(\mathcal{Y}\right)\left(e^{is\mathcal{Y}}-1\right). \tag{3.67}$$

Chapter 4

Stochastic Energetics

Abstract

In this chapter, we briefly review the stochastic energetics proposed by Sekimoto [44–46]. After the brief introduction in Sec. 4.1, we explain and derive basic relations for stochastic energetics in Sec. 4.2, and discuss the attainability of the Carnot efficiency within the framework of stochastic energetics, following Ref. [152] in Sec. 4.3. In Sec. 4.4, we explain a recent experimental result on the finite-time thermodynamics on the basis of stochastic energetics.

4.1 Introduction

There are three levels of understanding the nature. One relies on microscopic Hamiltonian dynamics, where the system is completely deterministic. Another is based on thermodynamics or hydrodynamics described by a few slow variables. The other understanding is by mesoscopic description, where some degree of freedom are traced out, and thus, a stochastic description in terms of the Langevin equation is necessary. Equilibrium thermodynamics provides the universal relations in terms of ensemble averaged quantities, while stochastic energetics provides the corresponding relations even for a single trajectory of the Langevin equation [44, 45].

4.2 Basic relations for stochastic energetics

We consider the one-dimensional underdamped Langevin equation driven by a Gaussian white noise:

$$m\frac{d\hat{v}}{dt} = -\frac{\partial U}{\partial \hat{x}}(\hat{x}; a(t)) - \gamma\hat{v} + \sqrt{2\gamma T}\hat{\xi}_G(t), \tag{4.1}$$

$$\frac{d\hat{x}}{dt} = \hat{v}, \tag{4.2}$$

where $a = a(t)$ represents an external control parameter. A single colloidal particle trapped by an optical tweezer is a typical example to realize Eqs. (4.1) and (4.2) and a represents the width of the tweezer [44, 45].

First law of thermodynamics in the single realization

By multiplying $\hat{v}$ to Eq. (4.1), we obtain the following equations.

$$d\hat{E} = d\hat{W} + d\hat{Q} \tag{4.3}$$

$$\hat{E} \equiv \frac{m\hat{v}^2}{2} + U(\hat{x}; a), \tag{4.4}$$

$$\hat{W} \equiv \int \frac{\partial U}{\partial a}(\hat{x}; a)da, \tag{4.5}$$

$$\hat{Q} \equiv \int (-\gamma\hat{v} + \sqrt{2\gamma T}\hat{\xi}_G(t)) \circ \hat{v}dt. \tag{4.6}$$

Here, $\hat{E}$ and $\hat{W}$ represents the total energy of the Brownian particle and the work done by the external agent. $\hat{Q}$ represents the work done by the viscous environment, which can be interpreted as the heat. Thus, Eq. (4.3) is interpreted as the first law of thermodynamics in the single realization. We note that the ensemble average of Eq. (4.3) leads to the conventional first law of equilibrium thermodynamics.

The heat current (4.6) is rewritten as

$$d\hat{Q} = -\frac{2\gamma}{m}\left(\frac{m\hat{v}^2}{2} - \frac{T}{2}\right)dt + \sqrt{2\gamma T}\hat{v} \cdot d\hat{B}, \tag{4.7}$$

where we have used Eq. (3.32) and $d\hat{B}^2 = dt$. By taking the ensemble average, we obtain the expression for the heat current:

$$\langle d\hat{Q}\rangle = -\frac{2\gamma dt}{m}\left(\left\langle\frac{m\hat{v}^2}{2}\right\rangle - \frac{T}{2}\right). \tag{4.8}$$

It should be noted that the direction of the heat is completely determined by the difference between kinetic energy of the Brownian particle and the bath temperature, where the current is independent of potential U. Equation (4.8) can be rewritten as

$$\begin{aligned}\langle d\hat{Q}\rangle &= d\left[\int E\mathcal{P}dxdp\right] - da\int\frac{\partial E}{\partial a}\mathcal{P}dxdp \\ &= \int E\frac{\partial\mathcal{P}}{\partial t}dxdp,\end{aligned} \tag{4.9}$$

where we have introduced the energy $E(x, p, a) = p^2/m + U(x, a)$ and the momentum $p = mv$. $\mathcal{P} = \mathcal{P}(x, p, t)$ represents the PDF for the Brownian particle.

Recalling that the Kramers equation can be written in a compact form:

$$\frac{\partial \mathcal{P}}{\partial t} = -\frac{\partial J_x}{\partial x} - \frac{\partial J_p}{\partial p}, \tag{4.10}$$

$$J_x \equiv \frac{p}{m}\mathcal{P}, \tag{4.11}$$

$$J_p \equiv \left(-\frac{\partial U}{\partial x} - \gamma\frac{p}{m}\right)\mathcal{P} - \frac{\partial}{\partial p}\gamma T\mathcal{P}, \tag{4.12}$$

we obtain

$$\langle d\hat{Q}\rangle = dt\left[\int\left(\frac{\partial E}{\partial x}J_x + \frac{\partial E}{\partial p}J_p\right)dxdp\right]. \tag{4.13}$$

H-theorems

Let us define the Shanon entropy $S_{\rm B}$ of the Brownian particle:

$$S_{\rm B} \equiv -\int \mathcal{P}\log\mathcal{P}dxdp, \tag{4.14}$$

where we have adopted the dimensionless unit for the entropy. The total derivative of $S_{\rm B}$ leads to

$$\frac{dS_{\rm B}}{dt} - \frac{1}{T}\frac{\langle d\hat{Q}\rangle}{dt} = \int \frac{1}{\mathcal{P}}\frac{\gamma}{T}\left[\frac{p}{m}\mathcal{P} + T\frac{\partial\mathcal{P}}{\partial p}\right]^2 dxdp \geq 0, \tag{4.15}$$

which means that $S_B - \langle\hat{Q}\rangle/T$ is non-decreasing. The second term on the left-hand side of Eq. (4.15) represents the entropy changes of the heat bath.

Following the similar procedure, we can obtain expressions for first law of thermodynamics, the average heat current, and the total entropy change for the overdamped Langevin system:

$$0 = -\frac{\partial U}{\partial\hat{x}}(\hat{x};a(t)) - \gamma\frac{d\hat{x}}{dt} + \hat{\xi}_G(t). \tag{4.16}$$

We summarize the formulas as follows:

$$dU = d\hat{E} + d\hat{Q}, \tag{4.17}$$

$$\langle d\hat{Q}\rangle = -\frac{dt}{\gamma}\left[\left\langle\left(\frac{\partial U}{\partial\hat{x}}\right)^2\right\rangle - T\left\langle\frac{\partial^2 U}{\partial\hat{x}^2}\right\rangle\right]$$

$$= dt\int\left[\frac{\partial U}{\partial x}J_x\right]dx, \tag{4.18}$$

$$\frac{dS_{\rm B}}{dt} - \frac{1}{T}\frac{\langle d\hat{Q}\rangle}{dt} = \int\frac{1}{\mathcal{P}}\frac{\gamma J_x^2}{T}dx \geq 0. \tag{4.19}$$

4.3 Attainability of Carnot's efficiency for a Brownian engine

Within the framework of stochastic energetics, we discuss the Brownian engine whose attainable efficiency is given by η_C in a quasi-static operation following Ref. [152].

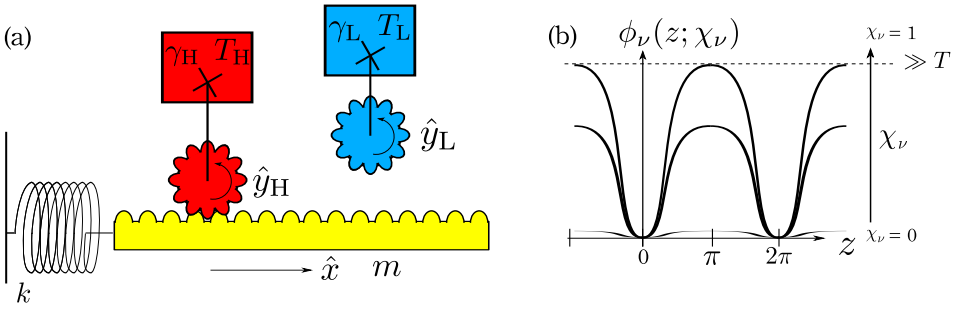

Figure 4.1: (a) A schematic figure of the Brownian heat engine, whose efficiency under the quasi-static operation is given by the Carnot efficiency. (b) A schematic figure of the attachment and detachment potential.

Setup

The schematic setup is shown in Fig. 4.1 (a) [152]. We consider the single particle $\hat{x}$ connected to a harmonic spring $U(\hat{x};k) = -k\hat{x}^2/2$ and heat baths via 2π-periodic interacting potentials $\phi_\nu(\hat{z};\chi_\nu)$ ($\nu = $ H or L):

$$\frac{d\hat{p}}{dt} = -k\hat{x} - \sum_{\nu={\rm H,L}} \frac{\partial \phi_\nu}{\partial \hat{x}}(\hat{x} - \hat{y}_\nu;\chi_\nu), \tag{4.20}$$

$$\frac{d\hat{x}}{dt} = \frac{\hat{p}}{m}, \tag{4.21}$$

where $\hat{y}_\nu$ represents the stochastic variable attached to a heat bath $\nu = $ H or L. The heat baths are assumed to be characterized by the overdamped Langevin equations:

$$0 = -\gamma_\nu \frac{d\hat{y}_\nu}{dt} + \sqrt{2\gamma_\nu T_\nu}\hat{\xi}_G(t) - \frac{\partial \phi_\nu}{\partial \hat{y}_\nu}(\hat{x} - \hat{y}_\nu;\chi_\nu), \tag{4.22}$$

where $\max_z\{\phi_\nu(z;\chi_\nu = 1)\} \gg T$ and $\phi_\nu(\hat{z},\chi_\nu = 0) = 0$ hold. Here, $0 \le \chi_\nu \le 1$ represents the detachment/attachment parameter as follows. $\chi_\nu = 1$ corresponds to the attached state, where the system $\hat{x}$ and the bath $\hat{y}_\nu$ are tightly coupled, i.e., the probability for $\hat{x} - \hat{y}_\nu = 2l\pi (l = 0, 1, 2, \cdots)$ with the integer l is almost 1. On the other hand $\chi_\nu = 0$ corresponds to the detached state, where the system $\hat{x}$ and the bath $\hat{y}_\nu$ are not correlated at all. See Fig. 4.1 (b) for the schematic figure of $\phi_\nu(\hat{z},\chi_\nu)$.

The reason why we have introduced the stochastic variable $\hat{y}_\nu$ and the parameter χ_ν is to discuss the cost of attachment/detachment [152]. Once an isolated system is attached to a heat bath, its energy fluctuates in time. After the detachment, the relaxation time toward the canonical distribution diverges, because the energy of the isolated system is fixed. Thus, it is necessary to consider the cost of operations [45].

Operation protocol

The schematic figure of the operation protocol is shown in Fig. 4.2, where the attachment/detachment protocols are represented by χ_ν axes. Initially, the system is at the state A_0. The spring constant is strengthened to be the state B_0 (adiabatic process). The heat bath $T_{\rm H}$ is attached to the system ($B_0 \to B_{\rm H}$). The isothermal expansion process change the state from $B_{\rm H}$ to $C_{\rm H}$. Then, the heat bath is detached ($C_{\rm H} \to C_0$). After the adiabatic expansion process $C_0 \to D_0$, we attach and detach to compress the system isothermally and the system comes back to the initial state ($D_0 \to D_{\rm L} \to A_{\rm L} \to A_0$).

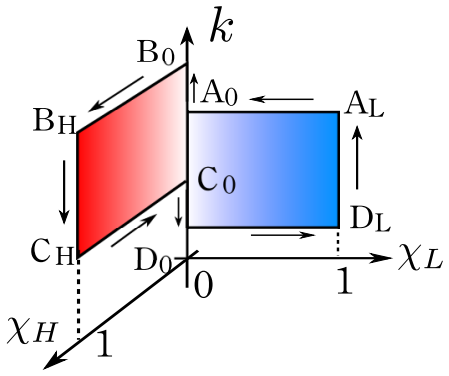

Figure 4.2: Operation protocol in Ref. [152]. Attachment and detachment processes are explicitly shown as $\chi_\nu(\nu = \text{H or L})$ axis.

Efficiency

We can show that the average work for the attachment and detachment processes are cancelled by choosing a proper choice of the ratio between the expansion and compression as follows. The Helmholtz free energy is calculated to be

$$\begin{aligned} e^{-F(T_\nu,k,\chi_\nu)/T_\nu} &= \int dxdpdy_\nu \exp\left[-\{\mathcal{H}(x,p,k)+\phi_\nu(x-y_\nu,\chi_\nu)\}/T_\nu\right] \\ &= \int dxdpe^{-\mathcal{H}(x,p,k)/T_\nu}\int dze^{-\phi_\nu(z,\chi_\nu)/T_\nu}, \end{aligned} \tag{4.23}$$

i.e.

$$F(T_\nu, k, \chi_\nu) = -\frac{T_\nu}{2}\ln\frac{mT_\nu^2(4\pi)^4}{k} + \tilde{F}(T_\nu, \chi_\nu) + \text{Const.}, \tag{4.24}$$

where we have introduced the Hamiltonian $\mathcal{H}(x, p, k) = p^2/2m + U(x; k)$. Here, $\tilde{F}$ is defined by $\tilde{F}(T_\nu, \chi_\nu) \equiv -T_\nu \log \int dz \exp[-\phi_\nu(z; \chi_\nu)/T_\nu]$. The sum of the following works for four processes is equal to zero:

$$\begin{aligned}
W(A_{\rm L} \to A_0) &= F(T_{\rm L}, k_{\rm A}, 0) - F(T_{\rm L}, k_{\rm A}, 1), & (4.25)\\
W(D_0 \to D_{\rm L}) &= F(T_{\rm L}, k_{\rm D}, 1) - F(T_{\rm L}, k_{\rm D}, 0), & (4.26)\\
W(B_0 \to B_{\rm H}) &= F(T_{\rm H}, k_{\rm B}, 1) - F(T_{\rm H}, k_{\rm B}, 0), & (4.27)\\
W(D_0 \to D_{\rm L}) &= F(T_{\rm H}, k_{\rm C}, 0) - F(T_{\rm H}, k_{\rm C}, 1), & (4.28)
\end{aligned}$$

because $W(A_{\rm L} \to A_0) + W(D_0 \to D_{\rm L}) = 0$ and $W(B_0 \to B_{\rm H}) + W(D_0 \to D_{\rm L}) = 0$ hold from Eq. (4.24) [45].

Works during the adiabatic operations (along k axis in Fig. 4.2) can be cancelled as follows. Let us recall that there exists an adiabatic invariant for a harmonic oscillator:

$$I(E, k) = \frac{E}{2\pi}\sqrt{\frac{m}{k}}. \tag{4.29}$$

Thus, before and after the adiabatic processes, the energy is changed as $E \to E' = E\sqrt{k'/k}$, where $'$ represents the quantities after the processes. The average work for each adiabatic process is given by

$$\begin{aligned}
\langle W(A_0 \to B_0)\rangle &= T_{\rm L}\left(\sqrt{\frac{k_B}{k_A}} - 1\right), & (4.30)\\
\langle W(C_0 \to D_0)\rangle &= T_{\rm H}\left(\sqrt{\frac{k_D}{k_C}} - 1\right). & (4.31)
\end{aligned}$$

The sum of Eqs. (4.30) and (4.31) is vanished, if we choose the condition

$$\sqrt{\frac{k_B}{k_A}} = \frac{T_{\rm H}}{T_{\rm L}}, \sqrt{\frac{k_D}{k_C}} = \frac{T_{\rm L}}{T_{\rm H}}. \tag{4.32}$$

Therefore, the average work for the attachment and detachment processes can be regarded as zero by the proper choice of the expansion and compression ratio.

The work in isothermal processes can be calculated by the integration of the free energy. The total work in a single realization is given by

$$W_{\rm tot} = W(B_{\rm H} \to C_{\rm H}) + W(D_{\rm L} \to A_{\rm L}) = \frac{T_{\rm H} - T_{\rm L}}{2}\ln\frac{k_{\rm C}}{k_{\rm B}}. \tag{4.33}$$

From the energy balance, we obtain

$$Q_{\rm H}(B_{\rm H} \to C_{\rm H}) = \Delta E(B_{\rm H} \to C_{\rm H}) - W(B_{\rm H} \to C_{\rm H}), \tag{4.34}$$

where $\Delta E(B_{\rm H} \to C_{\rm H})$ denotes the energy change from the state $B_{\rm H}$ to $C_{\rm H}$. From Eq. (4.24), the average energy $\langle E(B_{\rm H} \to C_{\rm H})\rangle = -T_{\rm H}^2 \partial (F(T_{\rm H}, k, 1)/T_{\rm H})/\partial T_{\rm H}$ does not depend on k. Hence, we obtain $\langle \Delta E(B_{\rm H} \to C_{\rm H})\rangle = 0$ and

$$\langle Q_{\rm H}(B_{\rm H} \to C_{\rm H})\rangle = -\langle W(B_{\rm H} \to C_{\rm H})\rangle = \frac{T_{\rm H}}{2} \ln \frac{k_{\rm C}}{k_{\rm B}}. \tag{4.35}$$

From Eqs. (4.33) and (4.35), the efficiency is given by the Carnot efficiency:

$$\eta = \frac{-W_{\rm tot}}{\langle Q_{\rm H}(B_{\rm H} \to C_{\rm H})\rangle} = \eta_C. \tag{4.36}$$

4.4 Finite time engine for stochastic energetics

In this section, we briefly explain an experimental setup corresponding to a finite-time thermodynamic cycle in a fluctuating system. We can use the analogy between a gas partitioned by a piston and a single colloidal particle trapped by an optical tweezer, where the volume for the former corresponds to the width of the optical tweezer for the latter. Thus, repeating heating and cooling processes and changing the width of the optical tweezer, the single particle heat engine can be realized experimentally [128]. Figure 4.3 represents the schematic figure of Ref. [128], where a Brownian particle is trapped by the optical tweezer and operated cyclically in two different baths at $T_{\rm H}$ and $T_{\rm L}$. In Ref. [128], a single melamine bead of diameter 2.94 μm trapped by a parabolic potential in water is heated or cooled by a laser and the efficiency at MP agrees with $\eta_{\rm CA}$ within experimental errors.

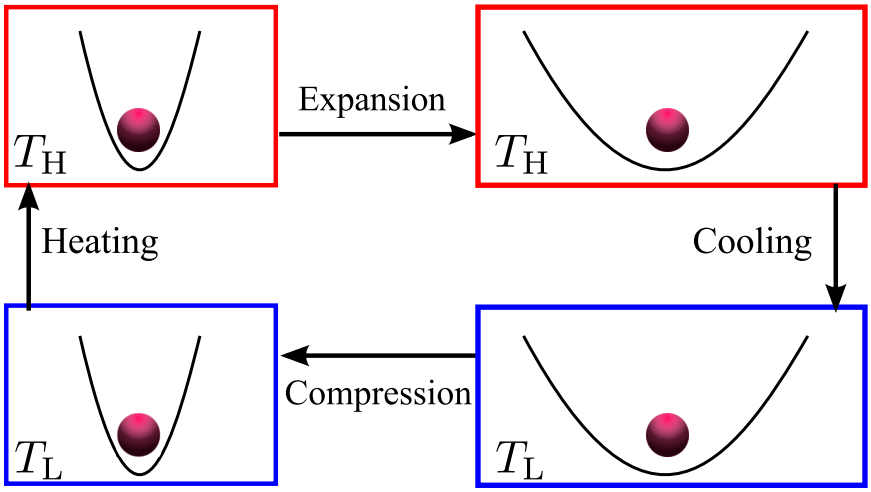

Figure 4.3: Schematic figure of the experimental realization for a micrometer-sized stochastic heat engine in Ref. [128].

Chapter 5

Adiabatic piston problem under nonlinear friction

Abstract

The motion of an adiabatic piston under nonlinear sliding friction is investigated to clarify the roles of the sliding friction in the fluctuating motion of an adiabatic piston. We clarify that dry friction can reverse the direction of the piston motion and causes a discontinuity or a cusp-like singularity for the VDFs of the piston. Furthermore, we show that the direction of the piston motion depends on the amplitude of the friction and nonlinearity of the friction. We also show that the heat fluctuation relation is modified under dry friction.

5.1 Introduction

Friction is ubiquitous in nature from a biological surface to an atomic-scale surface [15–17,25]. However, the ubiquitousness yields problems, such as wear and rupture, in manufacturing small machines. We study energy transfer, such as momentum or heat transfer, of a fluctuating object subjected to sliding friction. For this purpose, we study the motion of an adiabatic piston under the mechanical equilibrium, which is located between two equilibrium environments characterized by two different temperatures and densities. Lieb suggested that the equilibrium thermodynamics cannot tell us whether the adiabatic piston moves or not [153,154]. This problem is solved analytically by using Boltzmann-Lorentz equation [155] and is recently phenomenologically understood through the concept of the momentum transfer deficit due to dissipation (MDD) [156]. However, the motion of the adiabatic piston under nonlinear sliding friction including dry friction is little known.

Let us clarify the difference from previous studies [38–40]. Although the roles of dry friction in the asymmetric granular piston with the different restitution

coefficient have already been discussed in Ref. [38], its roles in the symmetric piston exposed to two thermal gases of different temperatures have not been analyzed yet. Baule and Sollich have studied a solvable model for a fluctuating piston whose two faces are respectively kicked by a single state-independent Poissonian noise under dry friction, assuming an exponential distribution for the amplitude and the constant event probability for each noise [39, 40]. However, the motion of the piston surrounded by the two thermal gases, which are characterized by state-dependent compound Poissonian noises, under dry friction has not been analyzed yet.

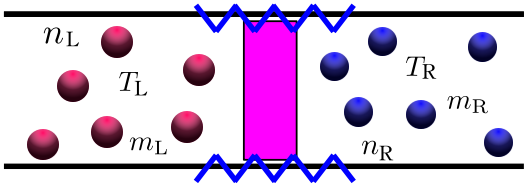

Figure 5.1: Schematic picture for the system with a fluctuating boundary under sliding friction. Blue zigzag lines represent the sliding friction. Ideal gas molecules are enclosed in a container and the piston with a finite mass M separate gas into two regions. Molecule mass for the left and right gas is respectively given by $m_{\rm L}$ and $m_{\rm R}$. Gas densities $n_{\rm L}, n_{\rm R}$ and temperatures $T_{\rm L}, T_{\rm R}$ are assumed to be constants.

5.2 Setup

We consider the fluctuating piston of mass M and area S, which moves along the frictional cylinder one-dimensionally, attached to two environments as follows. The density of the gas, temperature and molecule mass are respectively given by n_ν, T_ν and m_ν (ν = L or R). See Fig. 5.1. The time evolution of the probability distribution function (PDF) for the piston velocity V is given by the Boltzmann-Lorentz equation:

$$\begin{aligned}\frac{\partial P}{\partial t}+\frac{\partial}{\partial V}\frac{F_{\rm fri}}{M}P &= \int dV'\left\{\mathbb{W}_{\rm L}(V\leftarrow V')P(V',t)-\mathbb{W}_{\rm L}(V'\leftarrow V)P(V,t)\right\}\\ &\quad+\int dV'\left\{\mathbb{W}_{\rm R}(V\leftarrow V')P(V',t)-\mathbb{W}_{\rm R}(V'\leftarrow V)P(V,t)\right\},\\ &= J_{\rm L}+J_{\rm R}. \end{aligned} \tag{5.1}$$

where we have introduced the transition rate $\mathbb{W}_\nu(V'\leftarrow V)$ and velocity-dependent side-wall friction $F_{\rm fri}=F_{\rm fri}(V)$. See also Chapter 3 for the Rayleigh piston problem. We assume that $F_{\rm fri}(V)$ is an odd function of V as $F_{\rm fri}(-V)=-F_{\rm fri}(V)$.

We have introduced the collision integral $J_\nu(\nu = \mathrm{L}\text{ or }\mathrm{R})$ as

$$\begin{aligned} J_\nu &\equiv n_\nu S \int dv|v-V|\{\Lambda\Theta(\varepsilon^\nu(V''-v''))P(V'',t)\phi(v'',T_\nu,m_\nu) \\ &\quad -\Theta(\varepsilon^\nu(V-v))P(V,t)\phi(v,T_\nu,m_\nu)\}, \end{aligned} \tag{5.2}$$

where v'' and V'' represent the pre-collision velocities of the molecule vertical to the piston and those of the piston, respectively, which lead to the corresponding velocities v and V, and $\Lambda \equiv 1/e^2$. Here, we have introduced the area of the piston S, Maxwell distribution $\phi(v,T,m) \equiv \sqrt{m/2\pi T}\exp(-mv^2/2T)$, and Heaviside function $\Theta(x) = 1(x \geq 0)$ and $\Theta(x) = 0(x < 0)$ with $\varepsilon^{\mathrm{L}} \equiv -1$ and $\varepsilon^{\mathrm{R}} \equiv +1$. P_ν^v represents the one-dimensional momentum change of the piston for each collision between the gas molecule of velocity v in ν side and the piston.

The Kramers-Moyal expansion of Eq. (5.1) results into

$$\frac{\partial P}{\partial t} + \frac{\partial}{\partial V}\frac{F_{\mathrm{fri}}}{M}P = \sum_{n=1}^{\infty}\frac{(-1)^n}{n!}\frac{\partial^n}{\partial V^n}\left\{\epsilon_{\mathrm{L}}^n A_n^L(V) + \epsilon_{\mathrm{R}}^n A_n^L(V)\right\}P. \tag{5.3}$$

Here we have introduced the small parameter $\epsilon_\nu \equiv m_\nu/M$, and

$$A_n^L = \left(\frac{1+e_{\mathrm{L}}}{1+\epsilon_{\mathrm{L}}}\right)^n v_{\mathrm{L}}^{n+1} n_{\mathrm{L}} S K_n^-\left(\frac{V}{v_{\mathrm{L}}}\right), \tag{5.4}$$

$$A_n^R = \left(-\frac{1+e_{\mathrm{R}}}{1+\epsilon_{\mathrm{R}}}\right)^n v_{\mathrm{R}}^{n+1} n_{\mathrm{R}} S K_n^+\left(\frac{V}{v_{\mathrm{L}}}\right), \tag{5.5}$$

$(n = 1, 2, \cdots)$. We also define

$$K_n^+(x) \equiv \int_{-\infty}^{x} dy\tilde{\phi}_{\mathrm{R}}(y)(x-y)^{n+1}, \tag{5.6}$$

$$K_n^-(x) \equiv \int_{x}^{\infty} dy\tilde{\phi}_{\mathrm{L}}(y)(y-x)^{n+1}, \tag{5.7}$$

where $\tilde{\phi}_\nu(\nu = \mathrm{L}\text{ or }\mathrm{R})$ is the dimensionless VDF for each bath. Assuming the symmetric property of the VDF $\tilde{\phi}_\nu(x) = \tilde{\phi}_\nu(-x)$, $K_n^\pm(x)$ has the symmetric property and the recurrence relation:

$$K_n^+(-x) = K_n^-(x), \tag{5.8}$$

$$K_{n+2}^\pm(x) = \pm x K_{n+1}^\pm(x) + \left(1+\frac{n}{2}\right)K_n^\pm(x), \tag{5.9}$$

whose derivations are straightforward. We should note that the Botlzmann-Lorentz equation Eq. (5.1) is equivalent to the SDE driven by the state-dependent compound Poissonian processes:

$$M\frac{d\hat{V}}{dt} = F_{\mathrm{fri}}(\hat{V}) + F_L(t;\hat{V}) + F_R(t;\hat{V}), \tag{5.10}$$

where $\hat{F}_\nu(\nu = \mathrm{L}\text{ or }\mathrm{R})$ is the stochastic force acting on the piston due to the kick from ν side of the piston, and $\hat{V}$ denote the stochastic velocity of the piston. We

assume that the stochastic forces $\hat{F}_\nu$ can be described by the state-dependent compound white Poissonian process:

$$\hat{F}_\nu \equiv \sum_v P_\nu^v(\hat{V}) \cdot \hat{\xi}_\nu^v(t|\hat{V}), \tag{5.11}$$

$$P_\nu^v(\hat{V}) \equiv \frac{1+e_\nu}{2}\frac{2\epsilon_\nu^2}{1+\epsilon_\nu^2}M(v-\hat{V}), \tag{5.12}$$

($\nu =$ L or R), where $\hat{\xi}_\nu^v(t|\hat{V})$ is one-sided Poissonian noise whose probability is equivalent to collision probability for gas molecules of the velocity between v and $v+dv$ on the piston:

$$\lambda_v^\nu \equiv dv|v-\hat{V}| \cdot \Theta(\varepsilon^\nu(\hat{V}-v))n_\nu A\phi(v,T_\nu). \tag{5.13}$$

Let us prove the equivalency between the stochastic equation of motion Eq. (5.10) and the Boltzmann-Lorentz equation (5.1). See also Chapter 3. For an arbitrary analytic function $h = h(\hat{V})$, its differentiation $dh(\hat{V}) \equiv h(\hat{V}+d\hat{V}) - h(\hat{V})$ can be represented as

$$\begin{aligned}
dh(\hat{V}) &= \sum_{n=1}^\infty \frac{(d\hat{V})^n}{n!} \cdot \frac{\partial^n h}{\partial V^n}\bigg|_{V=\hat{V}} \\
&= \sum_{n=1}^\infty \frac{1}{n!}\left\{\sum_v\left(\frac{P_\nu^v}{M}\cdot d\hat{L}_{\rm L}^v\right) + \sum_v\left(\frac{P_\nu^v}{M}\cdot d\hat{L}_{\rm R}^v\right) + \frac{\hat{F}_{\rm fri}}{M}dt\right\}^n \cdot \frac{\partial^n h}{\partial V^n}\bigg|_{V=\hat{V}} \\
&= \sum_{n=1}^\infty \frac{1}{n!}\sum_{\nu={\rm L,R}}\left\{\sum_v\left(\frac{P_\nu^v}{M}\cdot d\hat{L}_\nu^v\right)^n\right\} \cdot \frac{\partial^n h}{\partial V^n}\bigg|_{V=\hat{V}} + dt\frac{\hat{F}_{\rm fri}}{M}\cdot\frac{\partial h}{\partial V}\bigg|_{V=\hat{V}} \\
&\quad + o(dt),
\end{aligned} \tag{5.14}$$

where we substitute $d\hat{V} = \sum_{v,\nu}(P_\nu^v \cdot d\hat{L}_\nu^v/M) + \hat{F}_{\rm fri}dt/M$ into the Taylor expansion of h and pick up only $O(dt)$ terms. Here, we have introduced the total differentiation $d\hat{L}_\nu^v$ of $L_\nu^v(t|\hat{V}) \equiv \int_0^t \hat{\xi}_\nu^v(s|\hat{V})ds$ ($\nu =$ L or R), noting that $(d\hat{L}_\nu^v)^n = O(dt)$, $d\hat{L}_{\rm L}^v \cdot d\hat{L}_{\rm R}^v = o(dt)$ and $d\hat{L}_\nu^v \cdot d\hat{L}_\nu^{v'} = o(dt)$ for $v \neq v'$. The ensemble average and the partial integral of Eq. (5.14) leads to

$$\begin{aligned}
\frac{\partial P}{\partial t} &= -\frac{\partial}{\partial V}\left\{\frac{F_{\rm fri}}{M}P(V,t)\right\} + \sum_{n=1}^\infty \frac{(-1)^n}{n!}\frac{\partial^n}{\partial V^n}\left\{\sum_{\nu={\rm L,R}}\sum_v\left(\frac{P_\nu^v}{M}\right)^n\lambda_v^\nu P\right\} \\
&= -\frac{\partial}{\partial V}\left\{\frac{F_{\rm fri}}{M}P(V,t)\right\} \\
&\quad + \sum_{n=1}^\infty \frac{(-1)^n}{n!}\frac{\partial^n}{\partial V^n}\left[\left\{n_{\rm L}A\int_V^\infty dv\left(\frac{P_\nu^v}{M}\right)^n|v-V|\phi(v,T_{\rm L})\right\}P\right. \\
&\quad \left. + \left\{n_{\rm R}A\int_{-\infty}^V dv\left(\frac{P_\nu^v}{M}\right)^n|v-V|\phi(v,T_{\rm R})\right\}P\right],
\end{aligned} \tag{5.15}$$

where we have used the martingale property of Itô product as $\langle (P_\nu^v(\hat{V})/M)^n \cdot d\hat{L}_\nu^v \rangle = \langle (P_\nu^v(\hat{V})/M)^n \rangle \langle (d\hat{L}_\nu^v)^n \rangle = (P_\nu^v(V)/M)^n \lambda_v^\nu dt$. The last equation in Eq. (5.15) is well known to be derived through the Kramers-Moyal expansion of the right-hand side of Eq. (5.1) [7]. Thus, Eq. (5.10) is equivalent to the Boltzmann-Lorentz equation Eq. (5.1). In the macroscopic piston limit $\epsilon_{\rm L}$ and $\epsilon_{\rm R} \to 0$ and in the absence of sliding friction, Eq. (5.10) is reduced to the Langevin equation driven by a Gaussian noise without drift. To observe the motion with non-zero average velocity, the finiteness of $\epsilon_{\rm L}$ and $\epsilon_{\rm R}$ necessary.

5.3 Fluctuating motion of adiabatic piston under dry friction

We consider the case with $m_{\rm L} = m_{\rm R}$ and $p = n_{\rm L} T_{\rm R} = n_{\rm R} T_{\rm R}$ called the adiabatic piston problem. We define the small parameter $\epsilon \equiv \sqrt{\epsilon_{\rm L}} = \sqrt{\epsilon_{\rm R}}$.

Here, the piston is assumed to move along the container under the influence of dry friction from the side walls

$$\hat{F}_{\rm fri} \equiv -\epsilon \bar{F}_{\rm fri} f_{\rm fri}(\hat{V}), \tag{5.16}$$

$$f_{\rm fri}(V) = {\rm sgn}(V) \tag{5.17}$$

where ${\rm sgn}(x) = x/|x|$ is the sign function [33–40], and $\bar{F}_{\rm fri}$ will be determined later.

Let us derive the average velocity of the piston under dry friction. At first, we derive the steady VDF for the piston, and then we derive the average velocity. Truncating Eq. (5.3) at $O(\epsilon^2)$, we obtain the Fokker-Planck-like equation for $P = P(V,t)$ up to $O(\epsilon^2)$:

$$\begin{aligned} \frac{\partial P}{\partial t} &= \epsilon \frac{\gamma_0}{M} \left[\frac{\partial}{\partial V} \left\{ V + \mu_0 v_{T_e} {\rm sgn}(V) \right\} P + \frac{v_{T_e}^2}{2} \frac{\partial^2 P}{\partial V^2} \right] \\ &\quad + \epsilon^2 C \frac{\gamma_0}{M} \left[\frac{\partial}{\partial V} \frac{V^2}{v_{T_e}} P - \frac{v_{T_e}^3}{4} \frac{\partial^3 P}{\partial V^3} \right] + O(\epsilon^3). \end{aligned} \tag{5.18}$$

Here, the first two terms on the right-hand side of Eq. (5.18) proportional to the first derivative term in Eq. (5.18) represents the force. Thus, the proportional constant of the friction force in Eq. (5.16) can be determined as

$$\bar{F}_{\rm fri} \equiv \mu_0 \gamma_0 v_{T_e} \tag{5.19}$$

with $\gamma_0 \equiv \gamma_{\rm L} + \gamma_{\rm R}$,

$$\gamma_\nu \equiv \frac{2(1+e)}{\sqrt{\pi}} \frac{pS}{v_{T_\nu}} \tag{5.20}$$

($\nu = {\rm L}$ or R), the effective temperature $T_e \equiv (1+e)\sqrt{T_{\rm L} T_{\rm R}}/2$ and the friction constant μ_0. The steady state VDF $P_{\rm ss}(V)$ up to $O(\epsilon)$ can be readily obtained

from Eq. (5.18):

$$
\begin{aligned}
P_{\rm ss}(V) &= (1+\epsilon a_1(V)+O(\epsilon^2))P_0(V), && (5.21)\\
P_0(V) &\equiv \frac{1}{Z}\exp\left[-\frac{M}{2T_e}(V^2+2\mu_0 v_{T_e}|V|)\right], && (5.22)\\
a_1(V) &\equiv C\left\{-\mu_0 {\rm sgn}(V)\left(\frac{MV^2}{T_e}-1\right)\right. && (5.23)\\
&\quad \left.+\left(1-2\mu_0^2\right)\frac{V}{v_{T_e}}-\frac{V^3}{3v_{T_e}^3}\right\},\\
C &\equiv \sqrt{\pi T_e}\left(\frac{1}{\sqrt{T_{\rm L}}}-\frac{1}{\sqrt{T_{\rm R}}}\right), && (5.24)
\end{aligned}
$$

where we have introduced the normalized constant $Z \equiv \sqrt{\pi} v_{T_e} e^{\mu_0^2} {\rm erfc}(\mu_0)$, It should be noted that the restitution coefficient only appears through γ_0 and T_e.

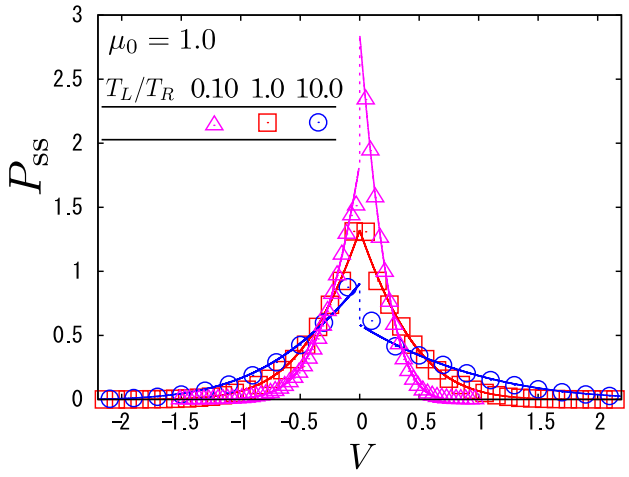

Figure 5.2: The obtained steady state VDFs Eqs. (5.21) - (5.24) for $\mu_0 = 1.0$ and $e = 0.9$ are verified through the simulation of Eq. (5.10). We average the data over 1000 ensembles with the time average for $0 < t/t_0 < 400$. Purple triangles, red squares and blue circles are data for $T_{\rm L}/T_{\rm R} = 0.10, 1.0, 10.0$, respectively, where the corresponding theoretical curves are represented by solid lines and dashed lines denote discontinuity at $V = 0$.

References [37–40] reports the existence of the discontinuity and the cusp singularity in VDFs of a stochastic motion of the piston under dry friction. As we expected, we obtain the consistent results with those in the previous studies, i.e. there exists a discontinuity at $V = 0$ for $T_{\rm L} \neq T_{\rm R}$, and the cusp-like singularity appears at $V = 0$ for $T_{\rm L} = T_{\rm R}$. The obtained singularity is close to that in Ref. [38, 39], while the singularities appear at $V \neq 0$, in addition to

$V = 0$ in Ref. [40]. We note that the amount of gap at $V = 0$ increases linearly with μ_0.

We numerically solve Eq. (5.10) for $0 < t/t_0 < 400$ and average the data over 1000 ensembles, to obtain the data for VDF and compare it with Eq. (5.21) in Fig. 5.2 for $e = 0.9$ and $\mu_0 = 1.0$. As can be seen from Fig. 5.2, it is obvious that our theory precisely reproduces the results of the simulation.

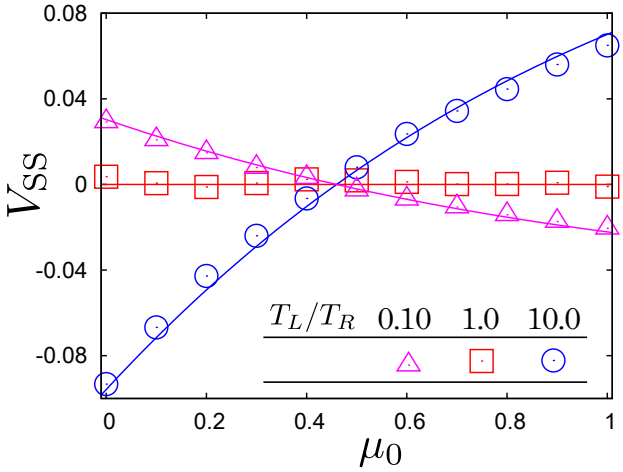

Figure 5.3: Reverse motion of the adiabatic piston against the friction constant μ_0 is verified for $e = 0.9$. We numerically solve Eq. (5.10) and take steady state average for $0 < t/t_0 < 400$. The numerical data are obtained from the ensemble average over 1000 samples. Purple triangles, red squares and blue circles are data for $T_{\rm L}/T_{\rm R} = 0.10, 1.0, 10.0$, respectively, where the corresponding theoretical curves are represented by solid lines.

To examine our theoretical consideration below, we adopt the velocity Verlet method for time integration of Eq. (5.10) with time interval $dt/t_0 = 0.01$, where we have introduced $t_0 \equiv x_0/v_{T_{\rm R}}$, and $x_0 \equiv M v_{T_{\rm R}}^2/pS$. We discretize the jump rates λ_v^ν by replacing dv by $\Delta v_\nu = v_{T_\nu}/50$ and v by v_i with $-10 v_{T_\nu} < v_i < 10 v_{T_\nu}$ for $\nu = {\rm L}$ or R and $1 \le i \le 1000$, with the thermal velocity $v_T \equiv \sqrt{2T/M}$ of the temperature T. $e = 0.9$ and $\epsilon = 0.1$ are fixed for our simulations.

In the absence of dry friction, it is known that the piston moves toward the high-temperature side under the condition $n_{\rm L} T_{\rm L} = n_{\rm R} T_{\rm R}$ and $T_{\rm L} \neq T_{\rm R}$. As will be shown, however, the direction of the piston motion can be reversed under the dry friction. Indeed, the averaged steady state velocity of the piston defined by $V_{\rm SS} \equiv \int dV V P_{\rm ss}(V)$ is given by:

$$V_{\rm SS} = V_{\rm ad} \left\{ 1 + 4\mu_0 \left(\mu_0 - \frac{\mu_0^3}{3} - \frac{7}{6\sqrt{\pi} e^{\mu_0^2} {\rm erfc}(\mu_0)} + \frac{\mu_0^2}{3\sqrt{\pi} e^{\mu_0^2} {\rm erfc}(\mu_0)} \right) \right\} + O(\epsilon^2), \tag{5.25}$$

where we have introduced $V_{\rm ad}$ as the steady velocity of the piston without any dry friction:

$$V_{\rm ad} \equiv \epsilon \frac{\sqrt{\pi}}{4} v_{T_e}^2 \left(\frac{1}{v_{T_{\rm L}}} - \frac{1}{v_{T_{\rm R}}} \right). \tag{5.26}$$

The notable fact in Eq. (5.25) is that the direction of the piston motion is changed around $\mu_0 \simeq 0.46$ (see Fig. 5.3).

The validity for Eq. (5.25) is verified through the direct simulation of Eq. (5.10) and is shown in Fig. 5.3, where we average the data for $0 < t/t_0 < 400$ and the ensemble average is taken over 1000 samples. As can be seen in Fig. 5.3, Eq. (5.25) correctly predicts the accurate behavior of Eq. (5.10).

Through the expansion in terms of ϵ up to $O(\epsilon^2)$, Eq. (5.10) under the steady state average is reduced to

$$0 \quad = \quad -\epsilon\gamma_0 V_{\rm SS} + \epsilon^2 \frac{C\gamma_0}{2v_{T_e}} \left\langle V^2 \right\rangle_{\rm SS} - \epsilon^2 C \bar{F}_{\rm fri} \check{f}(\mu_0), \tag{5.27}$$

where we have introduced the positive function

$$\check{f}(\mu_0) \equiv \frac{\mu_0}{2} + \frac{\mu_0^3}{3} + \frac{2-\mu_0^2}{3\sqrt{\pi}{\rm erfc}(\mu_0)e^{\mu_0^2}} > 0. \tag{5.28}$$

Here, the second term on the right-hand side of Eq. (5.27) is the force due to MDD [156], and the direction of the steady friction force is opposite to MDD, from which the change of direction of the piston motion originates. As the friction force becomes larger, it can be shown that the sign of $V_{\rm SS}$ is switched, because $\left\langle V^2 \right\rangle_{\rm SS} > 0$ and $\check{f}(\mu_0) > 0$. Thus, in contrast to systems without any dry friction, the direction of the piston motion under the dry friction does not correspond to that of the force due to MDD.

5.4 Roles of nonlinearity of sliding friction

We have discussed the inverse motion of the adiabatic piston under dry friction and the origin of the inverse motion on the basis of the Boltzmann-Lorentz equation in Sec. 5.3. One can ask whether the inverse motion is generic. Here, we consider several types of velocity dependence of the side-wall friction [25] and find that any nonlinear friction reverses the piston motion, while the linear one

does not. We consider the following velocity dependences of friction $F_{\rm fri}(V)$:

$$\text{Dry friction}: \qquad F_{\rm fri}(V) = -\mu_0' pS\,\mathrm{sgn}(V), \tag{5.29}$$

$$\text{Velocity weakening} + \text{strengthening} \qquad F_{\rm fri}(V) = -\mu_0' pS \times \left\{1 + (V/v_{\rm R} - \mathrm{sgn}(V))^2\right\} \mathrm{sgn}(V) \tag{5.30}$$

$$\text{Dry} + \text{Viscous friction}: \qquad F_{\rm fri}(V) = -\mu_0' pS \left\{ \frac{V}{v_{\rm R}} + \mathrm{sgn}(V) \right\}, \tag{5.31}$$

$$\text{Smoothed dry friction}: \qquad F_{\rm fri}(V) = -\mu_0' pS \tanh\left(\frac{V}{v_{\rm R}}\right), \tag{5.32}$$

$$\text{Viscous friction}: \qquad F_{\rm fri}(V) = -\mu_0' pS \frac{V}{v_R}, \tag{5.33}$$

where we have introduced a new dimensionless friction coefficient μ_0'. In Fig. 5.4, we plot the friction coefficient dependence of the average steady velocity of the piston $V_{\rm SS}$ fixing $T_{\rm L}/T_{\rm R} = 10.0$. It is remarkable that nonlinear frictions such as dry (squares), weakening and strengthening (diamonds), dry and viscous (piles), and smoothed dry (triangles) friction inverse the direction of the piston motion, while linear friction (circles) does not.

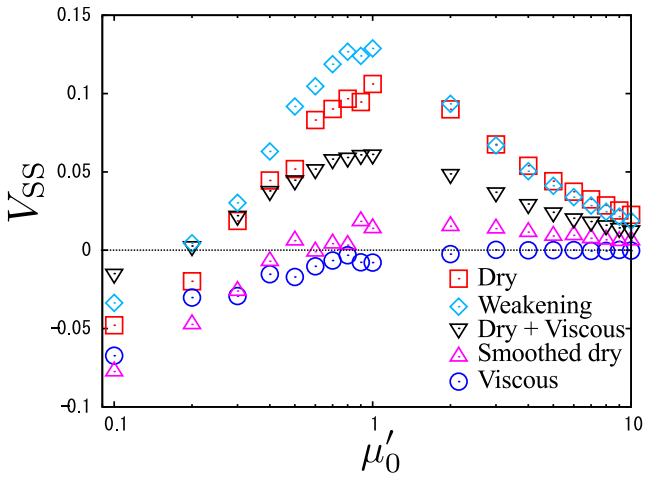

Figure 5.4: Average velocity of the piston $V_{\rm SS}$ against μ_0'. Nonlinear frictions such as dry (squares), weakening and strengthening (diamonds), dry and viscous (piles), and smoothed dry (triangles) friction inverse the direction of the piston motion, while linear friction (circles) does not.

The absence of the inverse motion of a piston under linear friction can be understood as follows. Let us write the side-wall friction as

$$F_{\rm lin}(V) = -\gamma_{\rm lin} V \tag{5.34}$$

where $\gamma_{\rm lin}$ represents the viscous friction coefficient. Taking the steady state average of Eq. (5.10), we obtain

$$0 = -\epsilon\gamma_0 V_{\rm SS} + \epsilon^2 \frac{C\gamma_0}{2v_{T_e}} \left\langle V^2 \right\rangle_{\rm SS} - \gamma_{\rm lin} V_{\rm ss}. \tag{5.35}$$

Hence, the average velocity is written as

$$V_{\rm ss} = \frac{V_{\rm ad}}{1 + \gamma_{\rm lin}/\epsilon\gamma_0}, \tag{5.36}$$

where the sign of $V_{\rm ss}$ turns out to be the same as $V_{\rm ad}$. The remarkable difference between Eqs. (5.27) and (5.35) is the third term on the right-hand side. The third term in Eq. (5.27) depends on C, while the one in Eq. (5.35) does not. We can conclude that the direction of piston motion depends on the amplitude and the nonlinearity of the velocity dependence for the side-wall friction.

5.5 Fluctuation theorems under dry friction

Let us discuss the large deviation property [157] for the work done by the system under dry friction. Fluctuation relation is one of the universal relations in non-equilibrium systems found in the last a few decades [158–162]. The fluctuation relation for frictionless granular systems has been reported recently [163]. The fluctuation relations under dry friction are derived for the work done by the non-fluctuating external system under the dry friction in Ref. [166], and experimentally discussed in Ref. [30, 164, 165]. However, the work done by the fluctuating gas under dry friction has not been investigated. Here, we derive a fluctuation relation for the work done by the gas under dry friction, considering the excess work defined by $d\hat{W}'_{\rm L} \equiv d\hat{W}_{\rm L} - F_0 \hat{V} dt$, $d\hat{W}_{\rm L}/dt \equiv \sum_v \{M(V^2 - V''^2)/2\} \cdot \hat{\xi}^v_{\rm L}(t|\hat{V})$, with the pre-collisional velocity V'' and $F_0 \equiv \langle \hat{F}_{\rm L}(V=0) \rangle = (1+e)pS/\{2(1+\epsilon^2)\}$ in terms of the perturbation of small μ_0, as shown in Appendix. A. Introducing the distribution for the excess power $\mathcal{P}(p_w, t) \equiv \langle \delta(\hat{W}'_{\rm L}(t) - p_w t) \rangle$, we obtain the fluctuation relation under dry friction up to $O(\epsilon, \mu_0)$:

$$\begin{aligned} \lim_{t\to\infty} \frac{1}{t} \ln \frac{\mathcal{P}(p_w, t)}{\mathcal{P}(-p_w, t)} &= \Delta\beta_e p_w + \frac{\bar{F}_{\rm fri}}{pS} B(p_w) p_w \\ &\quad + O(\epsilon^2, \mu_0^2), \end{aligned} \tag{5.37}$$

where we have introduced the difference of inverse temperatures

$$\Delta\beta_e \equiv \frac{2}{1+e} \left(\frac{1}{T_{\rm R}} - \frac{1}{T_{\rm L}} \right), \tag{5.38}$$

and the nonlinear function of p_w

$$B(p_w) \equiv \sqrt{\frac{v_{T_{\rm L}}}{v_{T_e}}} \frac{\sqrt{C^*(p_w)}}{(1+e)T_e} \tag{5.39}$$

$$C^{*2}(p_w) \equiv \frac{1 + (\tilde{T}^{1/4} - \tilde{T}^{-1/4})^2}{1 + 2\pi(p_w/\epsilon p S v_{T_e})^2/(1+e)^3} \tag{5.40}$$

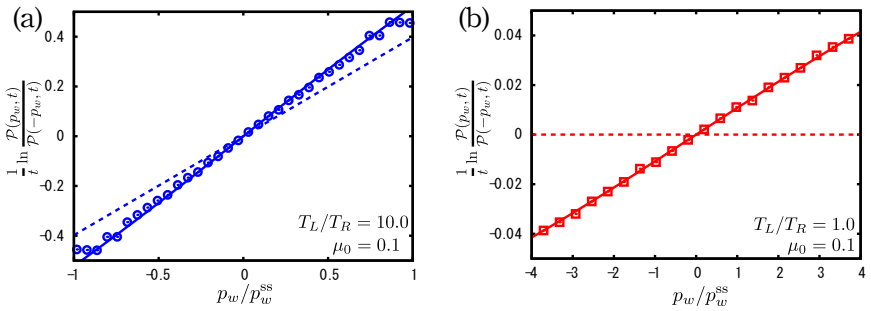

Figure 5.5: The fluctuation relation under dry friction Eq. (5.37) is verified through our simulation for $\mu_0 = 0.1, e = 0.9$ and $t/t_0 = 20.0$, where theoretical curves are represented by solid lines. The number of samples is 2.5×10^5. Blue circles in (a) and red squares in (b) are the numerical data for $T_{\rm L}/T_{\rm R} = 10.0, 1.0$, respectively. The blue and red dashed lines are theoretical lines without dry friction for $T_{\rm L}/T_{\rm R} = 10.0, 1.0$, respectively. The events satisfying $p_w < -p_w^{\rm ss}$ for $T_{\rm L}/T_{\rm R} = 10.0$ are so rare events that they could not be detected through our calculation, while numerical data for $T_{\rm L}/T_{\rm R} = 1.0$ agree with the theoretical curve for large $|p_w/p_w^{\rm ss}|$

with $\tilde{T} \equiv T_{\rm L}/T_{\rm R}$. See Appendix A for the derivation of the fluctuation relation. We solve Eq. (5.10) with $\mu_0 = 0.1$ and $e = 0.9$ for $0 < t/t_0 \leq 20.0$ to verify the validity of Eq. (5.37) as shown in Fig. 5.5 (a) for $T_{\rm L}/T_{\rm R} = 10.0$ and (b) for $T_{\rm L}/T_{\rm R} = 1.0$, where the number of samples is 2.5×10^5. Blue circles of Fig. 5.5 (a) and red squares of Fig. 5.5 (b) are the numerical data for $T_{\rm L}/T_{\rm R} = 10.0, 1.0$, respectively, and the solid curves denote the corresponding theoretical curves. The blue and red dashed lines are theoretical lines without dry friction for $T_{\rm L}/T_{\rm R} = 10.0, 1.0$, respectively. Here we use the scaled p_w by the corresponding steady state value $p_w^{\rm ss} = 0.2099$ for $T_{\rm L}/T_{\rm R} = 10.0$ and $p_w^{\rm ss} = 0.01281$ for $T_{\rm L}/T_{\rm R} = 1.0$, respectively. We only plot the data for $|p_w/p_w^{\rm ss}| < 1$ for $T_{\rm L}/T_{\rm R} = 10.0$ because the events satisfying $p_w < -p_w^{\rm ss}$ are so rare events that they could not be detected through our calculation. On the other hand, numerical data for $T_{\rm L}/T_{\rm R} = 1.0$ agree with the theoretical curve even for large $|p_w/p_w^{\rm ss}|$.

5.6 Summary and discussion

In this chapter, we have clarified the roles of nonlinear sliding friction in the fluctuating motion of an adiabatic piston surrounded by two thermal temperatures. Through the analysis of the Boltzmann-Lorentz equation Eq. (5.1) under dry friction, we have found the singularities only at $V = 0$ as those in Ref. [38, 39], while they are different from those in Ref. [40]. VDF of a fluctuating piston has a cusp-like singularity for $T_{\rm L} = T_{\rm R}$ and a discontinuity at $V = 0$ for $T_{\rm L} \neq T_{\rm R}$,

as in Eqs. (5.21) - (5.24) and Fig. 5.2. For dry frictional case, we have obtained the friction dependence of the velocity of the piston motion in Eq. (5.25), whose direction is changed above the threshold of the friction const μ_0, as in Fig. 5.3. The change of the direction of the piston motion has not been reported in the previous studies for the fluctuating piston under dry friction [38–40]. We have clarified the role of nonlinearity of sliding friction, by considering the various velocity dependences of the friction and have found that an arbitrary nonlinear friction can reverse the motion of the piston, while the linear (viscous) friction cannot. We have also demonstrated that the conventional fluctuation relation for the fluctuating work is modified due to the existence of dry friction.

Chapter 6

Non-equilibrium Brownian motion as a non-equilibrium probe

Abstract

The dynamics of a rotor under viscous or dry friction is investigated as a non-equilibrium probe of a granular gas numerically and analytically. In Sec. 6.2, we briefly explain the theory on a frictionless rotor introduced in Ref. [94]. We explain the setup of our simulation in Sec. 6.3 and show that the VDF for granular gases is cylindrically symmetric. In Sec. 6.4, we briefly explain the theoretical setup to derive the inverse formula for the cylindrically symmetric granular gas [92,93]. In Sec. 6.5, we show the existence of formulas between the VDF for the gas and the angular VDF for a rotor under a viscous friction around a rotating axis. The validity of these formulas is also numerically verified in this section. In Sec. 6.6, we discuss the position dependence of the viscous rotor. In Sec. 6.7, we examine the angular VDF for a dry frictional rotor using the numerical VDF for the granular gas under gravity. In Sec. 6.8, we conclude this paper with some remarks. In Appendix. B, we examine the rotor under viscous friction in an elastic gas without gravity as a benchmark test of our simulation and formulation, where the angular VDF for the rotor is analytically obtained. In Appendices C.1 and D.1, we show the detailed calculation of our analytic formulas for the viscous and dry frictional rotors, respectively. We explain the detailed procedure to apply our formulas to the viscous and dry frictional rotors in Appendices C.2 and D.2, respectively.

6.1 Introduction

In the previous chapter, we have rectified the motion of the piston from the temperature difference between two gases, where the fluctuations of the left and right gases are different. In this chapter, we consider a symmetric rotor in a single granular gas to clarify the role of the rotor as a non-equilibrium probe. We ask a question: can we rectify useful quantities from the fluctuating motion of the rotor? The molecular dynamics (MD) simulation of a realistic granular rotor is performed to demonstrate the role of a rotor as a probe to measure the VDFs of vibrating granular beds [29–32, 167–169]. We perform an event driven MD simulation of a rotating rotor around a fixed axis in a vertically vibrated granular gas under gravity as in Ref. [60].

6.2 Theory on a frictionless granular rotor

Before considering the motion of the rotor under the axial friction, let us review the theory on a frictionless granular rotor [94]. The fluctuating motion of the arbitrarily shaped rotor without the axial friction can be described by the following Boltzmann-Lorentz equation [3, 7, 8, 94–97]:

$$\frac{\partial P}{\partial t} = \int_{-\infty}^{\infty} dy \left\{ \mathbb{W}_{\epsilon_{\rm rot}}(\omega - y; y) P(\omega - y, t) - \mathbb{W}_{\epsilon_{\rm rot}}(\omega; y) P(\omega, t) \right\}, \quad (6.1)$$

where the transition rate $\mathbb{W}_{\epsilon_{\rm rot}}$ is introduced as

$$\begin{aligned} \epsilon_{\rm rot} \mathbb{W}_{\epsilon_{\rm rot}}(\omega; y) &\equiv \rho h \int_{\rm surf} d\varrho \int d\boldsymbol{v} \phi(\boldsymbol{v}) \Theta(V_n(\varrho) - v_n) \\ &\quad \times |V_n(\varrho) - v_n| \delta \left(\frac{y}{\epsilon_{\rm rot}} - \Delta\bar{\omega} \right), \quad (6.2) \\ \boldsymbol{V}(\varrho) &\equiv \omega \boldsymbol{e}_z \times \boldsymbol{r}(\varrho), \quad (6.3) \\ \Delta\bar{\omega} &\equiv (1+e) \frac{g(\varrho)}{R_I} \frac{V_n - v_n}{1 + \epsilon_{\rm rot} g^2(\varrho)}, \quad (6.4) \\ g(\varrho) &\equiv \frac{r_t(\varrho)}{R_I}. \quad (6.5) \end{aligned}$$

Here, $\boldsymbol{t}(\varrho) \equiv \boldsymbol{e}_z \times \boldsymbol{n}(\varrho), R_I \equiv \sqrt{I/M}$ are introduced, where the subscript n and t represent the normal and tangential component of the corresponding vector variable, respectively. $\boldsymbol{n}$ and $\boldsymbol{t}$ are normal and tangential unit vector on the surface of the rotor, respectively(Fig. 6.1). $\epsilon_{\rm rot} \equiv m/M$ represents the small parameter with the mass of the rotor M and that of a granular particle m. The restitution coefficient between rotor and particles are represented by e. The integral $\int_{\rm surf} d\varrho$ represents the integral along the surface of the rotor (Fig. 6.1), which depends on the shape of the rotor. Note that such a set of equations is widely used in systems, such as granular gases activated by a white noise thermostat [72, 170–174].

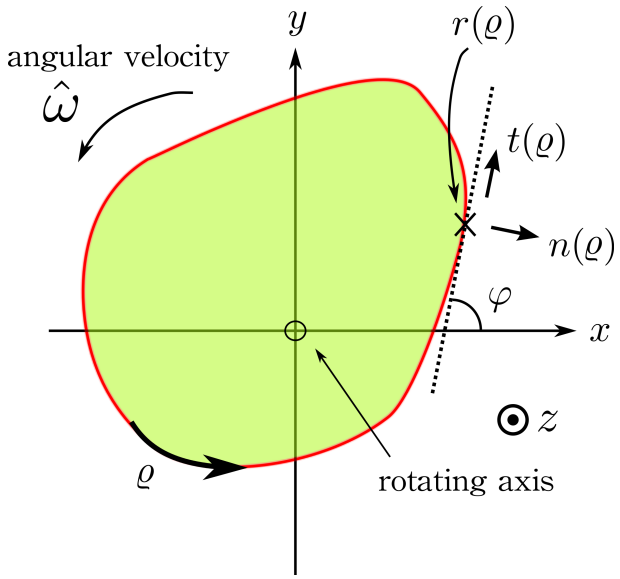

Figure 6.1: Schematic picture of an arbitrary shaped rotor

From next section, we analyze the dynamics of the rotor in vibrating granular beds to derive the relationship between the angular VDF of the rotor under viscous or dry friction and the VDF of the granular gas [92,93]. We demonstrate that the angular VDF of the rotor is correctly predicted from the VDFs of the granular gas, and is vice versa using our derived formulas. Because the motion of the rotor in vibrating beds can be easily observed in experiments, our method is, in particular, useful in the following two situations: Experiments for both vibrating granular gases deep inside a three dimensional container and the gases in an opaque container. Furthermore, we demonstrate that our formulas are valid even for the rotor near the boundary of the container. We thus indicate that the granular rotor under viscous or dry friction can be used as a local probe for a realistic granular gas.

6.3 Simulation Setup

A schematic figure of our setup is illustrated in Fig. 6.2. We prepare $N = 100$ frictionless grains of diameter $d = 0.02\sqrt{A}$ and mass m under gravity g in a quasi-two-dimensional container (area $A = L_{\rm box}^2$, height $H_{\rm box} = 0.1L_{\rm box}$). The VDF is different from the Gaussian for inelastic grains under gravity and vibration ($e_g < 1$). Following Refs. [175, 176], we adopt $e_g = 0.71$ for inelastic grains, which is the effective restitution coefficient for low-density polyethylene. The restitution coefficient between grains and the side wall is chosen to be identical to that for collisions between grains. We do not consider neither the

rotational motion of grains nor the tangential contact force between grains in this paper because the effect of the tangential friction of spherical grains can be absorbed into the effective normal restitution coefficient if the duration time of grains is negligible [177–180].

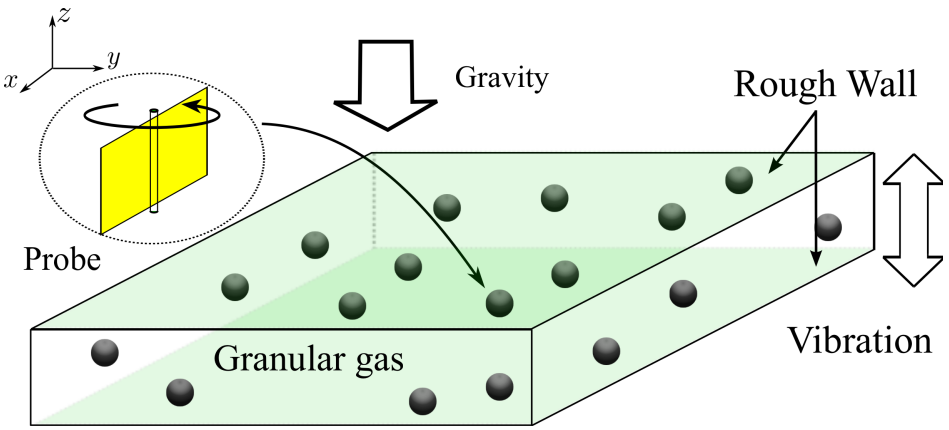

Figure 6.2: Schematic picture of our simulation.

The origin of the system in the laboratory frame $(x, y, z) = (0, 0, 0)$ is chosen to be the bottom center of the container at $t = 0$. We introduce a thin rotor of mass M rotating around the fixed axis $(x, y) = (x_0, y_0)$ under the frictional torque $\hat{N}_{\rm fri}(\hat{\omega})$ with width $w = 0.1L_{\rm box}$ and height $h = H_{\rm box} - d$ (Fig. 6.3 (a) and (b)). We introduce the restitution coefficient e between the rotor and grains and adopt $e = e_g = 0.71$. The density of the granular gas is $\rho = N/h(L_{\rm box} - d)^2$. We introduce the typical velocity of grains as $v_0 = \sqrt{gL_{\rm box}}$. We assume that the rotor is sufficiently macroscopic, i.e., $\epsilon_{\rm rot} = 0.01 \ll 1$. The local VDF for the granular gas is measured near the rotating axis in the region of $r = \sqrt{(x - x_0)^2 + (y - y_0)^2} < r_{\rm obs} \equiv 2w$ and $z_0 < z < z_0 + H_{\rm box}$.

Rough walls are introduced both on the top and the bottom of the container to distribute the energy into the horizontal direction. (See Fig. 6.3 (b).) When a grain collides against the rough wall, the post-collisional direction $\boldsymbol{n}'_\perp$ is randomized, while the kinetic energy is conserved during the collision. The scattered angles (θ_s, ϕ_s) are chosen from uniform random variables in $0 \le \phi_s \le \pi/2, 0 \le \theta_s \le 2\pi$. (See Fig. 6.3 (c).) Note that the probability density per a unit solid angle for small ϕ_s is higher than that for large ϕ_s, while that for the horizontal direction θ_s is uniform. The rough walls correspond to the walls where sandpapers are glued [181]. We inject energy into the granular gas by vertically vibrating the container in a piece-wise manner with a constant speed [182]. Figure 6.3 (d) illustrates the time evolution of the bottom wall $z = z_0$. The direction of the container motion is changed every $t_{\rm wall} = 0.1L_{\rm box}/v_0$. The maximum height of the bottom is $z_{\rm max} = 0.02H_{\rm box}$. It should be stressed that the rough wall is different from the thermal wall,

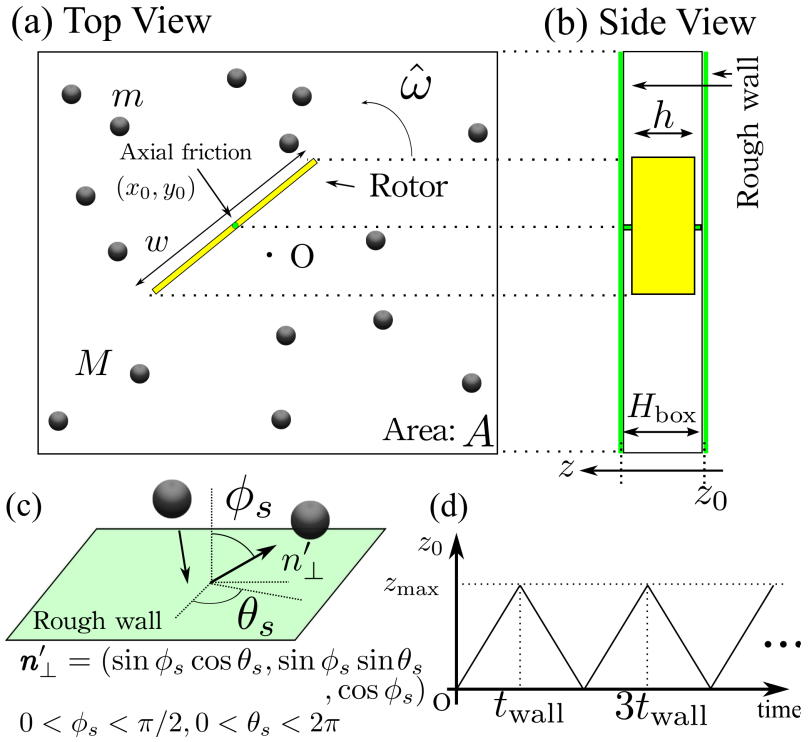

Figure 6.3: Schematics of (a) the top view and (b) the side view of our simulation. The rotor rotates around a fixed axis (x_0, y_0), and the origin O is the center of the container. Note that the size of the rotor is exaggerated. (c) The rough wall reflects the grain in random direction. (d) The container is vibrated vertically in a piece-wise linear manner. The time evolution of the bottom of the container is shown.

where the magnitude of velocity is randomly chosen from the Maxwell distribution function [183]. See Appendix B for the results of a simulation of grains associated with a thermal wall.

We here emphasize that the VDF for the gas is cylindrically symmetric. We observe the VDF in the two regions; the areas (i) and (ii). Here, the center of the area (i) is $(x, y) = (0, 0)$, and that of the area (ii) is $(x, y) = (-L_{\rm box}/4, -L_{\rm box}/4)$ (Fig. 6.4 (a)). The VDFs ϕ_α for $\alpha = x, y, z$ directions are shown in Fig. 6.4 (b), where the data are taken in the area (i). We note that VDFs even for horizontal direction deviate from Gaussian (dotted line) $\exp(-x^2/2)/\sqrt{2\pi}$ with $x = v_\alpha/v_0$. Because the rotor rotates around the vertical axis, the axis parallel to the z-axis, and the rotor cannot detect VDF for the z direction in our setup, we do not consider the VDF for v_z. Thus, we formulate the inverse formula for cylindrically symmetric gases on the basis of the Boltzmann-Lorentz equation.

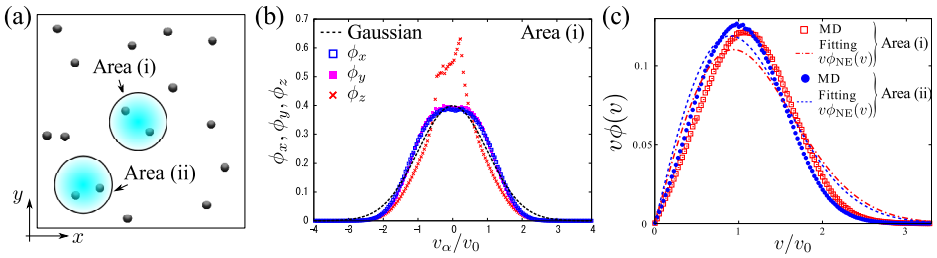

Figure 6.4: (a): The area (i) is the cylindrical area with the radius $r_{\rm obs}$ around $x = 0, y = 0$, and the area (ii) is the one around $x = -L_{\rm box}/4, y = -L_{\rm box}/4$. (b): VDFs for $\alpha = x, y, z$ directions are shown. The data are taken in the area (i). VDFs for horizontal direction are different from Gaussian (dotted line). VDF in the z direction is asymmetric due to the gravity. (c): The VDFs for $v = \sqrt{v_x^2 + v_y^2}$ in the areas (i) and (ii) are shown as open squares and filled circles, respectively. It should be noted that the VDF for the area (i) differs from that in the area (ii) due to the wall. Our observed VDFs cannot be fitted by the theoretical VDFs in Ref. [72] represented by the chain line and the dashed line for the area (i) and (ii), respectively.

We have confirmed that the VDFs are invariant whether the rotor is present or not. In Fig. 6.4 (c), the numerical data of VDFs for $v \equiv \sqrt{v_x^2 + v_y^2}$ are shown for both the areas (i) and (ii). It should be noted that the VDF in the areas (i) (open squares) differs from that in the area (ii) (filled circles) because of the influence of the wall. In this paper, we consider only the area (i) in Secs. 6.5 and 6.7, while we discuss the data for both area (i) and (ii) in Sec. 6.6.

Let us compare our obtained VDFs with that for granular gases activated by a white noise thermostat [72], which is phenomenologically used for the analysis of vibrating granular gases [76]. We note that our observed VDFs cannot be fitted by that in Ref. [72], which is written as $\phi_{\rm NE}(v) = (1 + a_2 S_2(v^2/v_{\rm th}^2))\phi_{\rm G}(v/v_{\rm th})/v_{\rm th}^2$ with $\phi_{\rm G}(x) \equiv \exp(-x^2/2)/2\pi$, $a_2 = 16(1-e_g)(1-2e_g^2)/\{185 - 153e_g + 30(1-e_g)e_g^2\}$, and $S_2(x) = x^2/2 - 2x + 1$. Here, $v_{\rm th}$ corresponds to a fitting parameter in our setup. The fitting results are shown in Fig. 6.4 (c) and $v_{\rm th}/v_0 = 0.935587$ and $v_{\rm th}/v_0 = 0.900656$ for the areas (i) (chain line) and (ii) (dashed line), respectively.

6.4 Theoretical starting point

We explain our theoretical starting point for the cylindrically symmetric granular gases. We only consider the two-dimensional VDF $\phi = \phi(v_x, v_y)$ for grains to calculate the angular VDF for the rotor. The time evolution of the PDF of the angular velocity of the rotor $P = P(\omega, t)$ can be described by the Boltzmann-

Lorentz equation [3, 7, 8, 94–97]:

$$\frac{\partial P}{\partial t} + \left\{ \frac{\partial}{\partial \omega} N_{\rm fri} P \right\} = \int_{-\infty}^{\infty} dy \left\{ \mathbb{W}_{\epsilon_{\rm rot}}(\omega - y; y) P(\omega - y, t) - \mathbb{W}_{\epsilon_{\rm rot}}(\omega; y) P(\omega, t) \right\}, \tag{6.6}$$

$$\epsilon_{\rm rot} \mathbb{W}_{\epsilon_{\rm rot}}(\omega; y) = \rho h \int_0^{2w} d\varrho \int_{-\infty}^{\infty} dv_x dv_y \phi(v_x, v_y) \Theta(V_n(\varrho) - v_n) \times |V_n(\varrho) - v_n| \delta \left(\frac{y}{\epsilon_{\rm rot}} - \Delta\bar{\omega} \right), \tag{6.7}$$

We have introduced ϱ as a coordinate variable along the surface of the rotor, running over $0 < \varrho < 2w$ [94]. According to Chapter. 3 and Refs. [92, 93], Eq. (6.6) is reduced to a Langevin equation for $\Omega \equiv \omega/\epsilon_{\rm rot}$ driven by the state-independent non-Gaussian noise in the large system size limit $\epsilon_{\rm rot} \to 0$ when the axial friction is sufficiently strong. In the following, we consider the two types of the axial friction, the viscous friction $N_{\rm fri} = -\gamma\omega$ and the dry friction $N_{\rm fri} = -\Delta {\rm sgn}(\omega)$ [33–40] and discuss the steady state distribution $P_{\rm ss}(\Omega) \equiv \lim_{t\to\infty} \mathcal{P}(\Omega, t)$ with $\mathcal{P}(\Omega, t) \equiv \epsilon_{\rm rot} P(\epsilon_{\rm rot}\Omega, t)$.

6.5 Granular Rotor under Viscous Friction

In this section, we consider the role of the rotor under viscous friction $N_{\rm fri} = -\gamma\omega$ as a probe of the granular gas. In Sec. 6.5.1, we analytically derive forward and inverse formulas, which connect the granular VDF with the rotor PDF. In Sec. 6.5.2, we verify the validity of the forward formula at first, where we estimate $P_{\rm ss}(\Omega)$ using the numerical data for $\phi(v)$. Next, in Sec. 6.5.3, we solve the inverse problem, i.e., we derive the granular VDF $\phi(v)$ from a given $P_{\rm ss}(\Omega)$, which enables us to infer the properties of granular gases from the motion of the probe, i.e., the rotor.

6.5.1 Analytic formula for PDF of the rotor

As is shown in Chapter 3 and Ref. [151], the steady angular VDF in the Fourier transform $\tilde{P}_{\rm ss}(s) \equiv \int_{-\infty}^{\infty} d\Omega e^{is\Omega} P_{\rm ss}(\Omega)$ can be expressed as

$$\tilde{P}_{\rm ss}(s) = \exp\left[\int_0^s \frac{I}{\gamma s'} \Phi(s') ds' \right], \tag{6.8}$$

where the cumulant generating function $\Phi(s) \equiv \sum_{l=1}^{\infty} \mathcal{K}_l (is)^l / l! = \int_{-\infty}^{\infty} \mathcal{W}(\mathcal{Y})(e^{i\mathcal{Y}s} - 1)$ with $\mathcal{K}_l \equiv \int_{-\infty}^{\infty} d\mathcal{Y} \mathcal{Y}^l \mathcal{W}(\mathcal{Y})$ and the scaled transition rate $\mathcal{W}(\mathcal{Y})$ can be represented by an integral transform of $\phi(v)$ for the cylindrically symmetric case:

$$\Phi(s) = -\frac{2\rho h w v_0}{\tilde{s}^2 \tilde{w}^2} \int_0^{\infty} dx \tilde{\phi}(x) \left\{ -(\tilde{w}\tilde{s}x)\pi {\rm H}_0(\tilde{w}\tilde{s}x) + 2(\tilde{w}\tilde{s}x)^2 \right\}. \tag{6.9}$$

Here, we have introduced dimensionless variables $\tilde{w} = (1+e)w/2R_I, \tilde{s} = sv_0/R_I, x = v/v_0$, and $\tilde{\phi}(x) = v_0^2\phi(v_0 x)$. We have used the Struve function $\mathrm{H}_\nu(x)$ with $\nu = 0$ defined by Eq. (C.6) [185]. See Appendix C.1 for the detailed derivation. We note that Eq. (6.9) is valid not only for the linear (viscous) frictional rotor but also for the nonlinear (dry) frictional rotor. Substituting Eq. (6.9) into Eq. (6.8), we obtain

$$\frac{\tilde{\gamma}}{\pi k}\left\{k^3\frac{d}{dk}\ln\tilde{P}_{\rm ss}\left(\frac{k}{\tilde{w}}\right) + Bk^2\right\} = \int_0^\infty dx x\tilde{\phi}(x)\mathrm{H}_0(kx), \tag{6.10}$$

where we have introduced $B = (2/\tilde{\gamma})\int_0^\infty dx x^2\tilde{\phi}(x)$, a dimensionless variable $k \equiv \tilde{w}\tilde{s}$, and a scaled friction coefficient $\tilde{\gamma} \equiv \gamma/(2\rho h w I v_0)$. The integral on the right-hand side of Eq. (6.10) is known as the Struve transformation, and its inverse transformation is the Y transform, which are kinds of the Bessel transformations [186]. Introducing the Neumann function $N_\nu(x)$ with $\nu = 0$ [185], we obtain the inverse estimation formula:

$$\tilde{\phi}(x) = \int_0^\infty G_{\rm vis}(k)N_0(kx)kdk, \tag{6.11}$$

$$G_{\rm vis}(k) \equiv \frac{\tilde{\gamma}}{\pi k}\left\{k^3\frac{d}{dk}\ln\tilde{P}_{\rm ss}\left(\frac{k}{\tilde{w}}\right) + Bk^2\right\}. \tag{6.12}$$

The VDF of the granular gas can be determined from Eqs. (6.11) and (6.12) only through the observation of the rotor dynamics. This implies that the rotor is regarded as a thermometer for the granular gas with the aid of the inverse formula Eqs. (6.11) and (6.12). The constant B in Eq. (6.12) can be determined numerically by the condition $\lim_{k\to\infty} G_{\rm vis}(k) = 0$.

6.5.2 Forward problem for viscous rotor

Before considering the inverse problem, we discuss the forward problem, i.e., the determination of the PDF for the rotor from the VDF for the granular gas. We verify the validity of the formulas (6.8) and (6.9) using the numerical data of the VDF $\phi(v)$ for the granular gas under gravity. In the following numerical simulation, we adopt $\gamma/mL_{\rm box}v_0 = 2.0$, which corresponds to $\tilde{\gamma} = 1.15248$. In Fig. 6.5 (a), we plot $P_{\rm ss}(\Omega)$ by the solid line on the basis of Eqs. (6.8) and (6.9) and the numerical data for $\phi(v)$ and the results of the MD simulation (circles). The agreement between the theory and the simulation is good except for the point near $\Omega = 0$, where the numerical error would be decreased by smaller bin-width for $\phi(v)$. We adopt the bin-width of the numerical histogram for $\phi(v)$ as $5.0 \times 10^{-3}v_0$. See Appendix C.2.1 for the detailed procedure to obtain the solid line in Fig 6.5 (a).

6.5.3 Inverse problem for granular gas

In this subsection, we show that the VDF for the granular gas can be inferred only through the numerical data of a steady distribution for the angular velocity

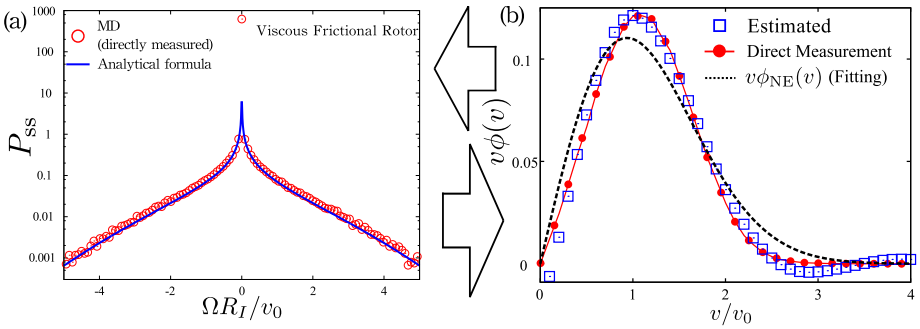

Figure 6.5: The demonstration of the applicability of our formulas (6.8)-(6.12) under viscous friction on (a) the forward and (b) the inverse estimation problems. The Fourier transform of Eq. (6.8) is shown as the solid line (a), which agrees with the directly measured MD data. (b) Our formula (6.11) represented by open squares are compared with the numerical data for the VDF $\phi(v)$ near the rotor (filled circles) We can successfully estimate the VDF for the granular gas only observing the angular VDF for the rotor. Note that there exists the numerical error for large v/v_0.

of a frictional rotor by using the formula Eq. (6.11) associated with Eq. (6.12).

The result for the inverse formula in Eqs. (6.11) and (6.12) is shown in Fig. 6.5 (b), where the parameter B is estimated as $B = 0.365556$ and we have used the bin-width $8.660211 \times 10^5 v_0/R_I$ for P_{SS}. The dotted line is $v\phi_{\rm NE}(v)$, and our formula (6.11) represented by open squares correctly predicts the numerical data for the VDF $\phi(v)$ near the rotor (filled circles). We adopt the bin-width for $P_{\rm ss}$ as $8.660211 \times 10^{-5} v_0/R_I$. Although numerical oscillation exists for large v/v_0, our estimation for the granular bath based on Eq. (6.11) agrees well with the directly measured VDF of granular particles in the MD simulation. This implies that the inverse formula (6.11) supplemented by Eq. (6.12) enables us to use the motion of the rotor as a non-equilibrium thermometer. See Appendix C.2.2 for the detailed procedure to obtain the estimated VDF.

6.6 Position dependence of the rotor

We now discuss the utility of the rotor as a local non-equilibrium probe. In Sec. 6.5.3, we have already demonstrated that the VDF for the surrounding gas in the area (i) can be inferred from the angular VDF for the viscous rotor $P_{\rm ss}$. Here, we discuss whether we can infer the local VDF in the area (ii) from the motion of the rotor using Eqs. (6.11) and (6.12).

In Fig. 6.6, we show that the VDF in the area (ii) can be also inferred from the angular VDF of the rotor. The estimated data and the directly measured data are represented by squares and circles, respectively. See also Appendix

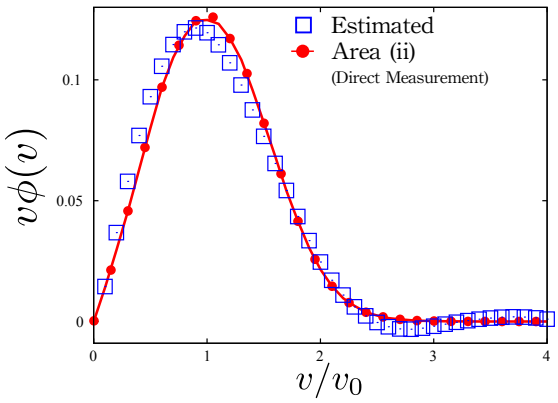

Figure 6.6: The demonstration of the inverse formula for the local VDF in the area (ii). Although the accuracy is a little worse than that in Fig. 6.5, the estimated data (squares) correctly predicts the direct measurement data (circles).

C.2.2 for the detailed procedure to obtain the estimated $\phi(v)$. Here, the parameter B is estimated as $B = 0.40278$. There also exists the numerical oscillation for large v/v_0. Although the accuracy is not as good as Fig. 6.5 (b), the estimated data are consistent with those obtained by the direct measurement. The reason for the small discrepancy would be the violation of the cylindrical symmetry because of the influence of the wall.

6.7 Granular Rotor under Dry Friction

We, now, consider a rotor under dry friction $N_{\rm fri} = -\Delta {\rm sgn}(\omega)$, because real experimental rotors are influenced by dry friction [33–40]. In Sec. 6.7.1, we derive an analytic formula for the angular VDF of the rotor, and verify its validity in Sec. 6.7.2. Note that we here only study the forward problem on the basis of the perturbative method developed in Ref. [93, 95].

6.7.1 Analytic formula for PDF of the rotor

The steady angular VDF $P_{\rm ss}(\Omega)$ can be obtained perturbatively in terms of $1/\tilde{\Delta}'$ with $\tilde{\Delta}' \equiv \Delta(1+e)/(\epsilon_{\rm rot} I \rho h v_0^2 4\pi) \gg 1$. The first-order solution in terms of $1/\tilde{\Delta}'$ is known as the independent kick model, which is originally introduced in Ref. [95] and can be systematically derived in Refs. [92, 93]. Introducing the Bessel function $J_\nu(x)$ [185], $\tilde{P}_{\rm ss}$ for the rotor under the dry friction can be

rewritten as:

$$\tilde{P}_{\rm ss}\left(\frac{k}{\tilde{w}}\right) = 1+\frac{\tilde{w}^2}{k^2}\frac{1}{\tilde{\Delta}'}\left[\frac{1}{2\pi}+C_1k^2-G_{\rm dry}(k)\right] +O(1/\tilde{\Delta}'^2), \quad (6.13)$$

$$G_{\rm dry}(k) \equiv \int_0^\infty dx x\tilde{\phi}(x)J_0(kx), \quad (6.14)$$

where we have introduced $C_1 = -\int_0^\infty dx x^3\tilde{\phi}(x)/4$. See Appendix D.1 for the detailed derivation.

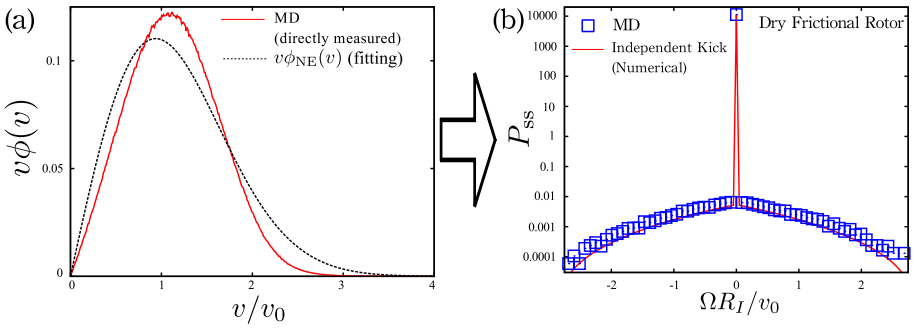

Figure 6.7: $P_{\rm ss}(\Omega)$ for the dry frictional rotor is calculated using the VDF represented (the solid line in (a)). The steady state angular VDF for the dry frictional rotor is shown in (b). The squares and the solid line are histogram for MD and the Fourier transform of Eq. (6.13), respectively. Our observed histogram in MD simulation can be correctly predicted by the Fourier transform of Eq. (6.13)

6.7.2 Forward problem for dry frictional rotor

Now, let us examine whether Eqs. (6.13) and (6.14) are consistent with the result of MD. For the MD simulation, we adopt $\Delta/mv_0^2 = 20.0$, which corresponds to $\tilde{\Delta}' = 31.36531$. The bin-width for $P_{\rm ss}$ is set to be $8.660211\times10^{-5}v_0/R_I$. As shown in Fig. 6.7 (b), the obtained PDF $P_{\rm ss}(\Omega)$ in the MD simulation is correctly predicted by the Fourier transform of Eq. (6.13) using the numerical data of VDF for the granular gas $\phi(v)$ (Fig. 6.7 (a)). We have also checked that the VDF for the granular gas is invariant even if we change the frictional torque $N_{\rm fri}$ of the rotor. We stress that the VDF of the granular gas obtained in MD cannot be fitted by that activated by the white noise thermostat [72]. In Fig. 6.7 (b), the squares and the solid line are histograms for MD and the Fourier transform of Eq. (6.13), respectively. For a given VDF of the granular gas, our framework agrees with the results of the MD simulation without introducing any fitting parameters. It should be noted that one can find the

small discrepancy between the theoretical result and the data for large $\Omega R_I/v_0$, because the independent kick model is correct only for small $\Omega R_I/v_0$. See the detailed implementation of Eqs. (6.13) and (6.14) in Appendix. D.2.

We here discuss the difficulty for the inverse estimation problem under dry friction in the present theoretical analysis. A possible reason is as follows: Although Eq. (6.13) can be formally solved in terms of $\tilde{\phi}$, the formal inverse formula is practically useless because the independent kick model under dry friction is only valid for small $\Omega R_I/v_0$ and the inverse Fourier transformation of Eq. (6.13) does not work well. Indeed, the exponential tail is reported for the dry frictional rotor for large $\Omega R_I/v_0$ in Ref. [93], which cannot be captured by the independent kick solution.

6.8 Summary and Discussion

We have shown the role of a granular rotor as a local non-equilibrium probe through the MD simulation of the rotor in vibrating granular beds under gravity (Figs. 6.2 and 6.3). We have approximately observed the cylindrically symmetric and spatially inhomogeneous VDFs (Fig. 6.4). We have formulated the inverse formula (6.11) in cylindrical coordinates to apply the MD simulation of a realistic viscous rotor. Starting from the Boltzmann-Lorentz equation (6.6), we have derived an analytic result Eq. (6.11) supplemented by Eq. (6.12) for the viscous frictional rotor. Using Eq. (6.11), we have numerically calculated the angular VDF for the rotor from the data of VDF for the granular gas near the rotor, and vice versa in Fig. 6.5. Furthermore, we have demonstrated that our inverse formula can be used even if the location of the rotor is different from the center of the container as shown in Fig. 6.6. Thus, the granular rotor is useful as a local probe for non-equilibrium baths.

For a dry frictional rotor, we have considered only the forward problem, and the result agrees with the MD result, as shown in Fig. 6.7. In other words, we cannot solve the inverse problem for the dry frictional rotor. To derive an alternative valid inverse formula for the dry frictional rotor, we expect that an appropriate interpolation is necessary between Eq. (6.13) and the exponential tail of the VDF for the rotor.

Chapter 7

Efficiency at maximum power output for a passive piston

Abstract

We study the efficiency at MP for a passive engine, which is an idealized model of internal combustion engines without mechanical controls. We consider a hard core gas confined by a massive piston in a chamber, where the piston freely moves in one-direction by the pressure difference (See Fig. 7.1). We use the molecular dynamics (MD) simulation of hard core gases to examine a theoretically derived efficiency at MP on the basis of an effective model, which we call stochastic mean field model (SMF). We explain our setup and operation protocol for the temperature of the thermal wall $T_{\rm bath}$ in Sec. 7.2. We introduce SMF in Sec. 7.3 to analyze the power and efficiency. We examine the validity of SMF in Sec. 7.4 comparing the time evolution of MD simulation and that of SMF. In Sec. 7.5, we obtain the efficiency at MP for our passive engines containing dilute hard core gases theoretically, which is close to the CNCA efficiency in the massive piston limit. We also find that the efficiency at MP for moderately dense gases is smaller than the CNCA efficiency even in the linear non-equilibrium regime. In Sec. 7.6, to clarify the efficiency in the linear non-equilibrium regime, we derive the Onsager matrix explicitly. We clarify the finite density effect for the efficiency and stress the importance of the heat flux when we attach a bath at $T_{\rm bath}$ on the efficiency at MP in this section. We discuss the difference between our results and previous works in Sec. 7.7 and conclude this chapter with some remarks in Sec. 7.8. In Appendix E, we review the kinetic theory of both elastic and inelastic hard core gases. In Appendix F, we consider the velocity auto-correlation of the piston attached to a dilute stationary gas. In Appendix G, the definition of the work and heat for our system is discussed and the effect of

the sidewall-friction on the piston is discussed in Appendix H.

7.1 Introduction

Up to now, we have examined the tracer motion attached to steady state gases. In this chapter, we consider the motion of the piston attached to a hard core gas under cyclic heating and cooling processes. The aim of this chapter is to clarify the efficiency at MP for the passive engine, which is an idealized model of internal combustion engines without mechanical controls. We consider a hard core gas confined by a massive piston in a chamber, where the piston freely moves in one-direction by the pressure difference (See Fig. 7.1). We use the MD simulation of hard core gases to examine a theoretically derived efficiency at MP on the basis of an effective model, which we call stochastic mean field model (SMF).

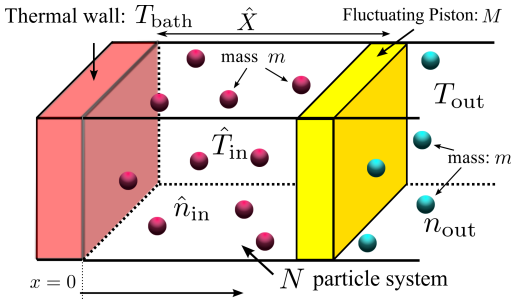

Figure 7.1: Schematic picture of our setup, where N identical hard core particles are enclosed in a container partitioned by an adiabatic piston of mass M at $x = \hat{X}$. The density $n_{\rm out}$ and the temperature $T_{\rm out}$ for the outside gas $x > \hat{X}$ are kept to be constants. The temperature $T_{\rm bath}$ of the thermal wall at $x = 0$ is controlled by an external agent, while thermodynamic quantities such as the density $\hat{n}_{\rm in}$ and the temperature $\hat{T}_{\rm in}$ fluctuate in time.

Because the engine we consider is an internal combustion engine, the maximum efficiency is smaller than the Carnot efficiency. Our study is relevant from the following two reasons. Firstly, we can find many situations, where the direct mechanical control of a piston is difficult. For example, the structure of internal combustion engines is usually too complicated to control inside mechanically [103]. Therefore, we need to clarify the effect of the uncontrollable motion of a piston on the efficiency. Secondly, the study on passive engines is important even for finite time thermodynamics. In the absence of mechanical control of a piston or a partitioning wall, heat flow when we attach a thermal wall is inevitable. Because heat flow from a reservoir is not usually taken into account in conventional finite time thermodynamics, it is important to verify whether the existing theoretical results should be changed, even if such heat

flow exist [107–126]. Indeed, we will show that conventional results are only valid for our system when the heat flow is negligible as in dilute gases. Thus, we believe that the detailed analysis of our system which is the simplest passive engine from a thermodynamic point of view is important.

7.2 Setup

In our system, N hard core particles of each mass m and diameter $d_{\rm in}$ are enclosed in a three-dimensional container partitioned by an adiabatic piston of mass M and the area A on the right side of x-direction, a diathermal wall attached with a thermal bath on the left side of x-direction and four adiabatic walls on the other directions (Fig. 1). We assume that adhesion between particles and the walls of the container as well as the one between particles can be ignored. The piston is assumed to move in one dimension without any sidewall friction. Post-collision velocity (v', V') and pre-collision velocity (v, V) in x-direction for a colliding particle and the piston are related as:

$$v'(v,V) = v - \frac{1}{m}P_v, \tag{7.1}$$

$$V'(v,V) = V + \frac{1}{M}P_v, \tag{7.2}$$

where the contribution from the horizontal motion of particles to the wall is canceled as a result of statistical average. Here, $P_v = P_v(V) \equiv M(V' - V) = (1+e)mM(v-V)/(m+M)$ represents the momentum change of the piston because of the collision for the particle of velocity v, where e is the restitution coefficient between the particles and the piston. The reason why we introduce the restitution coefficient is that the wall consists of a macroscopic number of particles and part of impulses of each collision can be absorbed into the wall as the excitation of internal oscillation.

We adopt the Maxwell reflection rule for a collision between a particle and a diathermal wall attached with the bath at $T_{\rm bath}$. The post-collisional velocity $\boldsymbol{v}' = (v'_x, v'_y, v'_z)$ toward the wall at $x = 0$ is chosen as a random variable obeying the distribution

$$\phi_{\rm wall}(\boldsymbol{v}', T_{\rm bath}) = \frac{1}{2\pi}\left(\frac{m}{T_{\rm bath}}\right)^2 v'_x \exp\left[-\frac{m\boldsymbol{v}'^2}{2T_{\rm bath}}\right], \tag{7.3}$$

whose domain is given by $0 < v'_x < \infty$ and $-\infty < v'_y, v'_z < \infty$.

Let us consider a heat cycle for heating $T_{\rm bath} = T_{\rm H} > T_{\rm out}$ and cooling $T_{\rm bath} = T_{\rm L} = T_{\rm out}$ processes (Fig. 7.2). Initially, the enclosed gas and the gas outside are in a mechanical equilibrium state, which satisfies $\hat{P}_{\rm in} = P_{\rm out}$ and $\hat{T}_{\rm in} = T_{\rm out} = T_{\rm bath}$. At $t = 0$, we attach a heat bath at $T_{\rm H}$ on the diathermal wall. For $0 < t < t_{\rm c}$, $T_{\rm bath}$ is kept to be $T_{\rm H}$ (Fig. 7.2 (a)), and at $t = t_{\rm c}$, $T_{\rm bath}$ is switched to be $T_{\rm L}$ simultaneously, and is kept to be this state until $t = 2t_{\rm c}$. Then, we again replace the bath at $T_{\rm L}$ by the one at $T_{\rm H}$ simultaneously (Fig.

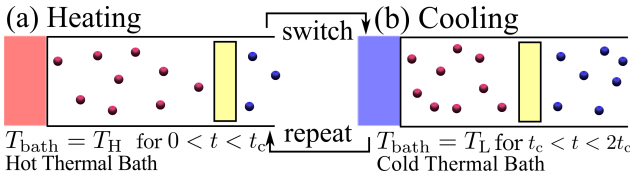

Figure 7.2: The operation protocol. We attach the heat bath $T_{\rm H}$ on the diathermal wall at $t = 0$. (a) For $0 < t < t_{\rm c}$, $T_{\rm bath}$ is kept to be $T_{\rm bath} = T_{\rm H}$, and at $t = t_{\rm c}$, $T_{\rm bath}$ is switched to be $T_{\rm L}$ simultaneously, and (b) $T_{\rm bath}$ is kept to be this state until $t = 2t_{\rm c}$. Then, we again replace the bath by $T_{\rm H}$ simultaneously. After repeating the switching of $T_{\rm bath}$, the heat cycle reaches a steady cycle.

7.2 (b)). After repeating the switching and attaching of the baths, the heat cycle reaches a steady cycle. It should be noted that the enclosed gas is no longer thermal equilibrium during the cycle. During the operation, we ignore the time necessary for the switching the heat bath. The finite switching time only lowers the power but does not affect the efficiency of the cycle and what the maximum-power-output process is.

In this paragraph, we explain some additional remarks in the MD simulation. We assume that particles are colliding elastically each other and with side walls. The collision rule between the piston and a particle is given by Eqs. (7.1) and (7.2). We introduce typical length and time scale as $X_{\rm ini} \equiv NT_{\rm out}/P_{\rm out}A$ and $t_0 \equiv X_{\rm ini}\sqrt{M/T_{\rm out}}$ for later convenience. The number of particle $N = 200$ is fixed through our simulation. The collisional force from outside the piston is modeled by $\hat{F}_{\rm out}$ as will be defined in Eq. (7.6).

7.3 Stochastic mean field model

Let us introduce the stochastic mean field (SMF) model to describe the dynamics of the piston and the energy balance of our system by using two independent stochastic variables: fluctuating density $\hat{n}_{\rm in}(t) = N/A\hat{X}(t)$ and fluctuating temperature $\hat{T}_{\rm in}(t)$. Here, $\hat{n}_{\rm in}(t)$ and $\hat{V} \equiv d\hat{X}/dt$ satisfy the stochastic equations:

$$\frac{d\hat{n}_{\rm in}}{dt} = -\frac{\hat{n}_{\rm in}}{\hat{X}}\hat{V}, \tag{7.4}$$

$$M\frac{d\hat{V}}{dt} = \hat{F}_{\rm in} + \hat{F}_{\rm out}, \tag{7.5}$$

where the stochastic force $\hat{F}_\nu(\nu = {\rm in}, {\rm out})$ is introduced as

$$\hat{F}_\nu \equiv \sum_v P_v \cdot \hat{\xi}^v_\nu(t|\hat{V}, \hat{n}_\nu, \hat{T}_\nu). \tag{7.6}$$

Here, $\hat{\xi}_\nu^v(\nu = \text{in, out})$ denotes Poissonian noise of the unit amplitude whose event probability is given by

$$\hat{\lambda}_\nu'^v \equiv \hat{\lambda}_\nu^v \left\{1 + 4\hat{\Phi} g_0(\hat{\Phi})\right\}, \tag{7.7}$$

$$\hat{\lambda}_\nu^v \equiv dv|v - \hat{V}|\Theta[\varepsilon^\nu(\hat{V} - v)]\hat{n}_\nu \phi_0(v, \hat{T}_\nu), \tag{7.8}$$

where we have introduced the radial distribution function at contact g_0 [191], $\varepsilon^{\text{in}} = -1$, and $\varepsilon^{\text{out}} = +1$. The symbol " $\cdot$ " in Eq. (7.6) represents Itô type stochastic product [7, 8]. $\Theta(x)$ is Heaviside function satisfying $\Theta(x) = 1$ for $x \geq 0$ and $\Theta(x) = 0$ for $x < 0$. The density and temperature for the gas outside are kept to be constants in time, i.e., $\hat{n}_{\text{out}} \equiv n_{\text{out}}$ and $\hat{T}_{\text{out}} \equiv T_{\text{out}}$. We note that a set of Eqs. (7.5) and (7.6) is an extension of the SDE discussed in Chapter 5 toward a finite density hard core gas when the density and the temperature change in time. We adopt the equation of state for hard core gases of volume fraction $\hat{\Phi} \equiv \hat{n}_{\text{in}} \pi d^3/6$ given by [192]

$$\hat{P}_{\text{in}} = \hat{n}_{\text{in}} \hat{T}_{\text{in}}(1 + 4\hat{\Phi} g_0(\hat{\Phi})). \tag{7.9}$$

Next, we propose the time evolution for $\hat{T}_{\text{in}}$. The differential of the internal energy for the gas $\hat{U}_{\text{in}} \equiv 3N\hat{T}_{\text{in}}/2$ is given by

$$d\hat{U}_{\text{in}} = d\hat{Q}_{\text{wall}} + d\hat{Q}_{\text{cond}} + d\hat{E}_{\text{pis}}, \tag{7.10}$$

$$\frac{d\hat{Q}_{\text{wall}}}{dt} \equiv A\hat{n}_{\text{in}}(T_{\text{bath}} - \hat{T}_{\text{in}})\sqrt{\frac{2\hat{T}_{\text{in}}}{\pi m}}, \tag{7.11}$$

$$\frac{d\hat{E}_{\text{pis}}}{dt} \equiv \sum_v \frac{m}{2}\left\{v'^2(v, \hat{V}) - v^2\right\} \cdot \hat{\xi}_{\text{in}}^v(\hat{V}, \hat{n}_{\text{in}}, \hat{T}_{\text{in}}), \tag{7.12}$$

$$d\hat{Q}_{\text{cond}} = -\frac{45\sqrt{\pi}}{64}\hat{J}_{\text{in}} A dt. \tag{7.13}$$

Here, $d\hat{Q}_{\text{wall}}$ and $d\hat{Q}_{\text{cond}}$ denote the heat flow from the thermal bath at T_{bath} [112] and heat flux due to the thermal conduction $\hat{J}_{\text{in}}$, respectively. $d\hat{E}_{\text{pis}}$ denotes the kinetic energy transfer from the piston to the gas. In summary, our SMF model consists of two coupled equations: the equation of motion for the piston (7.5) and the energy equation for the enclosed gas (7.10).

It is known that VDF for a hard core gas under the heat flux $\hat{J}_{\text{in}}$ [192, 193] is given by

$$\phi_{\text{flux}}(\boldsymbol{v}) = \left(1 + v_x g(\boldsymbol{v})\hat{J}_{\text{in}}\right)\phi_0(\boldsymbol{v}), \tag{7.14}$$

where we have introduced $\phi_0(\boldsymbol{v}) \equiv \prod_{\mu=x,y,z} \phi_0(v_\mu, \hat{T}_{\text{in}})$ and

$$\phi_0(v, \hat{T}_{\text{in}}) \equiv \sqrt{\frac{m}{2\pi\hat{T}_{\text{in}}}} \exp\left[-\frac{mv^2}{2\hat{T}_{\text{in}}}\right]. \tag{7.15}$$

In Eq. (7.14), $g(\boldsymbol{v})$ is written as

$$g(\boldsymbol{v}) \equiv -\frac{4}{5\hat{n}_{\rm in}\hat{T}_{\rm in}}\left(\frac{m\boldsymbol{v}^2}{2\hat{T}_{\rm in}}-\frac{5}{2}\right). \tag{7.16}$$

The energy flows $d\hat{Q}_{\rm wall}/dt$ and $d\hat{Q}_{\rm cond}/dt$ can be calculated as follows. The heat flows outgoing $\hat{q}^{\rm out}_{\rm wall}$ and incoming $\hat{q}^{\rm in}_{\rm wall}$ through the wall are, respectively, given by

$$\hat{q}^{\rm out}_{\rm wall} = \left\{\int_{-\infty}^{\infty}dv_ydv_z\int_{-\infty}^{0}dv_x\frac{m\boldsymbol{v}^2}{2}(-v_x)\hat{n}_{\rm in}A\phi_{\rm flux}(\boldsymbol{v})\right\} \tag{7.17}$$

$$\begin{aligned}\hat{q}^{\rm in}_{\rm wall} &= \left\{\int_{-\infty}^{\infty}dv_ydv_z\int_{-\infty}^{0}dv_x(-v_x)\hat{n}_{\rm in}A\phi_{\rm flux}(\boldsymbol{v})\right\}\\ &\quad\times\left\{\int_{-\infty}^{\infty}dv_ydv_z\int_{0}^{\infty}dv_x\frac{m\boldsymbol{v}^2}{2}\phi_{\rm wall}(\boldsymbol{v},T_{\rm bath})\right\}.\end{aligned} \tag{7.18}$$

Substituting Eqs. (7.17) and (7.18) into $d\hat{Q}_{\rm wall}+d\hat{Q}_{\rm cond}=(\hat{q}^{\rm in}_{\rm wall}-\hat{q}^{\rm out}_{\rm wall})dt$, we obtain Eqs. (7.11) and (7.13).

The heat flux $J_{\rm in}$ is estimated from the solution of the heat diffusion equation for the temperature profile $\mathcal{T}=\mathcal{T}(x,t)$:

$$\frac{\partial\mathcal{T}}{\partial t}-\frac{\kappa}{n}\frac{\partial^2\mathcal{T}}{\partial x^2}=0, \tag{7.19}$$

under the situation that the thermal conductivity κ and density $\hat{n}_{\rm in}=n$ are constants in space and time, where the piston position is fixed at $\hat{X}=L$. Imposing the boundary conditions $\mathcal{T}(x,t=0)\equiv T_{\rm ini}$, $\mathcal{T}(x=0,t)=T_{\rm bath}$ and $\partial_x\mathcal{T}(x=L,t)=0$ on Eq. (7.19), the solution of Eq. (7.19) is given by

$$\mathcal{T}(x,t) = T_{\rm bath}-(T_{\rm bath}-T_{\rm ini})\sum_{l=1}^{\infty}\frac{4}{\pi l}e^{-\left(\frac{l\pi}{2L}\right)^2\frac{\kappa t}{n}}\sin\left(\frac{l\pi x}{2L}\right). \tag{7.20}$$

Assuming that $T_{\rm ini}, L, \kappa$ and n change in time adiabatically, i.e. $T_{\rm ini}\to\hat{T}_{\rm in}(t), L\to\hat{X}(t), \kappa\to\hat{\kappa}(\hat{\Phi}(t),\hat{T}_{\rm in}(t))$ [192, 193] and $n\to\hat{n}_{\rm in}(t)$, we obtain the approximate heat flux $J_{\rm in}=\int_0^L-\kappa\partial_x\mathcal{T}(x,t)dx/L$ as

$$\hat{J}_{\rm in}(t) = \frac{4\hat{\kappa}}{\pi\hat{X}(t)}(T_{\rm bath}-\hat{T}_{\rm in}(t))\sum_{l=1}^{\infty}\frac{\sin(l\pi/2)}{l}\exp\left[-\left(\frac{l\pi}{2\hat{X}(t)}\right)^2\frac{\hat{\kappa}t}{\hat{n}_{\rm in}}\right], \tag{7.21}$$

where we have adopted expressions in Refs. [192, 193] for density and temperature dependence of the thermal conductivity $\hat{\kappa}(\Phi,T)=(75\sqrt{T/\pi}/64md^2_{\rm in}g_0(\Phi))[\{1+$

$(12\Phi g_0(\Phi)/5)\}^2 + (4608\Phi^2 g_0(\Phi)/225\pi)]$. See Appendix E for transport coefficients of inelastic hard core gases and the review for the kinetic theory.

Because the heat conduction relaxes very fast for the dilute gas, we can simplify Eq. (7.10) as

$$d\hat{U}_{\rm in} = d\hat{Q}_{\rm wall} + d\hat{E}_{\rm pis}, \tag{7.22}$$

although heat conduction exists. Indeed, we compare the dynamics of temperature in Fig. 7.3 for SMF and the dilute approximation of SMF using Eq. (7.22), the difference between two methods is negligible. Here we have adopted the initial volume fraction as $\Phi = 1.05 \times 10^{-4}$. We will also show that $dQ_{\rm cond}$ does not affect the efficiency at MP for the dilute gas later. Thus, we use Eq. (7.22) for the dilute gas instead of Eq. (7.10).

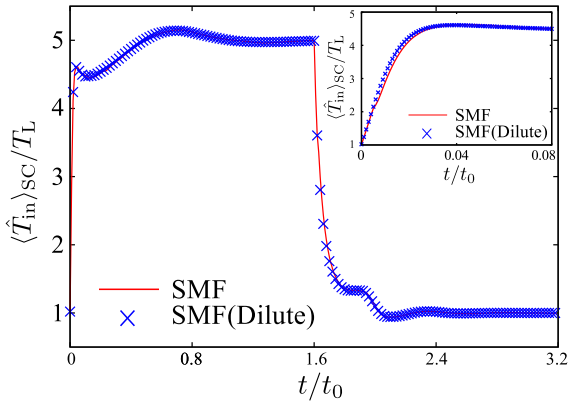

Figure 7.3: Comparison between SMF and the dilute approximation of SMF for $d_{\rm in}/\sqrt{A} = 0.01$. The initial volume fraction is calculated to be $\Phi = 1.05 \times 10^{-4}$. The solid line and the cross points represent the dynamics of temperature for SMF and the dilute version of SMF, respectively. The inset represents the detailed time evolution for $0 < t/t_0 < 0.08$.

In this paragraph, let us explain the numerical details of SMF. The numerical integration is performed through Adams-Bashforth method, with $dt/t_0 \equiv 0.01\epsilon$ and $\epsilon \equiv \sqrt{m/M}$. Calculating $\hat{\xi}_\nu^v$, v and dv are respectively replaced by v_i and Δv, where $v_i = i\Delta v - v_{\rm max} (i = 1, 2, \cdots, 600)$, $v_{\rm max} \equiv 6.0\sqrt{k_{\rm B} T_\nu / M} (\nu = {\rm in}, {\rm out})$ and $\Delta v \equiv v_{\rm max}/300$. Because Eq. (7.10) turns out to be unstable if the heat conduction in Eq. (7.13) is larger than that of Eq. (7.11), we impose the condition $dQ_{\rm cond} = 0$ if $dQ_{\rm cond} > dQ_{\rm wall}$ through the simulation for the numerical stability of our model. The simulation data are averaged in steady cycles, where the averaged quantity is represented by $\langle \cdots \rangle_{\rm SC}$.

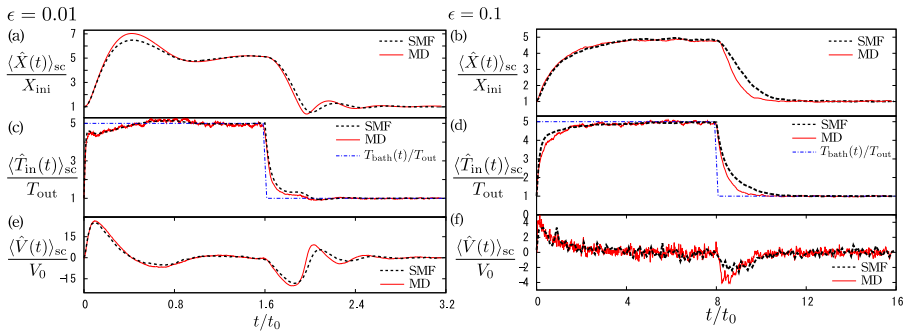

Figure 7.4: The time evolutions of steady cycles for $T_{\rm H}/T_{\rm L} = 5.0$. They are categorized into two types: damped oscillating type for $\epsilon = 0.01$ (left) and over-damped type for $\epsilon = 0.1$ (right). The time evolutions for the piston position ((a) and (b)), the temperature ((c) and (d)), and the piston velocity ((e) and (f)) are plotted. Time evolutions for the corresponding physical quantities for MD simulation (solid line) agree with those for the SMF model (dashed line).

7.4 Time evolution

To verify the validity of our effective model, we compare the time evolution of the MD simulation and SMF. We examine the dilute and moderately dense gases in Sec. 7.4.1 and 7.4.2, respectively.

7.4.1 Dilute case

We consider a dilute gas of the diameter $d_{\rm in}/\sqrt{A} = 0.01$ which corresponds to $\Phi = 1.05 \times 10^{-4}$ at $t = 0$. Time evolutions of the volume (the position of the piston) for $T_{\rm H}/T_{\rm L} = 5.0$ are drawn in Fig. 7.4 (a) for $\epsilon = 0.01$, $t_{\rm c}/t_0 = 1.60$ and (b) for $\epsilon = 0.1$, $t_{\rm c}/t_0 = 8.0$. The simulation data are averaged from 11th cycle to 20th cycle, where the solid and dashed lines, respectively, represent the data for MD simulation and those for simulation of our SMF model. Similarly, Figs. 7.4 (c) and (d) are the time evolutions for the temperature of the gas, and Figs. 7.4 (e) and (f) are the time evolutions for the piston velocity. Dot-dashed lines represent the operation protocol of $T_{\rm bath}$. It is remarkable that our SMF model correctly predicts the time evolution of MD.

Let us explain the behavior of the system shown in Fig. 7.4. When the heating process starts, the enclosed gas starts expanding, to find a new mechanical equilibrium density determined by the condition $\hat{P}_{\rm in} = P_{\rm out}$, because the pressure for the enclosed gas becomes larger than that for the outside after the heating. Similarly, the gas is compressed when the cooling process starts. It should be stressed that the heating (cooling) and expansion (compression) processes take place simultaneously.

The time evolutions of the physical quantities can be categorized into two types: (a) damped-oscillating type and (b) over-damped type depending on the

mass ratio $\epsilon \equiv \sqrt{m/M}$. Taking the average of Eq. (7.22) and assuming that the piston is heavy $\epsilon \ll 1$, the time evolution of the averaged temperature is written as

$$T_{\rm in}(t) = T_{\rm bath}\left(1 - a_0 V(t)\right) + O(\epsilon^2), \tag{7.23}$$

$$a_0 \equiv \sqrt{\frac{\pi m}{2T_{\rm bath}}}. \tag{7.24}$$

Assuming that the displacement of the piston is small $x/X_{\rm ini} \equiv (X - X_{\rm ini})/X_{\rm ini} \ll 1$, the average of Eq. (7.5) is written as

$$\frac{dV}{dt} = -\frac{P_{\rm out}A}{M}\frac{x}{X_{\rm ini}} - \bar{\gamma}V \tag{7.25}$$

where we introduced the viscous friction coefficients $\bar{\gamma} \equiv (\gamma_{\rm gas} + a_0 P_{\rm out}A)/M$ and $\gamma_{\rm gas} \equiv 4(1+e)P_{\rm out}A\sqrt{m/2\pi T_{\rm out}}$. The right-hand side of Eq. (7.25) is equivalent to the force acting on a harmonic oscillator in a viscous medium. If the viscous drag is sufficiently small, i.e. $\epsilon \to 0$, the motion of the piston is the damped-oscillating type (Fig. 7.4(a)), while the motion turns out to be the over-damped type, if ϵ is not small (Fig. 7.4(b)).

7.4.2 Moderately dense case

Let us examine the validity of SMF for a moderately dense gas. We adopt $d_{\rm in}/\sqrt{A} = 0.1$ which corresponds to $\Phi = 0.105$ at $t = 0$. In Fig. 7.5, simulation results for MD, SMF, and the dilute approximation of SMF are plotted. Although the time evolution of MD for small t/t_0 is well predicted by SMF (See the inset of Fig. 7.5), the agreement is relatively poor for $0.1 < t/t_0 < 0.5$. The agreement for $1.6 < t/t_0 < 2.0$ is also not good, though the difference is not large. Note that the discrepancy for $1.6 < t/t_0 < 2.0$ is not relevant for the efficiency at MP, because we need only $Q_{\rm H}$. The improvement of SMF for $0.1 < t/t_0 < 0.5$ is left as a future work.

7.5 Existence of Maximum Power and its Efficiency

In this section, we discuss the efficiency of the engine at MP. We show that the efficiency at MP for the dilute gas corresponds to the CNCA efficiency if the piston is sufficiently massive and elastic in Sec. 7.5.1, while that for the moderately dense gas is smaller than the CNCA efficiency as will be presented in Sec. 7.5.2

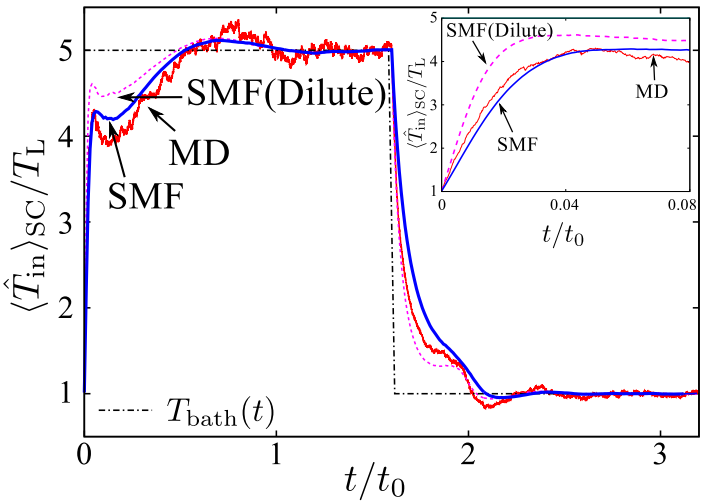

Figure 7.5: The time evolution of temperature for MD, the SMF, and the dilute approximation of SMF are compared. For heating regime $t/t_0 < 1.6$, the dilute SMF overestimates the heat gain, while the SMF works better than the dilute version, in particular, for small t/t_0. The inset represents the detailed time evolution for $0 < t/t_0 < 0.08$, where SMF captures the MD simulation results.

7.5.1 Dilute case

Let us illustrate that the MP exists for our engine. We define the work $\hat{W}_{\rm tot}$ and the heat spent per a cycle $\hat{Q}_{\rm H}$ as

$$\hat{W}_{\rm tot} \equiv \oint \frac{1+e}{2}(\hat{P}_{\rm in} - P_{\rm out}) A d\hat{X}, \tag{7.26}$$

$$\hat{Q}_{\rm H} \equiv \int_{T_{\rm H}} d\hat{Q}_{\rm wall}, \tag{7.27}$$

where $\oint$ and $\int_{T_\mu}$ represent the integral over a single cycle and the integral for the bath at $T_{\rm bath} = T_\mu (\mu = {\rm H \ or \ L})$, respectively, with the definition of $d\hat{Q}_{\rm wall}$ in Eq. (7.11). The validity for the definition of work Eq. (7.26) is discussed in Appendix **??**. The efficiency for a single operation protocol [194] is defined as

$$\hat{\eta} \equiv \frac{\hat{W}_{\rm tot}}{\hat{Q}_{\rm H}}. \tag{7.28}$$

We also introduce the conventional efficiency, which is defined as

$$\bar{\eta} \equiv \frac{\langle \hat{W}_{\rm tot} \rangle_{\rm SC}}{\langle \hat{Q}_{\rm H} \rangle_{\rm SC}}. \tag{7.29}$$

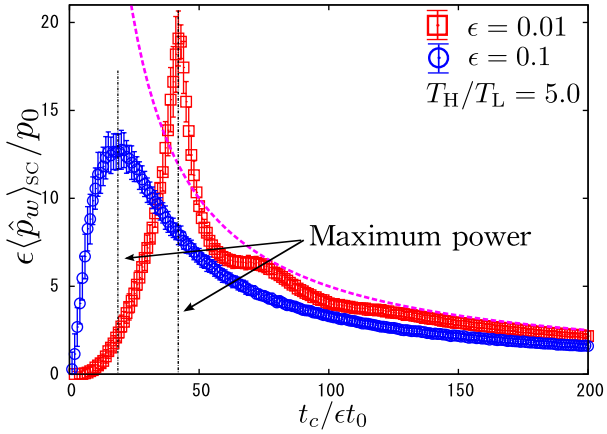

Figure 7.6: The average power is plotted against t_c. Apparently, there exists t_c for the maximum power operation, which corresponds to the necessary time for gas to expand toward the mechanical equilibrium. The dotted curve drawn as the guide line proportional to $1/t_c$.

In this section, we average the data from 11th cycle to 110th cycle.

The contact time dependence of the power $\hat{p}_w \equiv \hat{W}_{\rm tot}/2t_{\rm c}$, for the under-damped type $\epsilon = 0.01$ (squares) and the over-damped type $\epsilon = 0.1$ (circle) are shown in Fig. 7.6, where $T_{\rm H}/T_{\rm L} = 5.0$ and $e = 1.0$ are fixed and $p_0 \equiv T_{\rm out}/t_0$. Apparently, the MP is achieved at time $t_c^{\rm MP}$, which corresponds to the necessary time for the gas to expand toward the mechanical equilibrium. We note that the long time heating or cooling ruins the power, because the extracted work is, at most, $N(T_{\rm H} - T_{\rm L})\ln(T_{\rm H}/T_{\rm L})$. Thus, the power decreases as a function of t_c: $\langle\hat{p}_w\rangle_{\rm SC} \propto 1/t_c$ for $t_c \gg t_c^{\rm MP}$, which is drawn as a dashed line in Fig. 7.6.

We, here, explain that the obtained work is balanced with the work done by the viscous friction for gases. Multiplying V onto Eq. (7.25) and integrating over the cycle, we obtain $W_{\rm tot} = \oint M\bar{\gamma}V dX > 0$, because the integral of the left hand side of Eq. (7.25) is zero. Thus, the obtained work is balanced with the work done by the viscous friction for gases.

We present the results for the efficiency at MP (Fig. 7.7) for (a) $\epsilon = 0.01$ and (b) $\epsilon = 0.1$. The main figures represent the results for the elastic piston ($e = 1.0$), and the insets are those for the corresponding inelastic piston ($e = 0.9$). The open squares $\langle\hat{\eta}\rangle_{\rm SC}$ and triangles $\bar{\eta}$ are the simulation data for the SMF for the dilute gas characterized by Eq. (7.22), while filled ones are the data for the corresponding MD simulation. Although $\bar{\eta}$ and $\langle\hat{\eta}\rangle_{\rm SC}$ are different quantities, they agree with each other. As a comparison with previous studies, we plot the CNCA efficiency $\eta_{\rm CA}$ (dotted lines). Our SMF model correctly predicts the efficiency at MP for MD simulations, at least for $\epsilon = 0.01$, while our model is lower than the CNCA efficiency for $\epsilon = 0.1$. We note that the efficiency for our

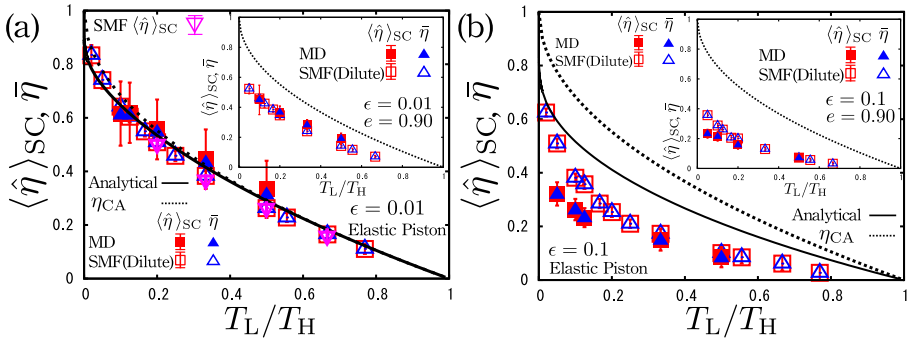

Figure 7.7: Efficiencies at maximum power operations for dilute gases for (a) $\epsilon = 0.01$ and (b) $\epsilon = 0.1$. The main figures represent the results for the elastic piston case, and the insets are those for the corresponding inelastic piston. In the main figure of (a), we plot the result of SMF (open piles). The open squares $\langle\hat{\eta}\rangle_{\rm SC}$ and open triangles $\bar{\eta}$ are simulation data for the dilute approximation of SMF, while filled ones are the data for the corresponding MD simulation. For the elastic piston of $\epsilon = 0.01$, the observed efficiencies are close to $\eta_{\rm CA}$ (dashed line) and Eq. (7.35)(solid line).

model with $e = 1.0$ and $\epsilon = 0.01$ are close to the CNCA efficiency.

Here, we derive the semi-analytical expression on $\bar{\eta}$ on the basis of SMF in the limit $\epsilon \to 0$. In this limit, $\hat{T}_{\rm in}$ rapidly relaxes to bath temperature, right after $T_{\rm bath}$ is switched. The average of the work Eq. (7.26) can be approximated by

$$\langle\hat{W}_{\rm tot}\rangle_{\rm SC} \simeq N(T_{\rm H} - T_{\rm L})\ln\tilde{X}(t_c), \tag{7.30}$$

where we have introduced the volume change of the gas through the cycle $\tilde{X}(t_c) \equiv \langle\hat{X}(t_c)\rangle_{\rm SC}/\langle\hat{X}(0)\rangle_{\rm SC}$ and choose $e = 1$. Integrating the equation of the energy conservation (7.22), we obtain

$$\Delta\hat{U} \quad = \quad \hat{Q}_{\rm H} + \hat{E}^{(H)}_{\rm pis} \tag{7.31}$$

where we have introduced $\Delta\hat{U} = 3N(T_{\rm H} - T_{\rm L})/2$ and $\hat{E}^{(H)}_{\rm pis} \equiv \int_{T_{\rm H}} d\hat{E}_{\rm pis}$. Averaging Eq. (7.31) and expanding in terms of ϵ, we obtain

$$\langle\hat{Q}_{\rm H}\rangle_{\rm SC} = \frac{3}{2}N(T_{\rm H} - T_{\rm L}) + NT_{\rm H}\ln\tilde{X}(t_c) + O(\epsilon), \tag{7.32}$$

where we have ignored the heat leak due to the fluctuation of the piston $O(\epsilon)$. Therefore, the efficiency $\bar{\eta}$ is given by

$$\bar{\eta} \quad = \quad \frac{T_{\rm H} - T_{\rm L}}{T_{\rm H} + \frac{3}{2}\frac{T_{\rm H}-T_{\rm L}}{\ln\tilde{X}(t_c)}} = \frac{\eta_C}{1 + \frac{3}{2}\frac{\eta_C}{\ln\tilde{X}(t_c)}}. \tag{7.33}$$

Assuming that $\tilde{X}(t_{\rm c}^{\rm MP})$ depends on the power of $T_{\rm H}/T_{\rm L}$:

$$\tilde{X}(t_{\rm c}^{\rm MP}) = \left(\frac{T_{\rm H}}{T_{\rm L}}\right)^{\alpha} = (1-\eta_C)^{-\alpha}\,, \tag{7.34}$$

we obtain the analytical expression on $\bar{\eta}$ for MP:

$$\begin{aligned}\bar{\eta}_{\rm MP} &= \eta_C\left(1-\frac{3}{2\alpha}\frac{\eta_C}{\ln(1-\eta_C)}\right)^{-1} \\ &= \frac{1}{1+\frac{3}{2\alpha}}\eta_C + \frac{3}{4\alpha}\left(\frac{1}{1+\frac{3}{2\alpha}}\right)^2\eta_C^2 + \frac{\alpha+6}{8\alpha^2}\left(\frac{1}{1+\frac{3}{2\alpha}}\right)^3\eta_C^3 + O(\eta_C^4),\end{aligned} \tag{7.35}$$

which is shown in Fig. 7.7 by solid lines. The exponent α is estimated from the simulation of SMF, where $\alpha = 1.5$ for $\epsilon = 0.01$ and $\alpha = 0.79$ for $\epsilon = 0.1$ (Fig. 7.8). As is shown in Fig. 7.7, Eq. (7.35) agrees with the results of MD for $\epsilon = 0.01$, while the agreement is not good for $\epsilon = 0.1$. The integration of $O(\epsilon)$ term would be necessary for the better agreement of $\epsilon = 0.1$. We expect that the exponent α is reduced to $\alpha = 3/2$ in the limit $\epsilon \to 0$ and $e \to 1$, as follows. Although there exist the tiny heat leak during the expansion process, we may approximately ignore the leak because the heating process is almost isochoric, as will be discussed in Sec. 7.7. Recalling Poisson's relation for an adiabatic process of ideal gases between state 1 and 2: $(T_{\rm in}^{(2)}/T_{\rm in}^{(1)})^{3/2}(X^{(2)}/X^{(1)}) = 1$, where $X^{(a)}$ and $T_{\rm in}^{(a)}$ $(a = 1, 2)$ respectively represent the position of the piston and temperature for the state a, the exponent $\alpha = 3/2$ agrees with the simulation result. In Sec. 7.6, we will prove that $\alpha = 3/2$ corresponds to the tight coupling condition for the Onsager matrix in linearly irreversible thermodynamics. Substituting the obtained $\alpha = 3/2$ for $\epsilon = 0.01$ into Eq. (7.35), we obtain

$$\bar{\eta}_{\rm MP} = \frac{\eta_C}{2} + \frac{\eta_C^2}{8} + \frac{5\eta_C^3}{96} + O(\eta_C^4) \tag{7.36}$$

We note that Eq. (7.36) is identical to the expansion of $\eta_{\rm CA}$ up to $O(\eta_C^2)$:

$$\eta_{\rm CA} = \frac{\eta_C}{2} + \frac{\eta_C^2}{8} + \frac{\eta_C^3}{16} + O(\eta_C^4). \tag{7.37}$$

However, the existence of ϵ lowers the efficiency from $\eta_{\rm CA}$ even at the leading order $O(\eta_C)$, because $\alpha = 0.79 < 3/2$ for $\epsilon = 0.1$. We thus conclude that the efficiency at MP for passive engines confining dilute gases is the CNCA efficiency if the piston is sufficiently massive and elastic.

7.5.2 Moderately dense case

We have analyzed the efficiency for dilute gases in the previous subsection. Here, we discuss the efficiency at MP for a moderately dense hard core gas. The

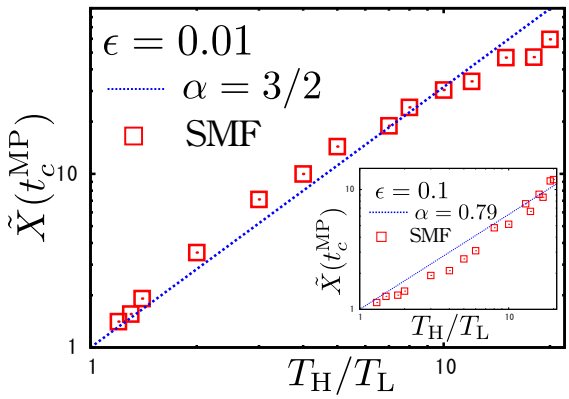

Figure 7.8: The volume change of the enclosed gas at MP $\tilde{X}(t_c^{\rm MP})$ is plotted against $T_{\rm H}/T_{\rm L}$. The main figure is for $\epsilon = 0.01$, and the inset is $\epsilon = 0.1$.

efficiency at MP is plotted in the main figure of Fig. 7.9, where SMF model almost correctly predicts the results of our MD simulation. The data for SMF at $T_{\rm H}/T_{\rm L} = 1.2, 1.3, 1.4$ are averaged over 1.0×10^4 cycles after 10 cycles for initial relaxation to improve their numerical accuracy. The other data are averaged from 11th cycle to 110th cycle. We find that the efficiency for moderately dense hard core gases is smaller than that for dilute ones to compensate the heat flux $J_{\rm in}$ as will be shown in the next section.

7.6 Linearly irreversible thermodynamics

In the previous section, we have suggested that the efficiency at MP output for the dilute gas can be described by the CNCA efficiency in the limit $\epsilon \to 0$ and $e \to 1$, while that for the moderately dense gas is smaller than the CNCA efficiency. In this section, we show that results in linear non-equilibrium situation $\eta_C \to 0$ can be understood by the relations between the currents $\mathcal{J}_i$ and the thermodynamic forces $\mathcal{X}_i$ on the basis of the Curie-Prigogine symmetry principle [149]:

$$\mathcal{J}_1 = L_{11}\mathcal{X}_1 + L_{12}\mathcal{X}_2, \tag{7.38}$$
$$\mathcal{J}_2 = L_{21}\mathcal{X}_1 + L_{22}\mathcal{X}_2, \tag{7.39}$$

where the Onsager matrix satisfies $L_{11}, L_{22} \geq 0, L_{12} = L_{21}$ and $\det L_{ij} = L_{11}L_{22} - L_{12}L_{21} \geq 0$. In the following, we assume that the piston is elastic $e = 1.0$ and massive limit $\epsilon \to 0$, and we abbreviate the average of an arbitrary stochastic quantity $\hat{\mathcal{A}}$ as $\mathcal{A} = \langle \hat{\mathcal{A}} \rangle_{\rm SC}$. We examine the dilute gas in Sec. 7.6.1 and clarify the finite density effect in Sec. 7.6.2.

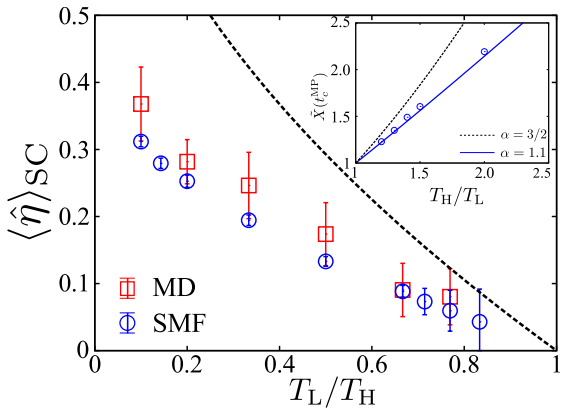

Figure 7.9: The main figure represents the efficiency at MP for moderately dense hard core gases. SMF almost correctly predicts the efficiency for MD simulation. We note that the efficiency is much smaller than the CNCA one, which is caused by the inevitable heat flux $dQ_{\rm cond}$. The inset represents the expansion ratio for the dense gases. The exponent α is estimated to be $\alpha = 1.141 \pm 0.009$.

7.6.1 Dilute case

Let us derive the Onsager matrix L_{ij} in our setup for the dilute gas following Refs. [113, 115]. We consider the linear non-equilibrium situation as $T_{\rm H,L} = T \pm \Delta T/2$, where T and ΔT are the mid-temperature $T \equiv (T_{\rm H} + T_{\rm L})/2$ and the temperature difference $\Delta T = T_{\rm H} - T_{\rm L}$, respectively, satisfying $\Delta T/T \ll 1$. Here, the total entropy production per a unit cycle $\Delta\sigma = -Q_{\rm H}/T_{\rm H} - Q_{\rm L}/T_{\rm L}$ is rewritten as

$$\Delta\sigma = -\frac{W_{\rm tot}}{T} + \frac{\Delta T}{T^2} Q_{\rm H}, \tag{7.40}$$

where we have used $W_{\rm tot} = Q_{\rm H} + Q_{\rm L}$ and $\Delta T/T \ll 1$. On the basis of the relation

$$\frac{\Delta\sigma}{2t_c} = \mathcal{J}_1\mathcal{X}_1 + \mathcal{J}_2\mathcal{X}_2, \tag{7.41}$$

$\mathcal{J}_i$ and $\mathcal{X}_i$ are respectively given by

$$\mathcal{J}_1 = \frac{T}{2t_c},\ \mathcal{J}_2 = \frac{Q_{\rm H}}{2t_c}, \tag{7.42}$$

$$\mathcal{X}_1 = -\frac{W_{\rm tot}}{T^2},\ \mathcal{X}_2 = \frac{\Delta T}{T^2} = \frac{\eta_C}{T}. \tag{7.43}$$

Let us derive L_{11} and L_{21} by taking $\eta_C = \Delta T/T \to 0$. $W_{\rm tot}$ is written as

$$W_{\rm tot} \simeq N\eta_C T \ln\tilde{X}(t_c) - 2a_0 NT \int_{X_{\rm L}}^{X_{\rm H}} V\frac{dX}{X}. \tag{7.44}$$

The first term on the right-hand side of Eq. (7.44) vanishes in the limit $\eta_C \to 0$. Then, from Eqs. (7.38), (7.42), and (7.43) we obtain

$$L_{11} = \frac{T^2}{4t_c N}\frac{1}{\tilde{E}} \geq 0, \tag{7.45}$$

$$\tilde{E} \equiv \int_{X_{\rm L}}^{X_{\rm H}} a_0 V \frac{dX}{X}. \tag{7.46}$$

Here, we have introduced $\tilde{E}$ as the inevitable dissipation due to the finite velocity of the piston. Now the heat $Q_{\rm H}$ is given by

$$Q_{\rm H} = \frac{3}{2}N\frac{\Delta T}{T}T + N\left(T+\frac{\Delta T}{2}\right)\ln\tilde{X}(t_c) - N\left(T+\frac{\Delta T}{2}\right)a_0\int_{X_{\rm L}}^{X_{\rm H}} V\frac{dX}{X}, \tag{7.47}$$

which can be rewritten as

$$\frac{Q_{\rm H}}{2t_c} = \frac{T^2}{4t_c}\frac{\ln\tilde{X}(t_c)-\tilde{E}}{\tilde{E}}\left(-\frac{W_{\rm tot}}{T^2}\right) \simeq \frac{T^2}{4t_c}\frac{\ln\tilde{X}(t_c)}{\tilde{E}}\mathcal{X}_1, \tag{7.48}$$

$$L_{21} = \frac{T^2}{4t_c\tilde{E}}\ln\tilde{X}(t_c), \tag{7.49}$$

in the leading order of $W_{\rm tot}/T$ and the limit $\eta_C \to 0$. Next, let us determine L_{12} and L_{22}. L_{12} can be determined from the condition $W_{\rm tot} = 0$, i.e., the work-consuming state:

$$W_{\rm tot} = N\mathcal{X}_2 T^2 \ln\tilde{X}(t_c) - 2NT\tilde{E} = 0. \tag{7.50}$$

Then, we obtain the reciprocal relation

$$L_{12} = \frac{T^2}{4t_c\tilde{E}}\ln\tilde{X}(t_c) = L_{21}. \tag{7.51}$$

Taking terms depending only on ΔT in Eq. (7.47), we obtain

$$\frac{Q_{\rm H}}{2t_c} \simeq \frac{1}{2t_c}\left(\frac{3}{2}NT^2 + \frac{NT^2}{2}\ln\tilde{X}(t_c)\right)\frac{\Delta T}{T^2}, \tag{7.52}$$

$$L_{22} = \frac{1}{2t_c}\left(\frac{3}{2}NT^2 + \frac{NT^2}{2}\ln\tilde{X}(t_c)\right) \geq 0, \tag{7.53}$$

where we have ignored the higher order term including a_0. Equations (7.45), (7.49), (7.51) and (7.53) are the explicit expressions of the Onsager matrix.

Here, we show that $\alpha = 3/2$ corresponds to the tight coupling limit of the Onsager matrix, where fluxes $\mathcal{J}_1$ is proportional to $\mathcal{J}_2$. Because the determinant is readily calculated as

$$\det L_{ij} = \frac{T^4}{8t_c^2\tilde{E}}\left(\frac{3}{2}+\frac{\alpha\eta_C}{2}-\alpha\right) \simeq \frac{T^4}{8t_c^2\tilde{E}}\left(\frac{3}{2}-\alpha\right) \geq 0. \tag{7.54}$$

The tight coupling limit $\det L_{ij} = 0$ corresponds to $\alpha = 3/2$, which is equal to the value obtained in Sec. 7.5. The CNCA efficiency is derived on the basis of Eqs. (7.38) and (7.39) in the tight coupling limit, following the similar procedure in Ref. [111]. It should be noted that the control parameter for our engine is not $\mathcal{X}_1$ but $\mathcal{J}_1$, in contrast to Ref. [111].

7.6.2 Moderately dense case

We stress that the efficiency at MP of the engine for the moderately dense gas is much smaller than the CNCA efficiency even in linear non-equilibrium regime $\eta_C \ll 1$, which is the result of the inevitable loose coupling of the Onsager matrix L^*_{ij} as follows. Solving the average of Eq. (7.10) in terms of $T_{\rm in}$, we obtain

$$T_{\rm in}(t) = T_{\rm bath}(1 - a_0^*(t)V(t)) + O(\epsilon^2) \tag{7.55}$$

$$a_0^*(t) \equiv \frac{a_0}{1 + 4\Phi(t)g_0(\Phi(t)) + \tilde{j}_{\rm in}(t)}, \tag{7.56}$$

where we have introduced the scaled flux $\tilde{j}_{\rm in} = \{T_{\rm bath}/(T_{\rm bath} - T_{\rm in})\}dQ_{\rm cond}/dt$. See also Eq. (7.24) for the comparison with the dilute case. Because the additional heat flux $dQ_{\rm cond}$ exists, Eqs. (7.40) and (7.47) are, respectively, replaced by

$$\Delta\sigma = -\frac{W_{\rm tot}}{T} + \frac{\Delta T}{T^2}Q_{\rm H} + \frac{1}{T}Q_{\rm cond}, \tag{7.57}$$

$$\begin{aligned} Q_{\rm H} &= \frac{3}{2}N\frac{\Delta T}{T}T + N\left(T + \frac{\Delta T}{2}\right)\ln\tilde{X}(t_c) + Q^{\rm H}_{\rm cond} \\ &\quad -N\left(T + \frac{\Delta T}{2}\right)\int_{X_{\rm L}}^{X_{\rm H}} \epsilon a_0^*(t)V\frac{dX}{X}, \end{aligned} \tag{7.58}$$

where we have introduced

$$Q_{\rm cond} \equiv \sum_{\mu={\rm H,L}} Q^{\mu}_{\rm cond} \tag{7.59}$$

$$Q^{\mu}_{\rm cond} \equiv -\int_{T_\mu} dQ_{\rm cond}. \tag{7.60}$$

Note that the sign of $Q^{\rm H}_{\rm cond}$ and $Q^{\rm L}_{\rm cond}$ are positive and negative respectively, and they are $O(\Delta T)$, while $Q_{\rm cond} > 0$ is $O(\Delta T^2)$ (See Eqs. (7.13), (7.21), and (7.60)). Thus, we obtain the Onsager matrix as

$$L^*_{11} \equiv \frac{T^2}{4t_c N}\frac{1}{\tilde{E}^*} \geq 0, \tag{7.61}$$

$$L^*_{21} \equiv \frac{T^2}{4t_c\tilde{E}^*}\ln\tilde{X}(t_c) = L^*_{12}, \tag{7.62}$$

$$L^*_{22} \equiv \frac{1}{2t_c}\left(\frac{3}{2}NT^2 + \frac{NT^2}{2}\ln\tilde{X}(t_c) + \tilde{q}\right) \geq 0, \tag{7.63}$$

where we have introduced $\tilde{E}^* \equiv \int_{X_{\rm L}}^{X_{\rm H}} (V/X) a_0^*(t) dX$ and $\tilde{q} \equiv Q_{\rm cond}/N\Delta T + Q_{\rm cond}^{\rm H} T/N\Delta T^2 > 0$. We have checked that $\tilde{q} \simeq 2.04$ for the operation of MP with $T_{\rm H}/T_{\rm L} = 1.5$ through the simulation of SMF. The tight coupling condition for L_{ij}^* is, thus, reduced to

$$\alpha = \frac{3}{2} + \tilde{q} > \frac{3}{2}. \tag{7.64}$$

On the other hand, we find that $\alpha < 3/2$ holds, which might be justified by the parallel argument to that in Sec. 7.5. With the aid of Eq. (7.9), Poisson's relation for a moderately dense gas can be derived as:

$$\left(\frac{T_{\rm in}^{(2)}}{T_{\rm in}^{(1)}} \right)^{3/2} \left(\frac{X^{(2)}}{X^{(1)}} \right)^{1+\Psi} = 1. \tag{7.65}$$

Here, Ψ represents the correction term due to the finite density effect:

$$\begin{aligned} \Psi &\equiv -\frac{\Phi^{(2)} - \Phi^{(1)}}{\ln \frac{X^{(2)}}{X^{(1)}}} \frac{4 - 3(\Phi^{(2)} + \Phi^{(1)}) + 2\Phi^{(2)}\Phi^{(1)}}{(1-\Phi^{(2)})^2 (1-\Phi^{(1)})^2} \\ &\simeq 4 \frac{d_{\rm in}}{X^{(1)}}, \end{aligned} \tag{7.66}$$

where $\Phi^{(a)} (a = 1, 2)$ represents the volume fraction for the state a. Hence, we expect $\alpha = 3/\{2(1+\Psi)\} \simeq 1.07$, which agrees with $\alpha = 1.141 \pm 0.009 < 3/2$ in the simulation of SMF shown in the inset of Fig. 7.9. Although this agreement may be accidental because the heat leak exists in the process, it is interesting to look for the reason why Poisson's relation works well. Thus, the system does not satisfy the tight coupling condition for moderately dense gases because of the existence of $dQ_{\rm cond}$.

7.7 Discussion

Let us discuss the difference between our results and previous works. Here, we explain that our engine contains isochoric and quasi-adiabatic heating/cooling processes, i.e., our engine is similar but different from the Otto engine. The pressure-volume graph for $\epsilon = 0.01$ and $T_{\rm H}/T_{\rm L} = 5.0$ is plotted in the main figure of Fig. 7.10. We also plot the time evolutions of the heat flux (solid line), the piston position (chain line), and the pressure (dashed line) for $0 < t/t_0 < 1.6$ in the inset of Fig. 7.10, where the heat flux is scaled by $\dot{q}_0 \equiv 5.0 \times 10^5 T_{\rm out}/t_0$. We notice that the heating process ends very fast $t/t_0 \sim 0.1$, and it can be regarded as the isochoric process. Then, the system expands with smaller heat flux which is less than 10% of the isochoric regime for $t/t_0 < 0.5$. For $0.5 < t/t_0 < 1.6$, the system is approximately adiabatic, i.e. the heat flux is negligible. Thus, our engine is similar but different from the Otto engine.

Let us explain the reason why the heat flux $dQ_{\rm cond}$ for a moderately dense gas is relevant to the efficiency at MP in contrast to the conventional finite time

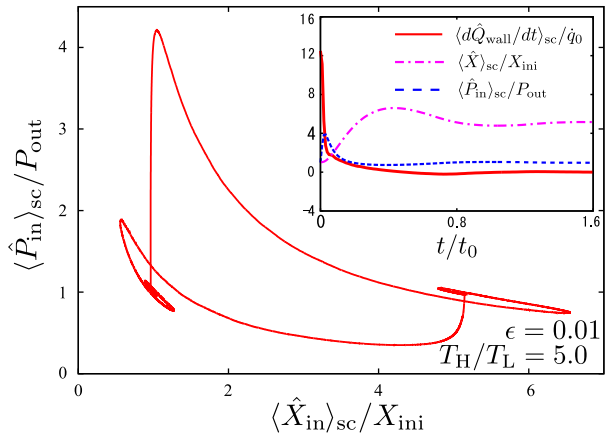

Figure 7.10: The main figure represents the pressure-volume figure for $\epsilon = 0.01, T_{\rm H}/T_{\rm L} = 5.0$. The inset represents the time evolution of the heat flux from the thermal wall (solid line), the position of the piston (chain line) and the pressure for the enclosed gas (dashed line) for $0 < t/t_0 < 1.6$. The heat process ends fast, and can be regarded as an isochoric one.

thermodynamics. As a counter example, let us consider the finite time Carnot cycle, which contains isothermal and adiabatic processes. When we attach the thermal bath to the gas, the amount of heat flux for a finite time Carnot cycle is too small and $dQ_{\rm cond}$ does not exist, because the temperature of the gas and that of the bath are essentially identical as the result of the adiabatic processes with mechanical control of the piston. On the other hand, the amount of heat flux for our engine is large because the temperature of the gas and that of the bath are different when we attach the bath onto the gas. Thus, the effect of the heat flux $dQ_{\rm cond}$ is significant for the efficiency for the passive engine.

For a macroscopic piston in the limit $\epsilon \to 0$, the one-dimensional momentum transfer model (Eqs. (7.1) and (7.2)) is too simple for the realistic motion of the piston, where the side-wall friction [240], the excitation of atoms on the piston surface [241] and tilting of the piston, etc. should be relevant for the real piston motion. In Appendix H, we discuss the effect of side-wall friction on the efficiency for our protocol and show that the side-wall friction lowers the efficiency.

7.8 Conclusion

In this chapter, we have investigated the efficiency at MP for a passive engine. We have considered an operation protocol for a hard core gas partitioned by a massive piston (Figs. 7.1 and 7.2). SMF has been proposed and its relevance has been demonstrated from the comparison of its result with the result of the

MD simulation for the dilute gas (Fig. 7.4) and the moderately dense gas (Fig. 7.5). We have found the existence of the MP in Fig. 7.6 and examined the efficiency at MP for the dilute gas in Fig. 7.7. The efficiency at MP for dilute gases is close to the CNCA efficiency for an elastic and massive piston. We have derived the analytical expressions for the efficiency at MP on the basis of SMF as Eqs. (7.35) and (7.36). To understand the linear non-equilibrium regime, we have derived the Onsager matrix explicitly Eqs. (7.45), (7.49), (7.51), and (7.53), and have found that the tight coupling condition is satisfied for the dilute gas. In contrast to the dilute gas, we have found that the efficiency at MP for moderately dense gases is smaller than the CNCA efficiency even for an elastic and massive piston in linear non-equilibrium regime (Fig. 7.9). We have clarified the importance of the heat flux when $T_{\rm bath}$ is switched, which induces the inevitable loose coupling for the Onsager matrix.

Chapter 8

Discussion and Summary

Let us summarize the thesis with some remarks. In Chapter 5, we have examined the roles of sliding friction in the fluctuating motion of the adiabatic piston. We have found that an arbitrary nonlinear friction can reverse the direction of the motion of the piston, while the linear one cannot. We have also derived the fluctuation relation under dry friction. In Fig. 5.4, we have discussed the steady state velocity of the piston as a function of the friction coefficient. Notice that the velocity of the piston under nonlinear friction exhibits a peak around $\mu_0' \sim 1.0$ and the peak height depends on the functional form of the nonlinear friction. It is interesting and important to clarify the optimal friction to maximize the piston velocity on the basis of Ref. [93].

In Chapter 6, we have clarified the role of a granular rotor as a probe of the VDF of a non-equilibrium bath. We have shown that there exists a one-to-one relation between the VDF of a non-equilibrium bath and the angular VDF of the rotor, using the molecular dynamics simulation of a vibrating granular bed. Let us discuss the possible extension of results in Chapter 6. We have assumed the restitution coefficient of grains is constant [175, 176]. The restitution coefficient for a sphere depends on the impact velocity $v_{\rm imp}$ as $e(v_{\rm imp}) = 1 - \mathcal{B}_1 v_{\rm imp}^{1/5} + \cdots (\mathcal{B}_1 > 0)$ [61, 187]. As discussed in Ref. [188], the velocity dependence of the restitution coefficient can be also analyzed in our theory within the framework of the Boltzmann-Lorentz equation. The effects for the tangential interaction and the mutual rotation between grains are also necessary to be analyzed. The extension of the Boltzmann equation toward denser gas is known as the Enskog equation [73, 74] (See also Appendix E). It is possible and interesting to apply our framework to the rotor in dense granular media [189] or denser granular liquids near the jamming transition beyond Enskog equation [86] by modifying the transition probability $\mathbb{W}_{\epsilon_{\rm rot}}$ in Eq. (6.6) [190]. As a future problem, it is also necessary to estimate the amount of the errors in particular for the inverse estimation formulas Eqs. (6.11) and (6.12).

In Chapter 7, we have theoretically analyzed the efficiency at MP for a passive engine, which is the simplest model of internal combustion engines. We have illustrated that the efficiency at MP for an elastic massive piston confining

a dilute gas is given by the CNCA efficiency, while that for a moderately dense gas is smaller than the CNCA efficiency even for an elastic and massive piston in the linear non-equilibrium regime. We have shown that the heat flux when $T_{\rm bath}$ is switched induces the inevitable loose coupling for the Onsager matrix. We should note that such a loose coupling would appear not only for a passive engine but also other engines, e.g. the finite time Carnot cycle if the temperature of a working fluid is different from $T_{\rm bath}$. Thus, we conclude that the heat flux when $T_{\rm bath}$ is switched should be suppressed for higher efficiency at MP.

The model considered in Chapter 7 might be unrealistic if the gas is regarded as a molecular gas because the mass of a real piston must be much larger than the mass of each molecule and adhesion between molecules and walls cannot be ignored in such a small engine. Our model, however, would be experimentally realized through two kinds of setups: colloidal suspensions with a semi-permeable membrane and a highly excited granular gas with a movable piston. Although the hydrodynamic interaction between colloids is important, the osmotic pressure between two dilute solutions separated by a semi-permeable membrane is described by van't Hoff's formula which has an identical form to the equation of states for ideal gases. Inhomogeneity and non-Gaussianity of granular gases can be suppressed, at least, for a specific setup of a highly agitated granular gas [29–31]. Thus, our model can be regarded as a simplified and idealized one for such systems. It would be interesting to consider the stochastic version of the multi-component chemical engine discussed in Chapter 2 and the non-equilibrium engine consisting of an inelastic hard core gas whose transport coefficients are given in Ref. [193] and summarized in Appendix E. To improve SMF model, we need to solve hydrodynamic equations under the moving boundary in contrast to the treatment in this paper. We also need to investigate the nonlinear Onsager matrix to understand the efficiency in the nonlinear non-equilibrium regime [114, 115]. Finally, because thermodynamic studies of engines without any force controls are little known so far, their experimental studies will be expected near future.

Appendix A

Derivation of fluctuation relation under dry friction

In this appendix, we derive the fluctuation relation under dry friction Eq. (5.37), writing $\hat{W} \equiv \hat{W}'_{\rm L}$ and $d\hat{W} \equiv d\hat{W}_{\rm L} - F_0 \hat{V} dt$. Let us derive a Master equation for the joint probability $f(V,W,t) \equiv \langle \hat{f}(\hat{V}(t), \hat{W}'_{\rm L}(t)) \rangle$ with $\hat{f}(\hat{V}(t), \hat{W}'_{\rm L}(t)) \equiv \delta(V - \hat{V}(t))\delta(W - \hat{W}'_{\rm L}(t))$ following Ref. [8]. For an arbitrary function $g = g(\hat{V}, \hat{W})$, the differentiation $dg(\hat{V}, \hat{W}) \equiv g(\hat{V} + d\hat{V}, \hat{W} + d\hat{W}) - g(\hat{V}, \hat{W})$ is given by

$$
\begin{aligned}
dg(\hat{V},\hat{W}) \;=\; & \frac{1}{M}\left(\sum_v d\hat{L}^v_{\rm L}\cdot P_v\right)\cdot\left\{\left(\frac{\partial}{\partial V} + MV\frac{\partial}{\partial W}\right)g\right\} \\
& + \frac{1}{2M^2}\left(\sum_v d\hat{L}^v_{\rm L}\cdot P_v^2\right)\cdot\left\{\left(\frac{\partial}{\partial V} + MV\frac{\partial}{\partial W}\right)^2 g\right\} \\
& + \frac{1}{M}\left(\sum_v d\hat{L}^v_{\rm R}\cdot P_v\right)\cdot\frac{\partial g}{\partial V} + \frac{1}{2M^2}\left(\sum_v d\hat{L}^v_{\rm R}\cdot P_v^2\right)\cdot\frac{\partial^2 g}{\partial V^2} \\
& - F_0\hat{V}\cdot\frac{\partial g}{\partial W}dt - \epsilon\frac{\bar{F}_{\rm fri}}{M}\sigma(V)\cdot\frac{\partial g}{\partial V}dt \\
& + O(\epsilon^2 dt).
\end{aligned}
\tag{A.1}
$$

It should be noted that $\langle \sum_v d\hat{L}^v_\alpha \cdot P_v^{n+1} \rangle = O(\epsilon^n dt)$. By taking the ensemble average of Eq. (A.1) and expanding it up to $O(\epsilon)$, the Master equation for $f(V,W,t)$ is derived [8]. Introducing Laplace transformation of $f(V,W,t)$ as

$$
\tilde{f}_\beta \equiv \int dW e^{-\beta W} f(V,W,t), \tag{A.2}
$$

we obtain the time evolution for $\tilde{f}_\beta$:

$$
\frac{\partial}{\partial t}\tilde{f}_\beta = \epsilon\frac{\gamma_0}{M}\left(L_\beta + L_{\rm fri}\right)\tilde{f}_\beta + O(\epsilon^2), \tag{A.3}
$$

where L_β and $L_{\rm fri}$ denote the linear operators on $\tilde{f}_\beta$ as

$$
\begin{aligned}
L_\beta &= \frac{v_{T_e}^2}{2}\frac{\partial^2}{\partial V^2} + \left(1+\check{\beta}\frac{\gamma_{\rm L}}{\gamma_0}\sqrt{\frac{T_{\rm L}}{T_{\rm R}}}\right)\frac{\partial}{\partial V}V - \frac{\check{\beta}}{2}\frac{\gamma_{\rm L}}{\gamma_0}\sqrt{\frac{T_{\rm L}}{T_{\rm R}}} \\
&\quad + \frac{\gamma_{\rm L}}{\gamma_0}\check{\beta}\left(1+\sqrt{\frac{T_{\rm L}}{T_{\rm R}}}\frac{\check{\beta}}{4}\right)\frac{V^2}{v_{T_e}^2}, \qquad \text{(A.4)} \\
L_{\rm fri} &\equiv \mu_0 v_{T_e}\frac{\partial}{\partial V}\sigma(V). \qquad \text{(A.5)}
\end{aligned}
$$

with $\check{\beta} \equiv 2k_B T_e \beta$. The eigenvalues κ_n and eigenfunctions for the operator (A.4) and its adjoint operator $L_\beta^\dagger$ are discussed in Ref. [162] :

$$
\begin{aligned}
L_\beta \psi_n(V) &= \kappa_n \psi_n(V) \qquad \text{(A.6)} \\
L_\beta^\dagger \phi_n(V) &= \kappa_n \phi_n(V) \qquad \text{(A.7)}
\end{aligned}
$$

$$
\begin{aligned}
\psi_n(V) &= \sqrt{\frac{\zeta}{2\pi v_{T_e} 2^n n!}}\exp\left[-\frac{\zeta V^2}{2v_{T_e}^2}\right]H_n\left(\frac{\sqrt{\eta}V}{v_{T_e}}\right), \qquad \text{(A.8)} \\
\phi_n(V) &= \sqrt{\frac{2\eta}{\zeta v_{T_e}}}\exp\left[-\left(\eta-\frac{\zeta}{2}\right)\frac{V^2}{v_{T_e}^2}\right]H_n\left(\frac{\sqrt{\eta}V}{v_{T_e}}\right), \qquad \text{(A.9)}
\end{aligned}
$$

$$
\begin{aligned}
\kappa_n(\beta) &= \frac{1}{2}\left\{1-(1+2n)\eta(\beta)\right\}, \qquad \text{(A.10)} \\
\eta(\beta) &\equiv \sqrt{1+\frac{\sqrt{\tilde{T}}(2k_B T_e)^2}{(1+\sqrt{\tilde{T}})^2}\beta(\Delta\beta_e-\beta)}, \qquad \text{(A.11)}
\end{aligned}
$$

where Hermite polynomials are defined as $H_n(x) \equiv (-1)^n e^{x^2}(d/dx)^n e^{-x^2}$ and $\int_{-\infty}^{\infty} dx e^{-x^2} H_n(x) H_l(x) = \sqrt{\pi} 2^n n! \delta_{nl} (n, l = 0, 1, \cdots)$. $\kappa_n(\beta)$ has the Gallavotti-Cohen-type symmetry as $\kappa_n\left(\Delta\beta_e - \beta\right) = \kappa_n(\beta)$ [159, 161], which leads to the conventional fluctuation relation without dry friction:

$$
\lim_{t\to\infty}\frac{1}{t}\ln\frac{\mathcal{P}(p_w,t)}{\mathcal{P}(-p_w,t)} = \Delta\beta_e p_w + O(\epsilon^2). \qquad \text{(A.12)}
$$

Let us solve eigenvalue problem for $L_\beta + L_{\rm fri}$ perturbatively up to $O(\epsilon, \mu_0)$, assuming that μ_0 is small:

$$
\left(L_\beta + L_{\rm fri}\right)\bar{\psi}_n(V) = \bar{\kappa}_n(\beta)\bar{\psi}_n(V), \qquad \text{(A.13)}
$$

We assume that $\mathrm{Re}(\bar{\kappa}_n) \leq \mathrm{Re}(\bar{\kappa}_m)$ for $n > m$, where $\mathrm{Re}(a)$ represents the real part of any complex number a. Multiplying $\phi_n(V)$ on both sides of Eq. (A.13),

integrating them over V and substituting $\bar{\kappa}_n(\beta) = \kappa_n(\beta) + \mu_0 \kappa_n^{(1)}(\beta) + O(\mu_0^2)$, $\bar{\psi}_n(V) = \psi_n(V) + O(\mu_0)$ into Eq. (A.13) for $n = 0$, we obtain:

$$\mu_0 \kappa_0^{(1)}(\beta) = -\frac{\mu_0}{\sqrt{\pi \eta(\beta)}} \left(1 + \check{\beta} \frac{\sqrt{\tilde{\bar{T}}}}{1 + \sqrt{\tilde{\bar{T}}}} \right). \tag{A.14}$$

The largest eigenvalue of the operator $\epsilon \gamma_0 (L_\beta + L_{\rm fri})/M$ is known to be equal to the scaled cumulant generating function [236]:

$$\lim_{t \to \infty} \frac{1}{t} \ln \langle e^{-\beta \hat{W}'_{\rm L}(t)} \rangle = \epsilon \frac{\gamma_0}{M} \bar{\kappa}_0(\beta) \tag{A.15}$$

Thus, according to Ref. [157], the large deviation property for $\hat{W}'_{\rm L}$ under the dry friction is characterized by the Legendre transformation of the maximum eingenvalue of $L_\beta + L_{\rm fri}$:

$$\lim_{t \to \infty} \frac{1}{t} \ln \mathcal{P}(p_w, t) = p_w \beta^* + \epsilon \frac{\gamma_0}{M} \bar{\kappa}_0(\beta^*), \tag{A.16}$$

where $\beta^* = \beta^*(p_w)$ gives the minimum for $p_w \beta + \epsilon \gamma_0 \bar{\kappa}_0(\beta)/M$. Taking the asymmetric part in terms of p_w, we obtain Eq. (5.37).

Appendix B

Benchmark Test for Simulation

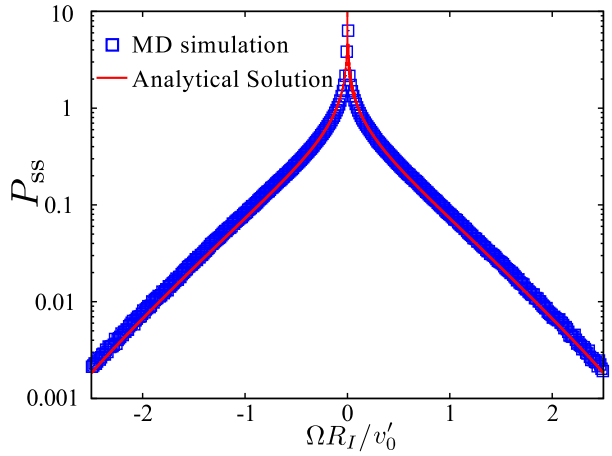

Figure B.1: The results of MD simulation for the rotor under viscous friction (squares) and our analytical solution are compared. The solid line represents the Fourier transform of Eq. (B.1). Our exact solution perfectly agrees with the MD simulation data.

In this appendix, we show that $P_{\rm ss}$ observed in our MD simulation for the granular rotor can be analytically predicted when the gas is elastic ($e_g = e = 1$) without gravity $g = 0$ and vibration, fixing $z_{\rm max} = 0$ as a benchmark test. We analyze a container heated by the thermal wall at the bottom. The top and the side walls of the container are chosen to be smooth elastic walls. The thermal wall is chosen to be the diffusive wall, i.e, the post collisional velocity of a grain $\boldsymbol{v} = (v_x, v_y, v_z)$ against the thermal wall is chosen to be random, following the

distribution $\phi_{\rm wall}(\boldsymbol{v}, T_{\rm bath}) = (m/T_{\rm wall})^2 v_z \exp\left[-m\boldsymbol{v}^2/2T_{\rm wall}\right]/2\pi$ [183]. We choose the typical velocity in this setup $v_0' = \sqrt{T_{\rm wall}/m}$ instead of v_0 as in Sec. 6.3. We have numerically checked that the VDF for the elastic gas can be regarded as the Gaussian $\tilde{\phi}(x) = \phi_{\rm G}(x)$ with $x = v/v_0'$. $P_{\rm ss}$ can be obtained analytically from our theory. The obtained solution is compared with the MD simulation data in Fig. B.1 for the viscous rotor.

With the aid of Eqs. (6.8) and (6.9), we obtain the analytic solution for $P_{\rm ss}(\Omega)$ as

$$\tilde{P}_{\rm ss}\left(\frac{k}{\tilde{w}}\right) = \exp\left[-\frac{1}{3\tilde{\gamma}\sqrt{2\pi}}\frac{k^2}{2}{}_2F_2\left(\begin{matrix}1,1\\2,\frac{5}{2}\end{matrix}\middle|-\frac{k^2}{2}\right)\right], \tag{B.1}$$

where we have used the following formulas $\tilde{\gamma}B = 1/\sqrt{2\pi}$, $\pi k\int_0^\infty dx x\phi_{\rm G}(x){\rm H}_0(kx) = kD_F\left(k/\sqrt{2}\right)/\sqrt{\pi}$, and

$$\int_0^{\frac{k}{\sqrt{2}}}\frac{ds'}{s'}\left(\frac{D_F(s')}{s'}-1\right) = -\frac{k^2}{6}{}_2F_2\left(\begin{matrix}1,1\\2,\frac{5}{2}\end{matrix}\middle|-\frac{k^2}{2}\right). \tag{B.2}$$

Here, $D_F(x)$ is the Dawson function [185]:

$$D_F(x) \equiv e^{-x^2}\int_0^x e^{t^2}dt \tag{B.3}$$

and ${}_qF_p$ is the generalized hypergeometric function [185, 238]:

$${}_qF_p\left(\begin{matrix}a_1,a_2,\cdots a_q\\b_1,b_2,\cdots b_p\end{matrix}\middle|z\right) \equiv \sum_{l=0}^{\infty}\frac{(a_1)_l(a_2)_l\cdots(a_q)_l}{(b_1)_l(b_2)_l\cdots(b_p)_l}\frac{z^l}{l!}, \tag{B.4}$$

where we have introduced the Pochhammer symbol as $(a)_l \equiv \Gamma(a+l)/\Gamma(a)$ with $l \geq 0$. To plot Fig. B.1, we adopt $\gamma/mL_{\rm box}v_0 = 1.0$, which corresponds to $\tilde{\gamma} = 0.57624$. The histogram for the angular velocity is shown in Fig. B.1 and the analytical solution (solid line) is consistent with the MD simulation result (squares), which ensures the accuracy of our MD code for the granular rotor and the validity of our framework.

Appendix C

Detailed calculation for a viscous frictional rotor

C.1 Derivation

In this appendix, we show the detailed derivation of the analytic results for the viscous frictional rotor in Sec. 6.5. Introducing $\mathcal{Y} \equiv y/\epsilon_{\rm rot}$, the transition rate given by $\mathcal{W}(\mathcal{Y}) \equiv \bar{\mathbb{W}}(\omega = 0; \mathcal{Y})$ is independent of $\epsilon_{\rm rot}$ and Ω. We note that $\mathbb{W}_{\epsilon_{\rm rot}}(\omega; y)$ satisfies the relation $\bar{\mathbb{W}}(\omega; \mathcal{Y})d\mathcal{Y} = \mathbb{W}_{\epsilon_{\rm rot}}(\omega; y)dy$ up to the leading order. We obtain the reduced time evolution equation for $\mathcal{P} = \mathcal{P}(\Omega, t)$ in $\epsilon_{\rm rot} \to 0$ limit from Eq. (6.6) when the axial friction is sufficiently strong, according to the generalized system size expansion method [92, 93]. For general frictional torque $N_{\rm fri} = N_{\rm fri}(\omega)$, we obtain

$$\frac{\partial \mathcal{P}}{\partial t} = -\frac{1}{I}\left\{\frac{\partial}{\partial \Omega}\tilde{N}_{\rm fri}(\Omega)\mathcal{P}\right\} + \int_{-\infty}^{\infty} d\mathcal{Y}\mathcal{W}(\mathcal{Y})\left\{\mathcal{P}(\Omega - \mathcal{Y}, t) - \mathcal{P}(\Omega, t)\right\}, \tag{C.1}$$

$$\mathcal{W}(\mathcal{Y}) = \rho h \int_0^{2w} d\varrho \int_{-\infty}^{\infty} dv_x dv_y \phi(v_x, v_y)\Theta(-v_n)|-v_n|\delta\left(\mathcal{Y} - \Delta\bar{\omega}'\right), \tag{C.2}$$

$$\Delta\bar{\omega}' \equiv -\frac{1+e}{R_I} g(\varrho) v_n, \tag{C.3}$$

where we have introduced the rescaled friction $\tilde{N}_{\rm fri}(\Omega) = N_{\rm fri}(\epsilon_{\rm rot}\Omega)/\epsilon_{\rm rot}$. It should be noted that $\tilde{N}_{\rm fri}(\Omega) = O(1)$ is assumed in $\epsilon_{\rm rot} \to 0$ limit.

The scaled friction is written as $\tilde{N}_{\rm fri} = -\tilde{\gamma}\Omega$ in Eq. (C.1) for the case of viscous friction with $\tilde{\gamma} = \gamma/(2\rho h w I v_0)$. We calculate the cumulant generating function $\Phi(s)$. For an even integer l, the cumulant $\mathcal{K}_l = \int d\mathcal{Y}\mathcal{Y}^l\mathcal{W}(\mathcal{Y})$ is

calculated as

$$\begin{aligned}
\mathcal{K}_l &= \rho h \int_0^{2w} d\varrho \int_{-\infty}^{\infty} dv_x dv_y \phi(v_x, v_y)\Theta(-v_n)|-v_n|(\Delta\bar{\omega}')^l \\
&= \rho h \frac{(1+e)^l}{R_I^l} 2 \int_{-w/2}^{w/2} d\varrho' \left(\frac{\varrho'}{R_I}\right)^l \int_0^{\infty} dv v \int_0^{2\pi} d\theta \phi(v)\Theta(-v\cos\theta)(-v\cos\theta)^{l+1} \\
&= \rho h \frac{(1+e)^l}{R_I^l} 4 \int_0^{w/2} d\varrho' \left(\frac{\varrho'}{R_I}\right)^l \int_0^{\infty} dv v^{l+2} \phi(v) \frac{\Gamma\left(\frac{l+2}{2}\right)}{\Gamma\left(\frac{l+3}{2}\right)} \sqrt{\pi} \\
&= \rho h \frac{\sqrt{\pi}(1+e)^l}{R_I^{2l}} \frac{\Gamma\left(\frac{l+2}{2}\right)}{\Gamma\left(\frac{l+3}{2}\right)} \frac{4}{l+1} \left(\frac{w}{2}\right)^{l+1} \int_0^{\infty} dv v^{l+2} \phi(v). \qquad \text{(C.4)}
\end{aligned}$$

We have changed the coordinate variable ϱ to ϱ' satisfying $-w/2 < \varrho' < w/2$, and used the front-back symmetry for the rotor. Here, $\Gamma(y)$ represents the Gamma function $\Gamma(y) = \int_0^{\infty} s^{y-1} e^{-s} ds$. Then, $\Phi(s)$ is written as

$$\begin{aligned}
\Phi(s) &= \int_0^{\infty} dv \phi(v) 2\sqrt{\pi}\rho h \sum_{l=1}^{\infty} \frac{w^{l+1} v^{l+2}}{R_I^{2l} 2^l} \frac{(is)^l (1+e)^l}{(l+1)!} \frac{\Gamma\left(\frac{l+2}{2}\right)}{\Gamma\left(\frac{l+3}{2}\right)} \\
&= -\int_0^{\infty} dv \phi(v) 2\sqrt{\pi}\rho h w \frac{R_I^4}{w^2 s^2} \left(\frac{2}{1+e}\right)^2 \\
&\quad \times \left\{ \sum_{j=2}^{\infty} \frac{(-1)^j}{(2j-1)!} \frac{\Gamma(j)}{\Gamma\left(j+\frac{1}{2}\right)} \left(\frac{1+e}{2} \frac{wsv}{R_I^2}\right)^{2j} \right\} \\
&= -\int_0^{\infty} d\tilde{v} \tilde{\phi}(\tilde{v}) \frac{2\rho h w v_0}{\tilde{s}^2 \tilde{w}^2} \left\{ -(\tilde{w}\tilde{s}\tilde{v})\pi \mathrm{H}_0(\tilde{w}\tilde{s}\tilde{v}) + 2(\tilde{w}\tilde{s}\tilde{v})^2 \right\}, \qquad \text{(C.5)}
\end{aligned}$$

where we have introduced the Struve function

$$\mathrm{H}_0(y) = \sum_{l=0}^{\infty} \frac{(-1)^l y^{2l+1}}{\{(2l+1)!!\}^2}. \qquad \text{(C.6)}$$

Because $\Phi(s)$ and $\tilde{P}_{\rm ss}$ satisfy the relation

$$\Phi(s) = s \frac{\gamma}{I} \frac{d}{ds} \ln \tilde{P}_{\rm ss}, \qquad \text{(C.7)}$$

we obtain

$$\tilde{s}^3 \frac{d}{d\tilde{s}} \ln \tilde{P}_{\rm ss} = \frac{2\rho h w I v_0}{\gamma \tilde{w}^2} \int_0^{\infty} d\tilde{v} \tilde{\phi}(\tilde{v}) \left\{ (\tilde{w}\tilde{s}\tilde{v})\pi \mathrm{H}_0(\tilde{w}\tilde{s}\tilde{v}) - 2(\tilde{w}\tilde{s}\tilde{v})^2 \right\}. \qquad \text{(C.8)}$$

Introducing variables $k = \tilde{w}\tilde{s}$ and $x = \tilde{v}$, we obtain

$$\tilde{\gamma} \left\{ k^3 \frac{d}{dk} \ln \tilde{P}_{\rm ss} \left(\frac{k}{\tilde{w}}\right) + Bk^2 \right\} = \pi k \int_0^{\infty} dx x \tilde{\phi}(x) \mathrm{H}_0(kx), \qquad \text{(C.9)}$$

where we have introduced $B = (2/\tilde{\gamma}) \int_0^{\infty} dx x^2 \tilde{\phi}(x)$. Thus, we obtain the formula (6.10).

C.2 Detailed procedure

C.2.1 Forward problem

Let us explain the detailed numerical technique to obtain $P_{\rm ss}(\Omega)$ using Eqs. (6.8) and (6.9). It contains the following four steps (a)-(d):

(a) Measure the VDF for the granular gas $\tilde{\phi}(x)$ around the rotor.

(b) Obtain the extrapolated data for $x\tilde{\phi}(x)$ in $x \to \infty$ limit. We fit the data in the range $x_- < x < x_+$ by a function $b_1 \exp(-b_2 x)$. We replace the data for $x > x_{\rm cut}$ and extrapolate the data by the fitting function in $x < x_{\rm end}$. We have checked whether the results are invariant if we use Gaussian as a fitting function instead.

(c) Apply the Struve transform in Eq. (6.9) using Eq. (C.6).

(d) Obtain the Fourier transform $\tilde{P}_{\rm ss}(s)$. Note that $P_{\rm ss}(\Omega)$ has a sharp peak around $\Omega = 0$, which is serious for the numerical Fourier transformation in terms of convergence. To solve this problem, we use the double exponential formula, which is a numerical technique for singular functions [237].

In Sec. 6.5.2, we adopt the fitting ranges as $x_- = x_{\rm cut} = 3.0, x_+ = 5.0$, and $x_{\rm end} = 60.0$, and obtained fitting parameters are $b_1 = 5910.96$ and $b_2 = 5.64439$.

C.2.2 Inverse estimation problem

Let us explain the detailed numerical technique to obtain $\phi(v)$ on the basis of Eqs. (6.11) and (6.12). It contains the following seven steps (a)-(g), to obtain $\tilde{\phi}$ from the data of $P_{\rm ss}(\Omega)$.

(a) Obtain the data of $P_{\rm ss}(\Omega)$.

(b) Obtain the extrapolated data of $P_{\rm ss}(\Omega)$ for $\Omega \to \infty$. We fit the data in the range $\Omega_- < \Omega < \Omega_+$ by the function $b_1' \exp(-b_2'\Omega)$. Replace the data for $\Omega > \Omega_{\rm cut}$ and extrapolate the data $\Omega < \Omega_{\rm end}$ by the fitting function. We have also checked that the results are invariant if we use the Gaussian fitting function instead.

(c) Obtain the Fourier transform $\tilde{P}_{\rm ss}(s)$. We have applied the double exponential formula [237], similarly to the forward problem.

(d) Estimate the parameter B. Fit the data of $k^3 d\log\tilde{P}/dk$ for $k \to \infty$ by the function $c' - Bk^2$. In our analysis, we fit the data in the region $k_c^- < k < k_c^+$.

(e) Calculate $G_{\rm vis}(k)$ using Eq. (6.12).

(f) Fit the numerically obtained data of $G_{\rm vis}(k)$ in the procedure (e) by $c/k + d/k^3$ in the $k \to \infty$ limit. In our analysis, we fit the data in the region $k_e^- < k < k_e^+$, and replace and extrapolate the data for $k_{\rm cut}' < k < k_{\rm end}'$ by the fitting function, where the cutoffs satisfy $k_e^- < k_{\rm cut}' < k_e^+$.

(g) Apply the Y transform (6.11) using the data of $G_{\rm vis}(k)$ obtained in the procedure (e).

Fitting ranges used in Sec. 6.5.3 are listed as $\Omega_- = 4.0v_0/R_I, \Omega_+ = 5.0v_0/R_I$, $\Omega_{\rm cut} = 4.0v_0/R_I, \Omega_{\rm end} = 20.0\Omega_{\rm cut}, k_c^- = 3.0, k_c^+ = 5.0, k_e^- = 2.5, k_e^+ = 3.5d = 0.603414, k_{\rm cut}' = 3.0$, and $k_{\rm end}' = 5.968133 \times 10^4$, and obtained fitting parameters are $b_1' = 0.438068 R_I/v_0, b_2' = 1.26993 R_I/v_0, c' = 0.40721$, and $c = 0.0942702$.

In Sec. 6.6, fitting ranges and parameters are listed as $\Omega_- = 4.0 v_0/R_I, \Omega_+ = 5.0 v_0/R_I, b'_1 = 0.463788 R_I/v_0, b'_2 = 1.31134 R_I/v_0, \Omega_{\rm cut} = 4.0 v_0/R_I, \Omega_{\rm end} = 20.0 \Omega_{\rm cut}, k_c^- = 3.0, k_c^+ = 5.0, c' = 0.660408, k_e^- = 2.5, k_e^+ = 3.5, c = 0.169773, d = 0.557026, k'_{\rm cut} = 3.0$, and $k'_{\rm end} = 5.968133 \times 10^4$.

Appendix D

Detailed calculation for a dry frictional rotor

D.1 Derivation

In this appendix, we show the detailed derivation of the analytical results for the dry frictional rotor in Sec. 6.7. The scaled dry friction in Eq. (C.1) is written as $\tilde{N}_{\rm fri}(\Omega) = -\tilde{\Delta}{\rm sgn}(\Omega)$, where we have introduced $\tilde{\Delta} \equiv \Delta/\epsilon_{\rm rot}$. The independent kick solution is written as

$$\tilde{P}_{\rm ss}(s) \;=\; 1 + \frac{I}{\tilde{\Delta}} \int_{-\infty}^{\infty} d\mathcal{Y} \mathcal{W}(\mathcal{Y}) \int_0^{\mathcal{Y}} \frac{d\Omega}{{\rm sgn}(\Omega)} \left[e^{is\Omega} - 1 \right] + O\left(\frac{1}{\tilde{\Delta}'^2} \right). \tag{D.1}$$

Equation (D.1) is rewritten as

$$\begin{aligned} \frac{\tilde{\Delta}}{I}(\tilde{P}_{\rm ss} - 1) &= \int_{-\infty}^{\infty} d\mathcal{Y} \mathcal{W}(\mathcal{Y}) \int_0^{\mathcal{Y}} \frac{d\Omega}{{\rm sgn}(\Omega)} \sum_{l=1}^{\infty} \frac{(is\Omega)^l}{l!} \\ &= \sum_{l=1}^{\infty} \frac{(is)^l}{l!} \int_{-\infty}^{\infty} d\mathcal{Y} \mathcal{W}(\mathcal{Y}) \frac{{\rm sgn}(\mathcal{Y}) \mathcal{Y}^{l+1}}{l+1} \\ &= \sum_{j=1}^{\infty} \frac{(-1)^j s^{2j+2}}{(2j+1)!} \int_{-\infty}^{\infty} d\mathcal{Y} |\mathcal{Y}| \mathcal{Y}^{2j} \mathcal{W}(\mathcal{Y}) \frac{1}{s^2}. \end{aligned} \tag{D.2}$$

By noting the following relations for an even integer l:

$$\begin{aligned} \int_{-\infty}^{\infty} d\mathcal{Y} |\mathcal{Y}| \mathcal{Y}^l \mathcal{W}(\mathcal{Y}) &= \frac{4\rho h (1+e)^{l+1}}{R_I^{2l+2}(l+2)} \left(\frac{w}{2} \right)^{l+2} \int_0^{\infty} dv v^{l+3} \phi(v) \int_{-\pi/2}^{\pi/2} d\theta \cos^{l+2}\theta \\ &= \frac{4\rho h (1+e)^{l+1} \sqrt{\pi}}{R_I^{2l+2}(l+2)} \left(\frac{w}{2} \right)^{l+2} \frac{l+4}{l+3} \frac{(\frac{l}{2}+\frac{3}{2})!}{(\frac{l}{2}+2)!} \int_0^{\infty} dv v^{l+3} \phi(v), \end{aligned} \tag{D.3}$$

$$\int_{-\pi/2}^{\pi/2} d\theta \cos^{l+2}\theta = \sqrt{\pi}\frac{\Gamma\left(\frac{l+3}{2}\right)}{\Gamma\left(\frac{l+4}{2}\right)} = \frac{l+4}{l+3}\frac{\left(\frac{l}{2}+\frac{3}{2}\right)!}{\left(\frac{l}{2}+2\right)!}, \tag{D.4}$$

$$\frac{(2j+4)\left(j+\frac{3}{2}\right)!}{(2j+3)!(j+2)!} = \sqrt{\pi}\left(\frac{1}{2^{j+1}(j+1)!}\right)^2, \tag{D.5}$$

$$J_0(x) = 1-\sum_{j=0}^{\infty}\frac{(-1)^j x^{2(j+1)}}{2^{2(j+1)}\{(j+1)!\}^2}, \tag{D.6}$$

we obtain

$$\frac{\tilde{\Delta}}{I}\left\{\tilde{P}_{\rm ss}\left(\frac{k}{\tilde{w}}\right)-1\right\}\left(\frac{k}{\tilde{w}}\right)^2 = \frac{4\pi\rho h v_0^2}{1+e}\int_0^\infty dx x\tilde{\phi}(x)\left\{1-\frac{k^2x^2}{4}-J_0(kx)\right\}. \tag{D.7}$$

We introduce coefficients here for Appendix D.2:

$$C_l \equiv \frac{(-1)^l}{2^{2l}(l!)^2}\int_0^\infty dx x^{2l+1}\tilde{\phi}(x), \tag{D.8}$$

with a positive integer $l = 1, 2, \cdots$. We thus obtain Eq. (6.13) and (6.14) from Eq. (D.7).

D.2 Detailed procedure

We, here, explain the detailed techniques to use the analytic PDF formulas (6.13) and (6.14). There are the following six steps (a)-(f) to obtain $P_{\rm ss}(\Omega)$ numerically.

(a) Observe the granular velocity around the rotor and make a histogram to numerically obtain the VDF $\tilde{\phi}(x)$.

(b) Introducing the sufficiently large x_- and $x_+(x_- < x_+)$, obtain the extrapolated data for $x\tilde{\phi}(x)$ in the $x \to \infty$ limit. We fit the data in the range $x_- < x < x_+$ by the exponential function $b_1\exp(-b_2 x)$. We replace the data for $x > x_{\rm cut}$ and extrapolate the data by $x < x_{\rm end}$ by the fitting function. We have also checked that the results are invariant if we use Gaussian as a fitting function instead.

(c) Obtain $G_{\rm dry}(k)$ as the Bessel transform of $\tilde{\phi}$ Eq. (6.14), and calculate C_1 and C_2 according to Eq. (D.8).

(d) Replace the data of $G_{\rm dry}(k)$ for $k < k_{\rm cut}^-$ by $1/2\pi + C_1k^2 + C_2k^4$, which corresponds to the Taylor expansion of Eq. (6.14) to avoid the numerical divergence of the second term in Eq. (6.13) in the $k \to 0$ limit. In the range $k_d^- < k < k_d^+$, fit the data of $G_{\rm dry}(k)$ by $d_1\exp(-d_2k^2)$. We extrapolate the data by $d_1\exp(-d_2k^2)$ in the region $k > k_{\rm cut}^+$.

(e) Calculate $P_{\rm inf} \equiv \lim_{s\to\infty} \tilde{P}_{\rm ss}(s) = 1 + C_1 \tilde{w}^2/\tilde{\Delta}'$, which corresponds to the delta function for $P_{\rm ss}(\Omega)$, and obtain the data for $\tilde{P}_{\rm ss}(s)$, following Eq. (6.13).

(f) Apply the Fourier transform to the data for $P_{\rm ss}(s) - P_{\rm inf}$, and obtain the smooth part $P_{\rm ss}^{\rm smooth}(\Omega)$. We note $P_{\rm ss}(\Omega = 0) = P_{\rm ss}^{\rm smooth}(0) + P_{\rm inf}/\Delta\Omega$. Here, $\Delta\Omega$ is the data mesh for Ω. Finally we obtain $P_{\rm ss}(\Omega) = P_{\rm inf}\delta(\Omega) + P_{\rm ss}^{\rm smooth}(\Omega)$.

We extrapolate the data in the procedure (b) and (d), because a large number of data are necessary to numerically perform integral transforms twice, in the Fourier and Bessel transform (6.13) and (6.14). The data are extrapolated also in Sec. 6.5.3, for the same reason.

In Sec. 6.7, we adopt the fitting ranges as $x_- = 3.0, x_+ = 5.0, x_{\rm end} = 20.0x_-, x_{\rm cut} = x_-$, $k_{\rm cut}^- = 0.5, k_d^- = 1.5, k_d^+ = 2.0$, and $k_{\rm cut}^+ = 1.75$, and obtained fitting parameters are $b_1 = 5910.96, b_2 = 5.64439, d_1 = 0.204485$, and $d_2 = 0.527407$.

Appendix E

Kinetic theory for hard core gases

In this appendix, we briefly review kinetic theory for both elastic and inelastic hard core gases. We review the history of kinetic theory such as Boltzmann equation, Enskog equation, Chapman-Enskog expansion, BBGKY hierarchy, Choh-Uhlenbeck equation and Revised Enskog equation. In Sec. E.1, we summarize the Boltzmann equation for elastic hard core gases and the Chapman-Enskog expansion. In Sec. E.2, we explain the Bogoliubov-Born-Green-Kirkwood-Yvon (BBGKY) hierarchy, which clarifies the foundation of the Boltzmann equation. In Sec. E.3, the extensions of the Boltzmann equation toward the moderately dense gases are summarized. In Sec. E.4, the kinetic theory for granular gases are summarized. The transport coefficients for moderately dense granular gases is summarized in Sec. E.5 [1]. There are many textbooks for the kinetic theory [196–203]. The history of the kinetic theory is also summarized and the original paper for Chapman-Enskog methods or Enskog theory is reprinted in Ref. [203]. In this appendix, the symbol "$\cdot$" represents an inner product of vectors.

E.1 Boltzmann equation

The Boltzmann equation, which is a time evolution equation for the one-body distribution function, is introduced to understand the second law of thermodynamics from mechanical point of view in 1872. The velocity before the collision $\boldsymbol{v}_l$ and after the collision $\boldsymbol{v}_l'$ of l th elastic particles ($l = 1, 2$) and the same mass are related as

$$\boldsymbol{v}_1' = \boldsymbol{v}_1 - (\boldsymbol{k} \cdot \boldsymbol{v}_{12})\boldsymbol{k} \tag{E.1}$$

$$\boldsymbol{v}_2' = \boldsymbol{v}_2 + (\boldsymbol{k} \cdot \boldsymbol{v}_{12})\boldsymbol{k}, \tag{E.2}$$

[1] A part of this chapter overlaps with the review part of the author's master thesis, *Numerical Analysis of Granular Jet Impacts* [195]

with the unit vector $\boldsymbol{k} \equiv (\boldsymbol{r}_2 - \boldsymbol{r}_1)/|\boldsymbol{r}_2 - \boldsymbol{r}_1|$ and relative velocities $\boldsymbol{v}_{12} \equiv \boldsymbol{v}_1 - \boldsymbol{v}_2$. We introduce the pre-collision velocities $\boldsymbol{v}_l''$, which lead $\boldsymbol{v}_l$ after the collision:

$$\boldsymbol{v}_1'' = \boldsymbol{v}_1 - (\boldsymbol{k}\cdot\boldsymbol{v}_{12})\boldsymbol{k} \tag{E.3}$$

$$\boldsymbol{v}_2'' = \boldsymbol{v}_2 + (\boldsymbol{k}\cdot\boldsymbol{v}_{12})\boldsymbol{k}. \tag{E.4}$$

Equations (E.1) and (E.2) are called direct collisions and Eqs. (E.3) and (E.4) are called inverse collisions.

The Boltzmann equation for elastic gases without external force is described as

$$\frac{\partial f_1}{\partial t} + \boldsymbol{v}_1 \cdot \nabla_1 f_1 = \int d^3v_2 d^2k S(\boldsymbol{k}\cdot\boldsymbol{v}_{12})(f_1'' f_2'' - f_1 f_2), \tag{E.5}$$

with the scattering cross section $S(\boldsymbol{k}\cdot\boldsymbol{v}_{12}) \equiv \sigma^2|\boldsymbol{k}\cdot\boldsymbol{v}_{12}|\Theta(\boldsymbol{k}\cdot\boldsymbol{v}_{12})$, where we have introduced Heaviside function $\Theta(x)$ with $\Theta(x) = 1(x \geq 0)$ and $\Theta(x) = 0(x < 0)$ and the particle diameter σ, with abbreviation $f_i \equiv f(\boldsymbol{r}_i, \boldsymbol{v}_i)(i = 1, 2)$ and $f_i'' \equiv f(\boldsymbol{r}_i, \boldsymbol{v}_i'')$ at the position of i th particle $\boldsymbol{r}_i$. The right hand side on Eq. (E.5) is called the collision integral

$$I_{\rm el}(f, f) \equiv \int d^3v_2 d^2k S(\boldsymbol{k}\cdot\boldsymbol{v}_{12})(f_1'' f_2'' - f_1 f_2). \tag{E.6}$$

The first term of the collision integral denotes the increase of the probability f_1 after the collision and the second term denotes the decrease of f_1. The Boltzmann equation has been used not only for classical gases but for electron gases or plasma [204, 205]. It is also known that the Boltzmann equation for elastic gases is equivalent to the direct simulation of Monte Carlo (DSMC) method [206–209].

Hydrodynamical equations can be derived from the Boltzmann equation by integrating over $\int d^3v_1$ after multiplying $\psi_1 \equiv 1, v_{1\alpha}, \boldsymbol{v}_1^2$, which are zero eigenvectors of the collision integral:

$$\int d^3v_1 \psi_1 I_{\rm el}(f, f) = \int d^3v_1 d^3v_2 \psi_1 \int d^2k S(g_{12})(f_1'' f_2'' - f_1 f_2) \tag{E.7}$$

$$= \frac{1}{4}\int d^3v_1 d^3v_2 \{\psi_1 + \psi_2 - \psi_1' - \psi_2')\} \times \int d^2k S(g_{12})(f_1'' f_2'' - f_1 f_2) \tag{E.8}$$

$$= 0, \tag{E.9}$$

with $g_{12} \equiv \boldsymbol{k}\cdot\boldsymbol{v}_{12}$. The time reversal symmetry during local collisions is used to derive the second equation, and the last equation results from the conservation of mass, momentum and kinetic energy. Because the derived hydrodynamical equations contain unknown functions such as the stress tensor or the heat flux we need the explicit expressions for f_1. The systematic perturbative method to obtain f_1 is known as the Chapman-Enskog expansion.

Chapman-Enskog expansion

The explicit calculation of the shear viscosity and the heat conductivity is performed in 1917 by Chapman and Enskog, where the Boltzmann equation (E.5) is perturbatively solved by assuming that the distribution function f_1 depends on space ant time variables through hydrodynamic variables $\boldsymbol{a}(\boldsymbol{r},t) = \{n(\boldsymbol{r},t), \mathcal{U}(\boldsymbol{r},t), \mathcal{T}(\boldsymbol{r},t)\}$ [210], i.e. the local density $n(\boldsymbol{r},t)$, the local velocity field $\mathcal{U}(\boldsymbol{r},t)$ and the local temperature $\mathcal{T}(\boldsymbol{r},t)$: $f_1(\boldsymbol{v}_1,\boldsymbol{r},t) \to f_1(\boldsymbol{v}_1|n,\mathcal{U},\mathcal{T})$ defined by

$$
\begin{aligned}
n(\boldsymbol{r},t) &\equiv \int d\boldsymbol{v}_1 f_1(\boldsymbol{v}_1,\boldsymbol{r},t), && \text{(E.10)}\\
\mathcal{U}(\boldsymbol{r},t) &\equiv \frac{1}{n(\boldsymbol{r},t)} \int d\boldsymbol{v}_1 \boldsymbol{v}_1 f_1(\boldsymbol{v}_1,\boldsymbol{r},t), && \text{(E.11)}\\
\mathcal{T}(\boldsymbol{r},t) &\equiv \frac{2}{3n(\boldsymbol{r},t)} \int d\boldsymbol{v}_1 \frac{m}{2} \left(\boldsymbol{v}_1^2 - \mathcal{U}^2(\boldsymbol{r},t)\right) f_1(\boldsymbol{v}_1,\boldsymbol{r},t), && \text{(E.12)}\\
& && \text{(E.13)}
\end{aligned}
$$

Namely, $\partial_t f_1 \to (\partial f_1/\partial \boldsymbol{a})\partial_t \boldsymbol{a}$. Because there is a large scale separation between the kinetic and the hydrodynamical regime, the small expansion parameter $\epsilon_{l_0} \sim l_0 \partial_\alpha$, which denotes the non-uniformity parameter, is introduced as a systematic expansion parameter with a mean free path l_0. The distribution function is expanded as $f_1 = f_M + \epsilon_{l_0} f^{(1)} + O(\epsilon_{l_0}^2)$, with local Maxwellian f_M and $\int d^3 v_1 f_M = n$. Here, $O(\epsilon_{l_0}^0)$ and $O(\epsilon_{l_0}^1)$ denote the Euler and Navier-Stokes order solutions, respectively. In summary, the Chapman-Enskog method is the method to solve following equations:

$$
\begin{aligned}
\frac{\partial f}{\partial t} + \epsilon_{l_0} \boldsymbol{v}_1 \cdot \nabla_1 f &= I_{\rm el}(f,f), && \text{(E.14)}\\
f &= f_M + \epsilon_{l_0} f^{(1)} + O(\epsilon_{l_0}^2), && \text{(E.15)}\\
f(\boldsymbol{v}_1,\boldsymbol{r},t) &= f(\boldsymbol{v}_1|n(\boldsymbol{r},t),\mathcal{U}(\boldsymbol{r},t),\mathcal{T}(\boldsymbol{r},t)). && \text{(E.16)}
\end{aligned}
$$

E.2 BBGKY hierarchy

Let us show the relation between the Boltzmann equation Eq. (E.5) and the microscopic equations of motion for N particles, following Ref. [202]. The dynamics of the system can be described as the trajectory of a phase point in the $6N$ dimensional phase space $(\boldsymbol{r}^N, \boldsymbol{p}^N)$ with momenta $\boldsymbol{p}^N = \boldsymbol{p}_1, \cdots \boldsymbol{p}_N$ and $\boldsymbol{r}^N = \boldsymbol{r}_1, \cdots, \boldsymbol{r}_N$. Let H be the Hamiltonian of the system, which we write in general form as

$$
H(\boldsymbol{r}^N, \boldsymbol{p}^N) = K_N(\boldsymbol{p}^N) + V_N(\boldsymbol{r}^N), \tag{E.17}
$$

with the total kinetic energy $K_N \equiv \sum_i \boldsymbol{p}_i^2/2m$ and potential energy $V_N(\boldsymbol{r}^N)$, where equations of motion are

$$
\dot{\boldsymbol{r}}_i = \frac{\partial H}{\partial \boldsymbol{p}_i}, \quad \dot{\boldsymbol{p}}_i = -\frac{\partial H}{\partial \boldsymbol{r}_i}, \tag{E.18}
$$

$(i = 1, \cdots N)$. We introduce a phase-space probability density $f^{[N]}(\boldsymbol{r}^N, \boldsymbol{p}^N, t)$.

$$\int dr^N dp^N f^{[N]}(\boldsymbol{r}^N, \boldsymbol{p}^N, t) = 1. \tag{E.19}$$

The time evolution of the probability density in phase space is governed by the Liouville equation, which is a $6N$ dimensional analogue of the equation of continuity of an incompressible fluid:

$$\frac{df^{[N]}}{dt} = \frac{\partial f^{[N]}}{\partial t} + \sum_i \left(\frac{\partial}{\partial \boldsymbol{r}_i} \cdot f^{[N]} \dot{\boldsymbol{r}}_i + \frac{\partial}{\partial \boldsymbol{p}_i} \cdot f^{[N]} \dot{\boldsymbol{p}}_i \right) = 0. \tag{E.20}$$

We rewrite Eq. (E.20) for convenience by introducing the pair force f_{ij} between i th and j th particles:

$$\left(\frac{\partial}{\partial t} + \sum_i \cdot \frac{\boldsymbol{p}_i}{m} \cdot \frac{\partial}{\partial \boldsymbol{r}_i} \right) f^{[N]} = -\sum_{ij} \boldsymbol{f}_{ij} \cdot \frac{\partial f^{[N]}}{\partial \boldsymbol{p}_i}, \tag{E.21}$$

with $f_{ii} = 0$. Because we are usually interested in the behavior of a subset of s particles, we introduce a reduced phase-space distribution function $f^{(s)}$:

$$f^{(s)}(\boldsymbol{r}^s, \boldsymbol{p}^s, t) \equiv \frac{N!}{(N-s)!} \int dr^{(N-s)} dp^{(N-s)} f^{[N]}(\boldsymbol{r}^N, \boldsymbol{p}^N, t), \tag{E.22}$$

with $\boldsymbol{r}^s \equiv \boldsymbol{r}_1, \cdots \boldsymbol{r}_s$, $\boldsymbol{p}^s \equiv \boldsymbol{p}_1, \cdots \boldsymbol{p}_s$, $\boldsymbol{r}^{(N-s)} \equiv \boldsymbol{r}_{s+1}, \cdots \boldsymbol{r}_N$ and $\boldsymbol{p}^{(N-s)} \equiv \boldsymbol{p}_{s+1}, \cdots \boldsymbol{p}_N$. The time evolution for $f^{(s)}$ can be calculated by integrating Eq. (E.21) over $dr^{(N-s)} dp^{(N-s)}$.

$$\begin{aligned} \left(\frac{\partial}{\partial t} + \sum_i^s \cdot \frac{\boldsymbol{p}_i}{m} \cdot \frac{\partial}{\partial \boldsymbol{r}_i} \right) f^{(s)} &= -\sum_{i,j=1}^s \boldsymbol{f}_{ij} \cdot \frac{\partial f^{(s)}}{\partial \boldsymbol{p}_i} - \frac{N!}{(N-s)!} \\ &\quad \times \sum_{i=1}^s \sum_{j=s+1}^N \int dr^{(N-s)} dp^{(N-s)} \boldsymbol{f}_{ij} \cdot \frac{\partial f^{[N]}}{\partial \boldsymbol{p}_i}. \end{aligned} \tag{E.23}$$

Because $f^{[N]}$ is symmetric with respect to interchange of particle labels and the sum of terms for $j = s+1$ to N in Eq. (E.23) is replaced by $N - s$ times the value of any one term. Thus, Eq. (E.23) can be simplified as

$$\left(\frac{\partial}{\partial t} + \sum_i^s \frac{\boldsymbol{p}_i}{m} \cdot \frac{\partial}{\partial \boldsymbol{r}_i} + \sum_{i,j=1}^s \boldsymbol{f}_{ij} \cdot \frac{\partial}{\partial \boldsymbol{p}_i} \right) f^{(s)} = -\sum_{i=1}^s \int d\boldsymbol{r}_{s+1} d\boldsymbol{p}_{s+1} \boldsymbol{f}_{i,s+1} \cdot \frac{\partial f^{(s+1)}}{\partial \boldsymbol{p}_i}. \tag{E.24}$$

The exact equation (E.24) which relates $f^{(s)}$ with $f^{(s+1)}$ is known as the Bogoliubov-Born-Green-Kirkwood-Yvon (BBGKY) hierarchy. The important case is $s = 1$:

$$\left(\frac{\partial}{\partial t} + \frac{\boldsymbol{p}_1}{m} \cdot \frac{\partial}{\partial \boldsymbol{r}_1} \right) f^{(1)} = -\int d\boldsymbol{r}_2 d\boldsymbol{p}_2 \boldsymbol{f}_{1,2} \cdot \frac{\partial f^{(2)}}{\partial \boldsymbol{p}_1} \equiv \left(\frac{\partial f}{\partial t} \right)_{\text{coll}}, \tag{E.25}$$

Although Eq. (E.25) is exact, we need all $f^{(n)}(n > 1)$ to obtain $f^{(1)}$. Thus, an approximate closure relation is necessary to obtain $f^{(1)}$. If we choose

$$\left(\frac{\partial f}{\partial t}\right)_{\rm coll} = I_{\rm el}(f^{(1)}, f^{(1)}), \tag{E.26}$$

we obtain the Boltzmann equation (E.5). Therefore, the assumption of the Boltzmann equation is that the two-body distribution function can be approximated as the product of the one-body distribution function. The transport coefficients for rarefied gases can be calculated via the Boltzmann equation supplemented by the Chapman-Enskog expansion. Because the Boltzmann equation is only suitable for dilute gases, it has been extended to treat moderately dense gases.

E.3 Extension of Boltzmann equation

There is a long history to extend the Boltzmann equation for dense fluids [211–221]. In 1922 [211], Enskog proposed one of the generalization of the Boltzmann equation for hard sphere fluid, which is now called "Standard Enskog Theory (SET)." $f^{(2)}$ is replaced as

$$f^{(2)} \to g(|\boldsymbol{r}_{12}| = \sigma) f(\boldsymbol{r}_1, \boldsymbol{v}_1, t) f(\boldsymbol{r}_1 - \boldsymbol{k}\sigma, \boldsymbol{v}_2, t), \tag{E.27}$$

i.e. the product of the distribution function for the two colliding spheres and $g(\sigma)$, which denotes static two-body correlations or the radial distribution function for a hard sphere fluids. For the SET, the static correlation g is the function of the number density as in fluid in uniform equilibrium evaluated at the contact point $(\boldsymbol{r}_1 + \boldsymbol{r}_2)/2$. SET has been criticized for the absence of the Onsager reciprocity relations in the case of a binary mixture of hard-sphere fluids [218].

After the formulation of the BBGKY hierarchy, in 1958, Choh and Uhlenbeck [212] extended the Boltzmann equations to include triple collision term $K(f, f, f)$

$$\frac{\partial f_1}{\partial t} + \boldsymbol{v}_1 \cdot \nabla f_1 = I_{\rm el}(f, f) + K(f, f, f) + \cdots, \tag{E.28}$$

and performed the density expansion, where the density dependence of the transport coefficients are calculated with the density of the system as an expansion parameter. Here, the correction in Eq. (E.27) is included in $I_{\rm el}(f, f)$. Choh and Uhlenbeck calculated the first order correction of the transport coefficient in three dimensions and Green and Cohen derived the formal structure of l-tuple collision terms ($l = 2, 3, 4, \cdots$). McLennan showed that the first correction term corresponds to the results from the Green-Kubo formula [213]. However, Dorfman and Cohen, Weinstock, as well as Goldman and Frieman show that the density expansion contains the logarithmic divergent in the second-order correction term in 3D and the first-order correction in 2D. Therefore, the convergence of the density expansion is questionable. Kawasaki and Oppenheim were the first to re-sum the divergent term, i.e. ring diagrams [214]. The details of the work by Choh Uhlenbeck are summarized by Ernst [221].

Revised Enskog Theory

The recent accepted phenomenological theory for the kinetic theory is called "Revised Enskog Theory (RET), " which is constructed in 1972 by van Beijeren and Ernst. [215–217, 219]. The RET equation is written as

$$(\frac{\partial}{\partial t} + \boldsymbol{v}_1 \cdot \nabla_1) f(\boldsymbol{r}_1, \boldsymbol{v}_1, t) = J_E^{\rm el}[\boldsymbol{r}_1, \boldsymbol{v}_1 | f(t)], \tag{E.29}$$

with the new collision operator

$$\begin{aligned} J_E^{\rm el}[\boldsymbol{r}_1, \boldsymbol{v}_1 | f(t)] \equiv & \int d^3\boldsymbol{v}_2 d^2k S(\boldsymbol{k}\cdot\boldsymbol{v}_{12})\{f^{(2)}(\boldsymbol{r}_1, \boldsymbol{v}_1''; \boldsymbol{r}_1 + \sigma\boldsymbol{k}, \boldsymbol{v}_2''; t) \\ & - f^{(2)}(\boldsymbol{r}_1, \boldsymbol{v}_1; \boldsymbol{r}_1 - \sigma\boldsymbol{k}, \boldsymbol{v}_2; t)\}, \end{aligned} \tag{E.30}$$

where the closure for the two body distribution $f^{(2)}$

$$f^{(2)}(\boldsymbol{r}_1, \boldsymbol{v}_1; \boldsymbol{r}_2\boldsymbol{v}_2; t) = \chi(\boldsymbol{r}_1, \boldsymbol{r}_2 | n(t)) f(\boldsymbol{r}_1, \boldsymbol{v}_1, t) f(\boldsymbol{r}_2, \boldsymbol{v}_2, t), \tag{E.31}$$

is adopted. The difference of RET from SET is χ, which is the functional of n as in a fluid in non-uniform under the local equilibrium [191]. RET dose not contradict to the Onsager reciprocal relation [217]. Haro and Garzó showed that the difference between SET and RET emerges in the case of a binary mixture of hard-sphere fluid at Navier-Stokes order [218] or a monatomic fluid at the Burnett order [220].

E.4 Kinetic Theory for Granular Flow

Boltzmann equation for granular flow

Let us derive the Boltzmann equation for granular gases intuitively, following Ref. [61]. The Boltzmann equation for granular gases consists of the collision integral $I(f, f)$, which denotes the increase or decrease of $f_1 d^3r_1$ after the collision per unit time. The number of direct collisions ν^- and that of inverse collisions ν^+ that occur during Δt and whose geometry is specified by d^2k are described as

$$\nu^- = f_1 f_2 d^3v_1 d^3v_2 S(\boldsymbol{k}\cdot\boldsymbol{v}_{12}) d^2k \Delta t d^3r_1 \tag{E.32}$$

$$\begin{aligned} \nu^+ &= f_1'' f_2'' d^3v_1'' d^3v_2'' S(\boldsymbol{k}\cdot\boldsymbol{v}_{12}'') d^2k \Delta t d^3r_1 \\ &= \Lambda f_1'' f_2'' d^3v_1 d^3v_2 S(\boldsymbol{k}\cdot\boldsymbol{v}_{12}) d^2k \Delta t d^3r_1 \end{aligned} \tag{E.33}$$

with

$$\Lambda \equiv \frac{1}{e_g} \frac{\partial(\boldsymbol{v}_1'', \boldsymbol{v}_2'')}{\partial(\boldsymbol{v}_1, \boldsymbol{v}_2)}. \tag{E.34}$$

Here, the Jacobian yields

$$\frac{\partial(\boldsymbol{v}_1'', \boldsymbol{v}_2'')}{\partial(\boldsymbol{v}_1, \boldsymbol{v}_2)} = \frac{1}{e_g}, \tag{E.35}$$

for inelastic hard core gases with a constant restitution coefficient $e_g < 1$. Thus, the Boltzmann equation for granular gases follows from the conservation of probability:

$$\frac{\partial f_1}{\partial t} + \boldsymbol{v}_1 \cdot \nabla_1 f_1 = \int d^3 v_2 d^2 k S(\boldsymbol{k} \cdot \boldsymbol{v}_{12}) \left(\frac{1}{e_g^2} f_1'' f_2'' - f_1 f_2 \right). \tag{E.36}$$

The difference from elastic gases is that the existence of the homogeneous cooling state (HCS) due to the inelastic collisions. Because the kinetic energy dissipates through inelastic collisions, $\mathcal{T}_g$, which is called the granular temperature, goes to zero as time passes. Although the exact solution is not known, the homogeneous solution for Eq. $(E.36)$ is conventionally analyzed by using the Sonine polynomial expansion:

$$f(\boldsymbol{v}, t) = f_M \left[1 + \sum_{p=1}^{\infty} a_p S_p(\boldsymbol{c}^2) \right], \tag{E.37}$$

with $\boldsymbol{c} \equiv \boldsymbol{v}_1 / \sqrt{2\mathcal{T}_g(t)/m}$ and the Sonine polynomials $S_p(x) (p = 0, 1, 2, \cdots)$, which satisfy the orthogonality conditions:

$$\int d\boldsymbol{c} \frac{e^{-\boldsymbol{c}^2}}{\pi^{-3/2}} S_p(\boldsymbol{c}^2) S_{p'}(\boldsymbol{c}^2) = 2\delta_{pp'} \left(p + \frac{1}{2} \right)!. \tag{E.38}$$

The first few Sonine polynomials in 3D read

$$S_0(x) = 1, \quad S_1(x) = -x + \frac{3}{2}, \quad S_2(x) = \frac{x^2}{2} - \frac{5x}{2} + \frac{15}{8}. \tag{E.39}$$

The corresponding coefficients for f are known to be $a_1 = 0$ and

$$a_2 = \frac{16(1 - e_g)(1 - 2e_g^2)}{81 - 17e_g + 30e_g^2(1 - e_g)}, \tag{E.40}$$

which are derived by van Noije and Ernst [72] on the basis of an earlier calculation by Goldstein and Shapiro [227]. The validity of the Sonine polynomial approximation is verified via the DSMC simulation [223]. We note that one-dimensional granular gas violates equipartition of energy [224].

RET for granular flow

We adopt RET to treat moderate dense granular flow [193]:

$$\left(\frac{\partial}{\partial t} + \boldsymbol{v}_1 \cdot \nabla_1 \right) f(\boldsymbol{r}_1, \boldsymbol{v}_1, t) = J_E[\boldsymbol{r}_1, \boldsymbol{v}_1 | f(t)], \tag{E.41}$$

where the collision operator is introduced as

$$\begin{aligned} J_E[\boldsymbol{r}_1, \boldsymbol{v}_1 | f(t)] \quad \equiv \quad & \int d^3 \boldsymbol{v}_2 d^2 k S(\boldsymbol{k} \cdot \boldsymbol{v}_{12}) \{ \Lambda f^{(2)}(\boldsymbol{r}_1, \boldsymbol{v}_1''; \boldsymbol{r}_1 + \sigma \boldsymbol{k}, \boldsymbol{v}_2''; t) \\ & - f^{(2)}(\boldsymbol{r}_1, \boldsymbol{v}_1; \boldsymbol{r}_1 - \sigma \boldsymbol{k}, \boldsymbol{v}_2; t) \}. \end{aligned} \tag{E.42}$$

Here, two-body distribution function is approximated as

$$f^{(2)}(\boldsymbol{r}_1, \boldsymbol{v}_1; \boldsymbol{r}_2, \boldsymbol{v}_2; t) = \chi(\boldsymbol{r}_1, \boldsymbol{r}_2 | n(t)) f(\boldsymbol{r}_1, \boldsymbol{v}_1, t) f(\boldsymbol{r}_2, \boldsymbol{v}_2, t), \tag{E.43}$$

with the equilibrium pair-correlation function χ as a functional of density n and the Jacobian for constant restitution coefficient case $\Lambda = 1/e_g^2$,

From the RET equation ($E.41$), the continuity equation for a physical quantity $\psi = \psi(\boldsymbol{v}_1)$ can be calculated through the integration $\int d^3 v_1$ after multiplying ψ on Eq. ($E.41$):

$$\frac{\partial}{\partial t} \langle \psi \rangle_f = -\frac{\partial}{\partial x_\alpha} J_\alpha(\psi) + I(\psi), \tag{E.44}$$

where $\langle \cdots \rangle_f \equiv \int d^3 v_1 f(\boldsymbol{x}_1, \boldsymbol{v}_1, t) \cdots$ and $J_\alpha = J_\alpha^c + J_\alpha^k$ with

$$J_\alpha^k \equiv \langle v_{1\alpha} \psi \rangle_f \tag{E.45}$$

$$J_\alpha^c \equiv \frac{\sigma}{4} \int d^3 v_1 d^3 v_2 d^2 k \int_0^1 d\lambda S(\boldsymbol{v}_{12} \cdot \boldsymbol{k}) k_\alpha \tag{E.46}$$
$$\Delta' \psi f^{(2)}(\boldsymbol{r}_1 + \sigma \boldsymbol{k}(1-\lambda), \boldsymbol{v}_1; \boldsymbol{r}_1 - \lambda \sigma \boldsymbol{k}, \boldsymbol{v}_2; t),$$

$$I(\psi) \equiv \frac{1}{2} \int d^3 v_1 d^3 v_2 d^2 k S(\boldsymbol{v}_{12} \cdot \boldsymbol{k}) \Delta \psi f^{(2)}(\boldsymbol{r}_1 + \sigma \boldsymbol{k}, \boldsymbol{v}_1; \boldsymbol{r}_1 \boldsymbol{v}_2; t), \tag{E.47}$$

with $\Delta' \psi \equiv (\psi_1' - \psi_1) - (\psi_2' - \psi_2)$ and $\Delta \psi \equiv (\psi_1' - \psi_1) + (\psi_2' - \psi_2)$. Hydrodynamical equations are derived by integrating over $\int d^3 v_1$ after multiplying $1, v_{1\alpha}$, and $\boldsymbol{v}_1^2/2$:

$$(\partial_t + \mathcal{U}_\beta \partial_\beta) n = -n \partial_\beta \mathcal{U}_\beta, \tag{E.48}$$

$$(\partial_t + \mathcal{U}_\beta \partial_\beta) \mathcal{U}_\alpha = -\frac{1}{mn} \partial_\beta \sigma_{\alpha\beta}, \tag{E.49}$$

$$(\partial_t + \mathcal{U}_\beta \partial_\beta) \mathcal{T}_g = -\frac{2}{3n} \{ \partial_\beta q_\beta + (\partial_\beta \mathcal{U}_\alpha) \sigma_{\alpha\beta} \} - \zeta \mathcal{T}_g, \tag{E.50}$$

with the density $n \equiv \langle 1 \rangle_f$, the velocity field $\mathcal{U}_\alpha \equiv \langle u_\alpha \rangle_f / n$, the granular temperature $\mathcal{T}_g \equiv \langle m \boldsymbol{u}^2 \rangle_f / 3n$ and $u_\alpha \equiv v_{1\alpha} - \mathcal{U}_\alpha$. Here, the stress tensor $\sigma_{\alpha\beta}$, the

heat flux q_α, and the cooling rate ζ are introduced:

$$\sigma_{\alpha\beta} = \sigma^k_{\alpha\beta} + \sigma^c_{\alpha\beta}, \tag{E.51}$$

$$\sigma^k_{\alpha\beta} \equiv m\langle u_{1\alpha}\tilde{u}_{1\beta}\rangle_f, \tag{E.52}$$

$$\sigma^c_{\alpha\beta} \equiv \frac{\sigma^3 m(1+e_g)}{4}\int dv_1^3 dv_2^3 \int d^2k\Theta(g_{12})g_{12}^2 k_\alpha k_\beta f^{(2)}(\boldsymbol{r}_1+\sigma\boldsymbol{k}(1-\lambda),\boldsymbol{v}_1;\boldsymbol{r}_1-\lambda\sigma\boldsymbol{k},\boldsymbol{v}_2;t), \tag{E.53}$$

$$q_\alpha = q^k_\alpha + q^c_\alpha, \tag{E.54}$$

$$q^k_\alpha \equiv m\langle u_{1\alpha}\boldsymbol{u}_1^2\rangle_f/2, \tag{E.55}$$

$$q^c_\alpha \equiv \frac{\sigma^3 m}{4}\int d^3v_1 d^3v_2 d^2k\Theta(g_{12})2(1+e_g)g_{12}^2 \tilde{V}_{12\beta}k_\beta k_\alpha f^{(2)}(\boldsymbol{r}_1+\sigma\boldsymbol{k}(1-\lambda),\boldsymbol{v}_1;\boldsymbol{r}_1-\lambda\sigma\boldsymbol{k},\boldsymbol{v}_2;t), \tag{E.56}$$

$$\zeta \equiv -\frac{I(m\boldsymbol{v}^2)}{3n\mathcal{T}_g}, \tag{E.57}$$

with $g_{12} \equiv \boldsymbol{v}_{12}\cdot\boldsymbol{k}$, $\tilde{V}_{12\alpha} \equiv V_{12\alpha} - \mathcal{U}_\alpha$, and $\boldsymbol{V}_{12} \equiv (\boldsymbol{v}_1+\boldsymbol{v}_2)/2$. The detailed derivations for Eqs. (E.44) and (E.48)-(E.50) are shown in Ref. [195].

Treatment of the rotational degrees of freedom

To solve hydrodynamical equations for frictional grains is laborious work. Including the collision rule of frictional grains, hydrodynamical equations can be derived from the Enskog equations. However, in addition to equations for the translational degree of freedoms $(n,\boldsymbol{\mathcal{U}},\mathcal{T}_g)$, those for the angular velocity fields $\bar{\boldsymbol{\omega}} \equiv \sum_i \boldsymbol{\omega}_i$ and the rotational temperature $\mathcal{T}_{\rm rot} \equiv \sum_i I_0(\boldsymbol{\omega}_i - \bar{\boldsymbol{\omega}})^2/2$ with moment of inertia of grains I_0 are necessary, which are quite complicated [225–233]. This difficulty can be avoided in the case of the slightly frictional grains, i.e. small frictional coefficient cases, where the effect of the tangential contact in collisions can be absorbed in the renormalized restitution coefficient [177, 178]. For slightly frictional spheres, Jenkins and Zhang [177] suggested that hydrodynamical equations for frictional grains are reduced to those for translational degree of freedoms by introducing an effective restitution coefficient $\bar{e}_g$

$$\bar{e}_g = e_g - \frac{\pi}{2}\mu_p + \frac{9}{2}\mu_p^2 + O(\mu_p^3), \tag{E.58}$$

as an expansion about the friction coefficient between grains μ_p, if μ_p is small. The validity of three-dimensional theory [177] has been tested by Xu *et al* [234] and Jenkins and Zhang [177]. The latter is consistent with Lun and Bent [235] in part. The validity of the case for slightly frictional disks [178] has been verified by Saitoh and Hayakawa [179]. Although the correlation between velocity and angular velocity of grains has been argued at the level of VDFs [230, 233], the transport coefficients for the large μ_p case have not been derived to our knowledge.

E.5 Transport coefficients for inelastic hard core gases

In this section, we summarize the results known as transport coefficients for inelastic hard core gases. We have used κ in the elastic limit $e_g = 1$ in Chap. 7. Let the one body VDF for hard core gas f, viscosity η, thermal conductivity κ, thermal conductivity from inelasticity μ. The superscript * in this appendix represents the dimensionless quantities, normalized by the corresponding dimensional ones, such as

$$\eta_0 \equiv \frac{5}{16\sigma^2}\sqrt{\frac{m}{\pi \mathcal{T}_g}} \tag{E.59}$$

$$\kappa_0 \equiv \frac{15\eta_0}{4m} \tag{E.60}$$

$$p^k \equiv n\mathcal{T}_g \tag{E.61}$$

$$\nu_0 \equiv \frac{p^k}{\eta_0}. \tag{E.62}$$

The dimensionless quantities are defined as

$$\begin{aligned} &\eta^* \equiv \frac{\eta}{\eta_0},\ \kappa^* \equiv \frac{\kappa}{\kappa_0},\ \gamma^* \equiv \frac{\gamma}{\eta_0},\ \mu^* \equiv \frac{n\mu}{\kappa_0 \mathcal{T}_g}, \\ &p^* \equiv \frac{p}{p^k},\ \zeta^* \equiv \frac{\zeta}{\nu_0},\ \nu_\eta^* = \frac{\nu_\eta}{\nu_0},\ \nu_\kappa^* = \nu_\mu = \frac{\nu_\mu}{\nu_0}. \end{aligned} \tag{E.63}$$

Transport coefficients are summarized in Table. E.1, where n^* represents the dimensionless density $n^* \equiv n\sigma^3$. We introduce

$$\tilde{S}_l(\boldsymbol{u}) \equiv u_l\left(\frac{mu^2}{2} - \frac{5\mathcal{T}_g}{2}\right)\ (l = x, y, z), \tag{E.64}$$

$$\tilde{E}(u) \equiv \left(\frac{mu^2}{2\mathcal{T}_g}\right)^2 - \frac{5mu^2}{2\mathcal{T}_g} + \frac{15}{4}. \tag{E.65}$$

Table E.1: Transport coefficients for moderately dense inelastic hard core gases in [73].

$$f = f_M \left\{ 1 + \tfrac{c^*}{4}\tilde{E}(u) - \tfrac{2m}{5n\mathcal{T}^3}\sum_{l=x,y,z}\left(\kappa^k\partial_l\mathcal{T} + \mu^k\partial_l n\right)\tilde{S}_l(\boldsymbol{u}) \right.$$
$$\left. -\tfrac{\mathcal{T}^2\eta^k}{2n}\sum_{ij=x,y,z}\left(\partial_i\mathcal{U}_j + \partial_j\mathcal{U}_i - \tfrac{2}{3}\delta_{ij}\sum_{l=x,y,z}\partial_l\mathcal{U}_l\right) + c_{\mathcal{D}}E_{\rm NE}(u)\sum_{l=x,y,z}\partial_l\mathcal{U}_l \right\}$$

$$f_M = \tfrac{n}{\pi^{3/2}}\left(\tfrac{2\mathcal{T}}{m}\right)^{3/2} e^{-mu^2/2\mathcal{T}}$$

$$\eta^* = \eta^{k*}\left[1 + \tfrac{2}{15}\pi n^*\chi(1+e_g)\right] + \tfrac{3}{5}\gamma^*$$
$$\eta^{k*} = \left(\nu_\eta^* - \tfrac{1}{2}\zeta^{(0)*}\right)^{-1}\left[1 - \tfrac{1}{15}(1+e_g)(1-3e_g)\pi n^*\chi\right]$$

$$\gamma^* = \tfrac{32}{45}\pi n^{*2}\chi(1+e_g)\left(1 - \tfrac{c^*}{32}\right)$$

$$\kappa^* = \kappa^{k*}\left[1 + \tfrac{\pi}{5}n^*\chi(1+e_g)\right] + \tfrac{64}{225}n^{*2}\chi(1+e_g)\left(1 + \tfrac{27}{32}c^*\right)$$
$$\kappa^{k*} = \tfrac{2}{3}(\nu_\kappa^* - 2\zeta^{(0)*})^{-1}\left(1 + \tfrac{1+p^*}{2}c^* + \tfrac{\pi}{10}n^*\chi(1+e_g)^2\left\{2e_g - 1 + \tfrac{3(1+e_g)^2-10}{6(1+e_g)}c^*\right\}\right)$$

$$\mu^* = \mu^{k*}\left[1 + \tfrac{\pi}{5}n^*\chi(1+e_g)\right]$$
$$\mu^{k*} = 2\left(2\nu_\kappa^* - 3\zeta^{(0)*}\right)^{-1}\left\{(1 + n\partial_n\ln\chi)\zeta^{(0)*}\kappa^{k*} + \tfrac{p^*}{3}(1 + n\partial_n\ln p^*)c^*\right.$$
$$\left. -\tfrac{2\pi}{15}n^*\chi(1 + \tfrac{n}{2}\partial_n\ln\chi)(1+e_g)\left(e_g - e_g^2 + \tfrac{c^*}{3} + \tfrac{e_g(1-e_g)}{4}c^*\right)\right\}$$

$$c_{\mathcal{D}} = \tfrac{1}{\nu_0}\left[\tfrac{\zeta^{(0)*}}{2} + \nu_\gamma^* + \tfrac{5c^*}{64}\left(1 + \tfrac{3c^*}{64}\right)\chi(1-e_g^2)\right]^{-1}\left[\tfrac{2\lambda^*}{45}\pi n\chi + (p^*-1)(\tfrac{2}{3} - e_g)c^*\right]$$

$$p^* = 1 + \tfrac{1+e_g}{3}\pi n^*\chi$$

$$\zeta^* = \zeta^{(0)*} + \zeta^{(1)*}, \zeta^{(0)*} = \tfrac{5}{12}\chi(1-e_g^2)\left(1 + \tfrac{3c^*}{32}\right),$$
$$\zeta^{(1)*} = [-\tfrac{1-e_g}{\nu_0}(p^*-1) + \tfrac{5}{32}(1-e_g^2)\left(1 + \tfrac{3c^*}{64}\right)\chi c_{\mathcal{D}}]\sum_{l=x,y,z}\partial_l\mathcal{U}_l,$$

$$c^* = 32(1-e_g)(1-2e_g^2)\left[81 - 17e_g + 30e_g^2(1-e_g)\right]^{-1},$$
$$\lambda^* = \tfrac{3}{8}(1+e_g)\left[(1-e_g)(5e_g^2 + 4e_g - 1) + \tfrac{c^*}{12}(159e_g + 3e_g^2 - 19e_g - 15e_g^3)\right],$$

$$\nu_\eta^* = \chi\left\{1 - \tfrac{1}{4}(1-e_g)^2\right\}\left(1 - \tfrac{c^*}{64}\right)$$
$$\nu_\kappa^* = \nu_\mu^* = \tfrac{1+e_g}{3}\chi\left[1 + \tfrac{33}{16}(1-e_g) + \tfrac{19-3e_g}{1024}c^*\right]$$
$$\nu_\gamma^* = \tfrac{1+e_g}{48}\chi\left[128 - 96e_g + 15e_g^2 - 15e_g^3 + \tfrac{c^*}{64}(15e_g^3 - 15e_g^2 + 498e_g - 434)\right]$$

Appendix F

Velocity auto-correlation

We demonstrate the utility of the SMF for the velocity auto-correlation function for a fluctuating piston in this appendix. In Ref. [239], the overdamped Langevin description is not adequate for the autocorrelation function for the piston velocity. Here, we compare the velocity autocorrelation function $C(t) \equiv \langle \hat{V}(t)\hat{V}(0)\rangle / \langle \hat{V}^2(0)\rangle$ obtained by MD for a dilute gas, by choosing $T_{\rm bath} = T_{\rm out}$. As can be seen in Fig. F.1 (a), due to the implementation of the fluctuation of $\hat{T}_{\rm in}$, the SMF model (solid line) agrees with the behavior of $C(t)$ for MD simulation with $\epsilon = 0.01$, which is better than that obtained by an underdamped Langevin equation at a constant temperature.

Taking the average of the SMF (7.5) and (7.22), the solid line in Fig. F.1(a) is derived. By solving Eq. (7.25), we obtain an analytic expression for $C(t)$ for the SMF $C_{\rm SMF}(t)$ as:

$$C_{\rm SMF}(t) = e^{-\epsilon\bar{\gamma}t/2}\left\{\cos(\omega t) - \frac{\epsilon\bar{\gamma}}{2\omega}\sin(\omega t)\right\}, \tag{F.1}$$

$$\omega \equiv \sqrt{\frac{P_{\rm out}A}{M}}\sqrt{1 - \frac{\epsilon^2 MNT_{\rm out}}{4P_{\rm out}^2A^2}}. \tag{F.2}$$

Equation (F.1) reproduces the result of the under-damped Langevin $C_{\rm L}(t)$ [239] replacing $\bar{\gamma} \to \gamma_{\rm gas}$. The only difference between the Langevin equation and the SMF is the back action of the temperature Eq. (7.23) due to the motion of the piston. It should be noted that the difference between $C_{\rm L}(t)$ and $C_{\rm SMF}(t)$ becomes smaller as $N \to \infty$ as is shown in Fig. F.1 (b).

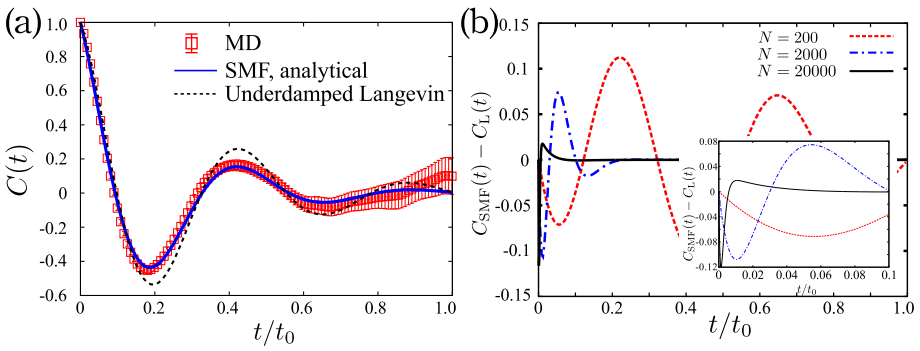

Figure F.1: (a) The comparison of results for the SMF model (solid line) and MD (squares) in terms of $C(t)$. The SMF model correctly predicts the MD data and shows better agreement with MD than the prediction of the underdamped Langevin equation (dotted line), due to the implementation of the time evolution of $\hat{T}_{\rm in}$. (b) The difference of the autocorrelation functions between MD and SMF is shown for $0 < t/t_0 < 1$ in the main figure. As $N \to \infty$, the difference becomes smaller. The inset represents the results for $0 < t/t_0 < 0.1$.

Appendix G

On the definition of work for a passive engine

In Chapter 7, we have defined the work as "Pressure × Volume change," which is not trivial. In this appendix, we justify the definition, i.e. we decompose the change of the kinetic energy of piston into heat and work by considering the path probability of $(\hat{X}(t), \hat{V}(t))$ under $\hat{T}_{\rm in}(t) = T_{\rm in}$. The discussion here is the extension of Ref. [242] toward the case that the volume of the enclosed gas fluctuates in time. Let us consider the path probability for the forward evolution $\mathcal{P}([\hat{X}, \hat{V}|\tau)$ of $(\hat{X}, \hat{V})$ during the interval τ from $(\hat{X}(0), \hat{V}(0))$ to $(\hat{X}(\tau), \hat{V}(\tau))$ and the backward one $\mathcal{P}([\hat{X}, \hat{V}]^\dagger|\tau)$ from $(\hat{X}(\tau), -\hat{V}(\tau))$ to $(\hat{X}(0), -\hat{V}(0))$, where n collisions between the piston and particles take place at time $\{t_i\}_{i=1}^n$ with $0 = t_0 < t_1 < \cdots < t_n = \tau$. The jump rates for the piston velocity from $V_{i-1} \equiv \hat{V}(t_{i-1})$ to $V_i \equiv \hat{V}(t_i)$ at the piston position $X_{i-1} \equiv \hat{X}(t_{i-1})$ caused by collisions from particles inside and outside the container are, respectively, written as

$$\begin{aligned} W_{\rm in}(V_i \leftarrow V_{i-1}|X_{i-1}) &\equiv n_{\rm in}(X_{i-1})A\int_{-\infty}^{\infty} dv|v - V_{i-1}| \\ &\quad \times\Theta(v - V_{i-1})\phi(v, T_{\rm in})\delta\left(V_i - V_{i-1} - \frac{P_v(V_{i-1})}{M}\right), \end{aligned} \tag{G.1}$$

$$\begin{aligned} W_{\rm out}(V_i \leftarrow V_{i-1}) &\equiv n_{\rm out}A\int_{-\infty}^{\infty} dv|v - V_{i-1}| \\ &\quad \times\Theta(V_{i-1} - v)\phi(v, T_{\rm out})\delta\left(V_i - V_{i-1} - \frac{P_v(V_{i-1})}{M}\right), \end{aligned} \tag{G.2}$$

$$W_{\rm tot}(V_i \leftarrow V_{i-1}|X_{i-1}) \equiv W_{\rm in}(V_i \leftarrow V_{i-1}|X_{i-1}) + W_{\rm out}(V_i \leftarrow V_{i-1}). \tag{G.3}$$

The escape rate per a unit time $\kappa(V_{i-1}|X_{i-1})$ for (X_{i-1}, V_{i-1}) is represented as

$$\begin{aligned}\kappa(V_{i-1}|X_{i-1}) &= \int_{-\infty}^{\infty} dV' W_{\rm tot}(V' \leftarrow V_{i-1}|X_{i-1}) \\ &= n_{\rm in}(X_{i-1}) A \int_{V_{i-1}}^{\infty} |v - V_{i-1}| \phi_0(v, T_{\rm in}) dv \\ &\quad + n_{\rm out} A \int_{-\infty}^{V_{i-1}} |v - V_{i-1}| \phi_0(v, T_{\rm out}) dv. \end{aligned} \tag{G.4}$$

Thus, $\mathcal{P}([X,V]|\tau)$ and $\mathcal{P}([X,V]^\dagger|\tau)$ are represented as

$$\mathcal{P}([X,V]|\tau) = \exp\left[-\sum_{i=0}^{n-1}\int_{t_i}^{t_{i+1}} \kappa(V_i|X(s_i)) ds_i\right]\left[\prod_{i=1}^{n} W_{\rm tot}(V_i \leftarrow V_{i-1}|X_{i-1})\right], \tag{G.5}$$

$$\mathcal{P}([X,V]^\dagger|\tau) = \exp\left[-\sum_{i=0}^{n-1}\int_{t_i}^{t_{i+1}} \kappa(-V_i|X(s_i)) ds_i\right]\left[\prod_{i=1}^{n} W_{\rm tot}(-V_{i-1} \leftarrow -V_i|X_{i-1})\right]. \tag{G.6}$$

Here, the position of the piston at time $t_i < s_i < t_{i+1}$ is given by $X(s_i) \equiv X_i + V_i(s_i - t_i)$. We obtain

$$\begin{aligned}\int_{t_i}^{t_{i+1}} \left\{\kappa(V_i|X_{s_i}) - \kappa(-V_i|X_{s_i})\right\} ds_i &= -N \ln\left(\frac{X_{i+1}}{X_i}\right) + n_{\rm out} A V_i (t_{i+1} - t_i) \\ &= -\beta_{\rm in}\int_{X_i}^{X_{i+1}} n_{\rm in}(X) T_{\rm in} A dX \\ &\quad + \beta_{\rm out} P_{\rm out} A V_j (t_{i+1} - t_i), \end{aligned} \tag{G.7}$$

$$\ln\left\{\frac{W_{\rm tot}(V' \leftarrow V|X)}{W_{\rm tot}(-V \leftarrow -V'|X)}\right\} = \begin{cases} \beta_{\rm in}\dfrac{m(v'^2 - v^2)}{2} \equiv \beta_{\rm in}\Delta E_{\rm in}(V' > V) \\ \beta_{\rm out}\dfrac{m(v'^2 - v^2)}{2} \equiv \beta_{\rm out}\Delta E_{\rm out}(V' < V), \end{cases} \tag{G.8}$$

Here we have introduced the inverse temperature $\beta_\nu \equiv 1/T_\nu$ and the energy change of ν side gas ΔE_ν through the piston fluctuation ($\nu = $ in, out). Using Eqs. (G.7) and (G.8), we obtain the following expression on the definition of the work:

$$\ln\left\{\frac{\mathcal{P}([X,V]|\tau)}{\mathcal{P}([X,V]^\dagger|\tau)}\right\} = \beta_{\rm in}\Delta Q_{\rm in} + \beta_{\rm out}\Delta Q_{\rm out} + \Delta S_{\rm inel}, \tag{G.9}$$

$$\Delta E_{\rm in} = \Delta Q_{\rm in} - \int_{X_{\rm ini}}^{X_\tau} \frac{1+e}{2} n_{\rm in} T_{\rm in} A dX, \tag{G.10}$$

$$\Delta E_{\rm out} = \Delta Q_{\rm out} + \frac{1+e}{2} P_{\rm out} A \int_{X_{\rm ini}}^{X_\tau} dX, \tag{G.11}$$

$$\Delta S_{\rm inel} \equiv \frac{1-e}{2}\int_{X_{\rm ini}}^{X_\tau} \left\{n_{\rm in} T_{\rm in} - P_{\rm out}\right\} A dX \tag{G.12}$$

where we have introduced the abbreviation $V_0 \equiv \hat{V}(0), X_\tau \equiv \hat{X}(\tau)$ and $V_\tau \equiv \hat{V}(\tau)$. From Eq. (G.10), the change of the internal energy for the enclosed gas ΔE_{in} is apparently decomposed into the change of work and heat. Thus, we adopt the definition of work Eq. (7.26).

Appendix H

Effect of side-wall friction on a passive engine

In this appendix, we discuss the effect of the side-wall friction on the efficiency for a passive engine, which exists for realistic situations. We implement the linear friction on the side-wall as $\hat{F}_{\rm fri} = -\gamma_{\rm lin}\hat{V}$. Then, the equation of motion Eq. (7.5) turns out to be

$$M\frac{d\hat{V}}{dt} = \hat{F}_{\rm in} + \hat{F}_{\rm out} + \hat{F}_{\rm fri} \tag{H.1}$$

We assume that $\gamma_{\rm lin}$ does not depend on ϵ and $\gamma_{\rm lin}/\gamma_{\rm gas} = O(1)$, where the motion of the piston becomes the over-damped type, even if the piston is heavy. Because the side-wall friction can be regarded as that attached with a zero temperature bath, we define the efficiency under friction [240] by introducing the frictional heat:

$$\hat{Q}_{\rm fri} \equiv \oint \gamma_{\rm lin}\hat{V}^2 dt \tag{H.2}$$

$$\hat{\eta}_{\rm fri} \equiv \frac{\hat{W}_{\rm tot}}{\hat{Q}_{\rm H} + \hat{Q}_{\rm fri}} \tag{H.3}$$

The simulated data for the efficiency at MP with $\gamma_{\rm lin}/\gamma_{\rm gas} = 2.0$ and $e = 1.0$ are plotted in Fig. H.1. The asymptotic behavior of $\langle\hat{\eta}\rangle_{\rm SC}$ and $\langle\hat{\eta}_{\rm fri}\rangle_{\rm SC}$ in the limit $\epsilon \to 0$ for $T_{\rm H}/T_{\rm L} = 5.0$ are shown in Fig. H.1 (a). In Fig. H.1 (b), we plot the temperature dependence of $\langle\hat{\eta}\rangle_{\rm SC}$ and $\langle\hat{\eta}_{\rm fri}\rangle_{\rm SC}$ at MP with $\epsilon = 0.001$, where the efficiencies are lower than $\eta_{\rm CA}$(see Fig. 7.7 (a)). Thus, as expected, the friction on the sidewall lowers the efficiency.

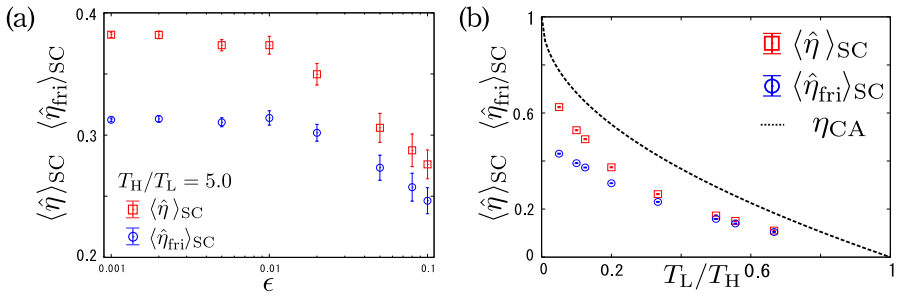

Figure H.1: The efficiency at MP under side-wall friction. The asymptotic behavior of the efficiencies in the limit $\epsilon \to 0$ (a), and their temperature dependence for $\epsilon = 0.001$ and $\gamma_{\rm lin}/\gamma_{\rm gas} = 2.0$ (b). The friction on the sidewall lowers the efficiency.

Bibliography

[1] R. Brown, *The miscellaneous botanical works of Robert Brown: Volume 1.*, Edited by John J. Bennett, (R. Hardwicke, London, 1866).

[2] A. Einstein, Ann. Phys. **17** 549 (1905).

[3] M. von Smoluchowski, Annalen der Physik, **21** 756 (1906).

[4] M. von Smoluchowski, Ann. Physik, **25**, 205 (1908).

[5] P. Langevin, C. R. Acad. Sci. (Paris) **146**, 530 (1908).

[6] *Selected papers on noise and stochastic processes*, Edited by N. Wax, (Dover, New York, 1954).

[7] N. G. van Kampen, *Stochastic Processes in Physics and Chemistry*, 3rd ed. (North-Holland Personal Library, 2007).

[8] C. Gardiner, *Stochastic Methods, 4th ed.* (Springer-Verlag, Berlin, 2009).

[9] P. Hänggi, *100 years of Brownian motion: historical items and surveys*, Original papers related to the history of Brownian motion are listed: `http://www.physik.uni-augsburg.de/theo1/hanggi/History/BM-History.html`.

[10] M. von Smoluchowski, Phys. Zeitschrift **13**: 1069 (1912).

[11] R. P. Feynman, *The Feynman Lectures on Physics*, Vol. 1. Chapter 46. (Massachusetts, USA: Addison-Wesley., 1963).

[12] J. M. R. Parrondo and P. Español, Am. J. Phys. **64**, 1125 (1996).

[13] P. Eshuis, K. van der Weele, D. Lohse, and D. van der Meer, Phys. Rev. Lett. **104**, 248001 (2010).

[14] Y. Yamamoto, *Historical development of thermological ideology* Volume 1-3., 1st ed. (Chikuma Shobō, Tokyo, 2009) (*written in Japanese*).

[15] A. Jagota and C. Y. Hui, Mater. Sci. Eng. R-Reports **72**(12), 253 (2011).

[16] Q. Li, Y. Dong, D. Perez, A. Martini, and R. W. Carpick, Phys. Rev. Lett. **106**, 126101 (2011).

[17] A. J. Weymouth, D. Meuer, P. Mutombo, T. Wutscher, M. Ondracek, P. Jelinek, and F. J. Giessibl, Phys. Rev. Lett. **111**, 126103 (2013).

[18] T. L. Hill, *Thermodynamics of Small Systems* (Dover, New York, 1964).

[19] D. M. Carberry, J. C. Reid, G. M. Wang, E. M. Sevick, Debra J. Searles, and Denis J. Evans, Phys. Rev. Lett. **92**, 140601 (2004).

[20] C. Bustamante, J. Liphardt, and F. Ritort, Phys. Today **58**(7), 43 (2005).

[21] A. Barreiro, R. Rurali, E. R. Heránndez, J. Moser, T. Pichler, L. Forró, and A. Bachtold, Science **320**, 5877 (2008).

[22] Martin G. L. van den Heuvel and C. Dekker, Science **317**, 333 (2007).

[23] J. Bath and A. J. Turberfield, Nature Nanotech. **2**, 275 (2007).

[24] R. Guerra, U. Tartaglino, A. Vanossi and E. Tosatti, Nature Materials **9**, 634 (2010).

[25] B. N. J. Persson, *Sliding Friction* (Springer-Verlag, Berlin, 2000).

[26] M. G. L. van den Heuvel, M. P. de Graaff, C. Dekker, Science **312**, 910 (2006).

[27] B. Wang, S. M. Anthony, S. C. Bae, and S. Granick, Proc. Natl Acad. Sci. USA **106**, 15160 (2009).

[28] B. Wang, J. Kuo, S. C. Bae and S. Granick, Nature Materials **11**, 481 (2012).

[29] A. Gnoli, A. Petri, F. Dalton, G. Pontuale, G. Gradenigo, A. Sarracino, and A. Puglisi, Phys. Rev. Lett. **110**, 120601 (2013).

[30] A. Gnoli, A. Sarracino, A. Puglisi and A. Petri, Phys. Rev. E **87**, 052209 (2013).

[31] A. Gnoli, A. Puglisi, and H. Touchette, Europhys. Lett. **102**, 14002 (2013).

[32] A. Sarracino, A. Gnoli, and A. Puglisi, Phys. Rev. E **87**, 040101(R) (2013).

[33] A. Kawarada, H. Hayakawa, J. Phys. Soc. Jpn. **73**, 2037 (2004).

[34] H. Hayakawa, Physica D **205** 48 (2005).

[35] P. G. de Gennes, J. Stat. Phys. **119**, 953 (2005).

[36] A. M. Menzel and N. Goldenfeld, Phys. Rev. E **84**, 011122 (2011).

[37] J. Talbot, R. D. Wildman, and P. Viot, Phys. Rev. Lett. **107**, 138001 (2011).

[38] J. Talbot and P. Viot, Phys. Rev. E **85**, 021310 (2012).

[39] A. Baule and P. Sollich, Europhys. Lett, **97**, 20001 (2012).

[40] A. Baule and P. Sollich, Phys. Rev. E **87**, 032112 (2013).

[41] A. Gnoli, A. Puglisi, and H. Touchette, Europhys. Lett. **102**, 14002, (2013).

[42] H. Touchette, E. Van der Straeten and W. Just, J. Phys. A: Math. Theor. **43**, 445002 (2010).

[43] Y. Chen, A. Baule, H. Touchette and W. Just, Phys. Rev. E **88** 052103 (2013).

[44] K. Sekimoto, J. Phys. Soc. Jpn. **66**, 1234 (1997).

[45] K. Sekimoto, *Stochastic Energetics*, Lecture Notes in Physics (Springer, New York, 2010).

[46] U. Seifert, Rep. Prog. Phys. **75** 126001 (2012).

[47] K. Kanazawa, T. Sagawa, and H. Hayakawa, Phys. Rev. Lett. **108**, 210601 (2012).

[48] L. D. Landau and E. Lifshitz, *Statistical Physics, Part 1* (Butterworth-Heinemann, Oxford, 1980).

[49] H. Callen, *Thermodynamics and an Introduction to Thermostatistics* (Wiley, New York, 1985).

[50] B. Abou and F. Gallet, Phys. Rev. Lett. **93**, 160603 (2004).

[51] K. Hayashi and S. Sasa, Phys. Rev. E **69**, 066119 (2004).

[52] J. Prost, J.-F. Joanny, and J. M. R. Parrondo, Phys. Rev. Lett. **103**, 090601 (2009).

[53] T. Hatano and D. Jou, Phys. Rev. E **67**, 026121 (2003).

[54] J. Ren and B. Li, Phys. Rev. E **81**, 021111 (2010).

[55] P. Pradhan, C. P. Amann, and U. Seifert, Phys. Rev. Lett. **105**, 150601 (2010).

[56] P. Pradhan, R. Ramsperger, and U. Seifert, Phys. Rev. E **84**, 041104 (2011).

[57] K. Kanazawa, T. Sagawa, and H. Hayakawa, Phys. Rev. E **87**, 052124 (2013).

[58] H. M. Jaeger, S. R. Nagel, and R. P. Behringer, Rev. Mod. Phys. **68**, 1259 (1996).

[59] I. S. Aranson and L. S. Tsimring, Rev. Mod. Phys. **78**, 641 (2006).

[60] T. Pöschel and T. Schwager, *Computational Granular Dynamics* (Springer, Berlin, 2005).

[61] N. V. Brilliantov and T. Pöschel, *Kinetic Theory of Granular Gases* (Oxford University Press, New York, 2010).

[62] S. F. Edwards, in *Granular Matter: An Interdisciplinary Approach*, edited by A. Mehta (Springer-Verlag, New York, 1994), p. 121, and references therein.

[63] S. F. Edwards and R. B. S. Oakeshott, Phys. A (Amsterdam) **157**, 1080 (1989).

[64] S. F. Edwards and D. V. Grinev, Phys. Rev. E **58**,4758 (1998).

[65] H. A. Makse and J. Kurchan, Nature **415**, 614 (2002).

[66] R. Blumenfeld and S. F. Edwards, Phys. Rev. Lett. **90**, 114303 (2003).

[67] R. K. Bowles and S. S. Ashwin, Phys. Rev. E **83**, 031302 (2011).

[68] G. Gradenigo, E. E. Ferrero, E. Bertin, and J.-L. Barrat, Phys. Rev. Lett. **115**, 140601 (2015).

[69] D. Bi, S. Henkes, K. E. Daniels, and B. Chakraborty, Annu. Rev. Condens. Matter Phys. **6**, 63 (2015).

[70] J. T. Jenkins and S. B. Savege, J. Fluid. Mech. **130**, 187 (1983).

[71] J. T. Jenkins and M. W. Richman, Phys. Fluids. **28**, 3485 (1985).

[72] T.P.C. van Noije and M.H. Ernst, Granul. Matt. **1**, 57 (1998).

[73] V. Garzó and J. W. Dufty, Phys. Rev. E **59**, 5895 (1999).

[74] J. F. Lutsko, Phys. Rev. E **72**, 021306 (2005).

[75] C. C. Maaß, N. Isert, G. Maret, and C. M. Aegerter, Phys. Rev. Lett. **100**, 248001 (2008).

[76] S. Tatsumi, Y. Murayama, H. Hayakawa, and M. Sano, J. Fluid. Mech. **641**, 521 (2009).

[77] GDR MiDi, Eur. Phys. J. E **14**, 341 (2004).

[78] Y. Forterre and O. Pouliquen, Annu. Rev. Fluid Mech. **40**, 1 (2008).

[79] T. G. Sano and H. Hayakawa, Phys. Rev. E **86**, 041308 (2012).

[80] T. G. Sano and H. Hayakawa, AIP Conf. Proc. **1542**, 622 (2013).

[81] T. G. Sano and H. Hayakawa, Prog. Theor. Exp. Phys. (**2013**) 103J02.

[82] X. Cheng, L. Gordillo, W. W. Zhang, H. M. Jaeger, and S. R. Nagel, Phys. Rev. E **89**, (2014).

[83] A. J. Liu and S. R. Nagel, Nature **396**, 21 (1998).

[84] M. Otsuki and H. Hayakawa, Phys. Rev. E **83**, 051301 (2011).

[85] H. Hayakawa and M. Otsuki, Phys. Rev. E **88**, 032117 (2013).

[86] K. Suzuki and H. Hayakawa, Phys. Rev. Lett. **115**, 098001 (2015).

[87] J. S. Olafsen and J. S. Urbach, Phys. Rev. E **60**, R2468(R) (1999).

[88] A. Kudrolli and J. Henry, Phys. Rev. E **62**, R1489(R) (2000).

[89] G. W. Baxter and J. S. Olafsen, Nature **425**, 680 (2003).

[90] J. J. Brey, M. J. Ruiz-Montero, and R. García-Rojo, Phys. Rev. E **60**, 7174 (1999).

[91] A. Sarracino, D. Villamaina, G. Costantini, and A. Puglisi, J. Stat. Mech. (**2010**)P04013.

[92] K. Kanazawa, T. G. Sano, T. Sagawa, and H. Hayakawa, Phys. Rev. Lett. **114**, 090601 (2015).

[93] K. Kanazawa, T. G. Sano, T. Sagawa, and H. Hayakawa, J. Stat. Phys. **160**, 1294 (2015).

[94] B. Cleuren and R. Eichhorn, J. Stat. Mech. (**2008**) P10011.

[95] J. Talbot, R. D. Wildman, and P. Viot, Phys. Rev. Lett. **107**, 138001 (2013).

[96] S. Chapman, Proc. Roy. Soc. Ser. A **119**, 34 (1928).

[97] A. Kolmogorov, Math. Ann. **104**, 415 (1931).

[98] H. Callen, *Thermodynamics and an Introduction to Thermostatistics* (Wiley, New York, 1985),

[99] L. D. Landau and E. Lifshitz, *Statistical Physics, Part 1* (Butterworth-Heinemann, Oxford, 1980).

[100] S. Carnot, *Reflexions sur la Puissance Motorice Du Feu et Sur Les Machines* (Ecole Polytechnique, 1824).

[101] C. D. West, *Principles and applications of Stirling engines*, Van Nostrand-Reinhold, New York (1986).

[102] M. O. Magnasco, Phys. Rev. Lett. **72**, 2656 (1994).

[103] V. Ganesan, *Internal Combustion Engines* (McGraw Hill Education, India Pvt Ltd, 2012)

[104] A. Vaudrey, F. Lanzetta, and M. Feidt, J. Non-Equilib. Thermodyn., **39**, 199 (2014).

[105] H. B. Reitlinger, *Sur lútilisation de la chaleur dans les machines á feu ("On the use of heat in steam engines," in French)*Vaillant-Carmanne, Liége, Belgium, (1929).

[106] J. Yvon, *Proceedings of the International Conference on Peaceful Uses of Atomic Energy*, (Geneva, Switzerland, (1955) USA).

[107] P. Chambadal, *Les centrales nucléaires* (Armand Colin, Paris, France, 1957).

[108] I. I. Novikov, At. Energy (N.Y.) **3**, 1269 (1957); J. Nucl. Energy **7**, 125 (1958).

[109] F. Curzon and B. Ahlborn, Am. J. Phys. 43, 22 (1975).

[110] A. De Vos, *Endoreversible Thermodynamics of Solar Energy Conversion* (Oxford University, Oxford, 1992); R. S. Berry, V. A. Kazakov, S. Sieniutycz, Z. Szwast, and A. M. Tsvilin, *Thermodynamic Optimization of FiniteTime Processes* (John Wiley & Sons, Chichester, 2000); P. Salamon, J. D. Nulton, G. Siragusa, T. R. Andersen, and A. Limon, Energy 26, 307 (2001).

[111] C. Van den Broeck, Phys. Rev. Lett. **95**, 190602 (2005).

[112] Y. Izumida and K. Okuda, Europhys. Lett. **83**, 60003 (2008).

[113] Y. Izumida and K. Okuda, Phys. Rev. E **80**, 021121 (2009).

[114] M. Esposito, R. Kawai, K. Lindenberg, and C. Van den Broeck, Phys. Rev. Lett. **105**, 150603 (2010).

[115] Y. Izumida and K. Okuda, Europhys. Lett. **97** 10004 (2012).

[116] J. Hoppenau, M. Niemann, and A. Engel, Phys. Rev. E **87**, 062127 (2013).

[117] U. Seifert, Phys. Rev. Lett. **106**, 020601 (2011).

[118] C. Van den Broeck, N. Kumar, and K. Lindenberg, Phys. Rev. Lett. **108** 210602 (2012).

[119] M. Mozurkewich and R. S. Berry, J. Appl. Phys. **53**, 34 (1982).

[120] F. Angulo-Browndag, J. A. Rocha-Martínezddag, and T. D. Navarrete-González, J. Phy. D: Appl. Phys. **29**, 80 (1996).

[121] X. Qin, L. Chen, F. Sun, and C. Wu, Eur. J. Phys. **24** 359 (2003).

[122] H. T. Quan, Y. D. Wang,Y. X. Liu, C. P. Sun, and F. Nori, Phys. Rev. Lett. **97**, 180402 (2006).

[123] H. T. Quan, Y. X. Liu, C. P. Sun, and F. Nori, Phys. Rev. E **76**, 031105 (2007).

[124] O. Abah, J. Roßnagel, G. Jacob, S. Deffner, F. Schmidt-Kaler, K. Singer, and E. Lutz, Phys. Rev. Lett. **109**, 203006 (2012).

[125] T. Schmiedl and U. Seifert, Phys. Rev. Lett. **98**, 108301 (2007).

[126] T. Schmiedl and U. Seifert, Europhys. Lett. **81** 20003 (2008).

[127] Z. C. Tu, J. Phys. A: Math. Theor. **41** 312003 (2008).

[128] V. Blickle and C. Bechinger, Nat. Phys., **8** 143 (2012).

[129] S. Rana, P. S. Pal, A. Saha, and A. M. Jayannavar, Phys. Rev. E **90**, 042146 (2014).

[130] E. Torricelli, Letter to Michelangelo Ricci (11th June, 1644).

[131] B. Pascal, *Scientific paper series*, (Iwanami-bunko, Tokyo, 1953) (*written in Japanese*).

[132] K. Koyanagi, *Pascal's hidden pictures*, (Chuokoron-shinsho, Tokyo, 1999) (*written in Japanese*).

[133] J. B. West, J. Appl. Physiol. **98**, 31 (2005).

[134] I. Newton, *The Principia: Mathematical Principles of Natural Philosophy* 1st ed. (Philosophical Transactions of the Royal Society, London, 1687).

[135] I. B. Cohen, Hist. Sci. Soc. **46** 99 (1955).

[136] E. W. J. Neave, Hist. Sci. Soc. **25**, 372 (1936).

[137] P.-S. Laplace and A.-L. de Lavoisier, *Memoire sur la chaleur* (Théophile Barrois le jeune, Paris, 1784).

[138] C. Rumford, Philos. T. R. Soc. Lond. **88**, 80 (1798).

[139] A. Shimizu, *Foundation of Thermodynamics*, 3rd. (Univ. Tokyo press, Japan, 2008) (written in Japanese).

[140] T. Shibata and S.-i. Sasa, J. Phys. Soc. J **67** 1918 (1998).

[141] E. Fermi, *Thermodynamics*, (Dover, New York, 1936).

[142] H. Hooyberghs, et al. J. Chem. Phys. **139** 134111 (2013).

[143] M. Doi J. Phys. A: Math. Gen. **9** 1465 (1976).

[144] M. Doi, J. Phys. A: Math. Gen. **9** 1479 (1976).

[145] L. Peliti, J. Physique **46** 1469 (1985).

[146] D. C. Mattis and M. L. Glasser, Rev. Mod. Phys. **70** 979 (1988).

[147] U. C. Tauber, M. Howard, and B. P. Vollmayr-Lee, J. Phys. A: Math. Gen. **38** R79 (2005).

[148] K. Itakura, J. Ohkubo and S.-i. Sasa, J. Phys. A: Math. Theor. **43** 125001 (2010).

[149] I. Prigogine, Etude *Thermodynamique des Phénomènes Irreéversibles* (Desoer, Liège, 1947); S. R. de Groot and P. Mazur, *Non-Equilibrium Thermodynamics* (Dover, New York, 1984).

[150] W. Driessler, J. Stat. Phys. **24**, 595 (1981).

[151] I. Eliazar and J. Klafter, J. Stat. Phys. **111**, 739 (2003).

[152] K. Sekimoto, F. Takagi and T. Hondou, Phys. Rev. E **62**, 7759 (2000).

[153] E. H. Lieb, Physica A **263**, 491499 (1999).

[154] H. Callen, *Thermodynamics and an Introduction to Thermostatistics* (Wiley, New York, 1985), 2nd ed. p. 53.

[155] Ch. Gruber and J. Piasecki, Physica A **268**, 412 (1999).

[156] A. Fruleux, R. Kawai, and K. Sekimoto, Phys. Rev. Lett. **108**, 160601 (2012).

[157] H. Touchette, Phys. Rep. **478**, 1 (2009).

[158] D. J. Evans, E. G. D. Cohen and G. P. Morriss, Phys. Rev. Lett. **71**, 2401 (1993).

[159] G. Gallavotti and E. G. D. Cohen, Phys. Rev. Lett. **74**, 2694 (1995).

[160] J. Kurchan, J. Phys. A: Math. Gen. **31**, 3719 (1998).

[161] J. L. Lebowitz and H. Spohn, J. Stat. Phys. **95**, 333 (1999).

[162] P. Visco, J. Stat. Mech. P06006 (2006).

[163] H. Hayakawa and M. Otsuki, Phys. Rev. E **88**, 032117 (2013).

[164] P. S. Goohpattader, S. Mettu and M. K. Chaudhury, Langmuir, **25**, 9969 (2009).

[165] S. Joubaud, D. Lohse, and D. van der Meer, Phys. Rev. Lett. **108**, 210604 (2012).

[166] A. Baule, H. Touchette, and E. G. D. Cohen, Nonlinearity **24**, 351, (2011).

[167] A. Naert, Europhys. Lett. **97**, 20010 (2012).

[168] S. Joubaud, D. Lohse, and D. van der Meer, Phys. Rev. Lett. **108**, 210604 (2012).

[169] C.-É. Lecomte and A. Naert, J. Stat. Mech. (**2014**) P11004.

[170] D. J. Evans and G. P. Morriss, *Statistical Mechanics of Nonequilibrium Liquids* (Academic Press, London, 1990).

[171] A. Puglisi, V. Loreto, U. Marini Bettolo Marconi, A. Petri, and A. Vulpiani, Phys. Rev. Lett. **81**, 3848 (1998).

[172] T. P. C. van Noije, M. H. Ernst, E. Trizac, and I. Pagonabarraga, Phys. Rev. E **59**, 4326 (1999).

[173] G. Gradenigo, A. Sarracino, D. Villamaina, and A. Puglisi, Europhys. Lett. **96**, 14004 (2011).

[174] N. Khalil and V. Garzó, J. Chem. Phys. **140**, 164901 (2014).

[175] A. Lorenz, C. Tuozzolo, and M.Y. Louge, Exp. Mech. **37**, 292 (1997).

[176] M. Louge (1999), Fall 1999 Impact Parameter Chart, `http://grainflowresearch.mae.cornell.edu/impact/data/Impact%20Results.html`

[177] J. T. Jenkins and C. Zhang, Phys. Fluids **14**, 1228 (2002).

[178] D. K. Yoon and J. T. Jenkins, Phys. Fluids **17**, 083301 (2005).

[179] K. Saitoh and H. Hayakawa, Phys. Rev. E **75**, 021302 (2007).

[180] J. T. Jenkins and D. Berzi, Granul. Matt. **12**, 151 (2010).

[181] S-S. Hsiau and W-L. Yang, Phys. Fluids. **14**, 612 (2002).

[182] D. van der Meer and P. Reimann, Europhys. Lett. **74**, 384 (2006).

[183] Y. Sone, (Birkhäuser, Boston, 2007).

[184] T. Baumberger and C. Caroli, Adv. Phys **55**, 279 (2006).

[185] M. Abramowitz and I. A. Stegun, *Handbook of Mathematical Functions: With Formulas, Graphs, and Mathematical Tables* (Dover, New York, 1964).

[186] E. C. Titchmarsh, Proc. London Math. Soc. **2**, 23 (1923).

[187] G. Kuwabara and K. Kono, Jpn. J. Appl. Phys. **26**, 1230 (1987).

[188] A. S. Bodrova, N. V. Brilliantov, and A. Yu. Loskutov, J. Exp. Theor. Phys. **109**, 946 (2009).

[189] C. Scalliet, A. Gnoli, A. Puglisi, and A. Vulpiani, Phys. Rev. Lett. **114**, 198001 (2015).

[190] J. Javier Brey, M. J. Ruiz-Montero, D. Cubero, and R. García-Rojo, Phys. Fluids **12**, 876 (2000).

[191] S. Torquato, Phys. Rev. E **51**, 3170 (1995).

[192] P. Résibois and M. de Leener, *Classical Kinetic Theory of fluids* (Wiley, New York, 1977).

[193] V. Garzó and J. W. Dufty, Phys. Rev. E **59** 5895 (1999).

[194] G. Verley, M. Esposito, T. Willaert and C. Van den Broeck, Nat. Com. **5**, 4721 (2014).

[195] T. Sano, Master Thesis, "*Numerical Analysis of Granular Jet Impacts,*" *Kyoto University*. The pdf file is available on the author's webpage.

[196] S. Chapman and T. G. Cowling, "The Mathematical Theory of Non-uniform Gases (Third Edition)," Cambridge University Press, 1970.

[197] J. A. MacLennan, "An Introduction to Nonequilibrium Statistical Mechanics," Prentice Hall, 1989.

[198] R. Balescu, "Equilibrium and Nonequilibrium Statistical Mechanics," John Wiley & Sons, 1975.

[199] P. Rèsibois and M. de Leener, "Classical Kinetic Theory of Fluids," John Wiley & Sons, 1977.

[200] L. E. Reichel, "A Modern Course in Statistical Physics," University Texas Press, 1980.

[201] E. M. Lifshitz and L. P. Pitaevski, "Physical Kinetics," Butterworth-Heinemann, 1981.

[202] J.-P. Hansen and I. R. McDonald, "Theory of Simple Liquids, " *the third edition*, 2006.

[203] S. G. Brush, Kinetic Theory, Vol. 3 (Pergamon Press, New York, 1972).

[204] I. P. Shkarofsky, T. W. Johnston, and M. P. Bachynski, "The Particle Kinetics of Plasmas (Addison-Wesley, Reading, MA)," 1966.

[205] C. Busch and U. Kortshagen, Phys. Rev. E **51**, 280 (1995).

[206] G. A. Bird, Phys. Fluids, **6**, 1518 (1963).

[207] G. A. Bird, J. Fluid Mech. **30**, 479 (1967).

[208] W. Wagner, J. Stat. Phys., **66** 1011 (1976).

[209] Y. Sone and K. Aoki, "Molecular Aerodynamics," (Asakura Publishing, Co., Ltd.), 1994.

[210] S. Chapman, Proc. R. Soc. Lond. A 93:1 (1916-1917); D. Enskog, Thesis, Uppsala (1917) [Both reprinted in [203]].

[211] D. Enskog, K. Sven Vetenskaps Akad. Handl., 63 (no. 4) (1922) English translation appears in: [203].

[212] S.T. Choh and G.E. Uhlenbeck, The kinetic theory of phenomena in dense gases, Ph.D. dissertation, University of Michigan, 1958.

[213] J. A. McLennan, Phys. Lett. **7**, 332 (1963).

[214] K. Kawasaki and I. Oppenheim, Phys. Rev. A **139**, 1763 (1965).

[215] van Beijeren and the M. H. Ernst, Physica **68** 437 (1973).

[216] van Beijeren and the M. H. Ernst, Physica **70** 225 (1973).

[217] van Beijeren and the M. H. Ernst, Phys. Rev. **43 A**, 167 (1973).

[218] J.M. Kincaid, Phys. Lett. A, **64**, 429 (1978).

[219] van Beijeren and the M. H. Ernst, J. Stat. Phys. **21** 2, (1979).

[220] M. López de Haro and V. Garzó, Physica A **197** 98, (1993).

[221] M. H. Ernst, arXiv:cond-mat/9707146 (1997).

[222] A. Goldstein and M. Shapiro, J. Fluid Mech. **282**, 75 (1995).

[223] J. Javier Brey, M. J. Ruiz-Montero, and D. Cubero, Phys. Rev. E **54**, 3664 (1996).

[224] Y. Du, H. Li and L. P. Kadanoff, Phys. Rev. Lett. **74**, 1268 (1995).

[225] K. Kanatani, Trans. Jpn. Soc. Mech. Eng. B **45**, 507 (1979);ibid.**45**, 515 (1979); J. Kano, A. Shimosaka, and J. Hidaka, J. Soc. Powder Techol. Jpn. **33**, 95 (1996).

[226] N. Mitarai, H. Hayakawa and H. Nakanishi, Phys. Rev. Lett. **88**, 174301 (2002).

[227] A. Goldstein and M. Shapiro, J. Fluid Mech. **282**, 75 (1995).

[228] I. Goldhirsch, S. H. Noskowicz, and O. Bar-Lev, Phys. Rev. Lett. **95**, 068002 (2005).

[229] B. Gayen and M. Alam, J. Fluid Mech. **567**, 195 (2006).

[230] N. V. Brilliantov, T. Pöschel, W. T. Kranz, and A. Zippelius, Phys. Rev. Lett. **98**, 128001 (2007).

[231] W. T. Kranz, N. V. Brilliantov, T. Pöeschell and A. Zippelius, Eur. Phys. J. Special Topics, **179**, 91 (2009).

[232] B. Gayen and M. Alam, Phys. Rev. Lett. **100**, 068002 (2008).

[233] B. Gayen and M. Alam, Phys. Rev. E **84**, 021304 (2011).

[234] H. Xu, M. Y. Louge, and A. P. Reeves, Continuum Mech. Thermodyn. **15**, 321 (2003).

[235] C. K. K. Lun and A. A. Bent, J. Fluid Mech. **258**, 335 (1994).

[236] T. Nemoto, Phys. Rev. E **85**, 061124 (2012).

[237] H. Takahasi and M. Mori, Double Exponential Formulas for Numerical Integration, *Publications of RIMS, Kyoto University* **9**, 721 (1974).

[238] G. E. Andrews, R. Askey, and R. Roy, *Special functions* (Cambridge University Press, Cambridge, England, 1999).

[239] L. Cerino, G. Gradenigo, A. Sarracino, D. Villamaina, and A. Vulpiani, Phys. Rev. E **89**, 042105 (2014).

[240] J. P. S. Bizzaro, J. App. Phys. **108**, 054907 (2010).

[241] M. Itami and S.-i. Sasa, Phys. Rev. E **89**, 052106 (2014).

[242] M. Itami and S.-i. Sasa, J. Stat. Phys. **158**, 37 (2015).